ANL-79-65

Part I

ANL-79-65

Part I

RADIOLOGICAL AND ENVIRONMENTAL RESEARCH DIVISION ANNUAL REPORT

Fundamental Molecular Physics and Chemistry

October 1978—September 1979

ARGONNE NATIONAL LABORATORY, ARGONNE, ILLINOIS

Prepared for the U. S. DEPARTMENT OF ENERGY
under Contract W-31-109-Eng-38

FOREWORD

This is the ninth Annual Report of our Section, summarizing our work on the chemical physics of atoms and molecules, especially their interaction with external agents such as photons and electrons. Even though the volume of work covered has increased and our activities have expanded into several additional scientific areas, this year's report has been reduced in size for easier reading.

As before, our programs are designed to address themselves to several of the DOE needs. First, we continue to determine cross sections for electron and photon interactions with molecules to provide a sound basis for the microscopic analysis of radiation actions on matter, including biological substances. We are also developing theories that predict the earliest events of radiation action by use of cross-section data. Second, we are studying the chemical physics of atmospheric-pollutant molecules (and related molecules) arising from coal and other energy technologies. More specifically, work in this area concerns electronic spectroscopy, as well as the kinetics of clustering of a small number of molecules. All these efforts are supported by the Office of Environment, DOE. In addition, a part of our work deals with spectral and collisional property of highly stripped ions — an important basic area of the fusion energy technology, both in the magnetic-confinement approach and in the intertial-heating approach. This part of the work is supported by the Office of Energy Research, DOE.

The articles in this report are loosely arranged according to the subject they treat although an article is often related to several topics. Papers 1-17 concern photoabsorption processes and their consequences. In particular, paper 1 reports on the initial operation of a new photoionization mass spectrometer. Paper 2 also reports a new activity, i.e., measurements of the polarization of fluorescence. Papers 18-32 concern electron interactions with atoms and molecules. Notice that in the above-mentioned two areas, both theoretical and experimental studies are conducted, often in close association. Papers 33-34 treat basic radiation physics, and papers 35-47 deal with various problems in theoretical atomic physics. Many of the latter papers (e.g., papers 36, 37, and 45-47)

represent work related to fusion-plasma studies.

In addition to the work in our laboratory, we have made numerous other scientific contributions. First of all, collaboration with workers at other institutions is too much to be listed here. An example is the new effort being made with the National Bureau of Standards, as seen in papers 2, 8, 9, 10, and 11. The addresses of the co-authors in this volume will give some idea of the extent of our collaborative work. I thank all the co-authors for their contributions to our programs, and sincerely hope that they feel it worth while to work with us for years to come. Second, we have played major roles in several scientific meetings; examples are the Sixth International Congress of Radiation Research, May 1979, Tokyo and the Eleventh International Conference on the Physics of Electronic and Atomic Collisions, August-September 1979, Kyoto. Finally, M. Inokuti is a Councilor for the Radiation Research Society and is Vice-Chairman of the Committee on Stopping Powers for the International Commission on Radiation Units and Measurements.

Mitio Inokuti

TABLE OF CONTENTS

Fundamental Molecular Physics and Chemistry

PHOTON FLUX MEASUREMENTS FROM THE NEW PHOTOIONIZATION MASS SPECTROMETER

P. M. Dehmer

The Hopfield continuum of helium was generated in approximately 75 torr of helium gas by a high voltage pulsed dc discharge generated by a Velonex Model 350 high power pulse generator, which was used as the driver for two additional stages of high power pulse amplification. The final output stage consisted of a pair of Machlett 6544 triode tubes in parallel. The voltage pulse is characterized by a 60 nsec rise time, 150 nsec width, and 9 to 10 kV amplitude. The voltage pulse from this pulse generator has a more rapid cutoff than a pulse from a typical thyratron pulse generator, thus allowing the use of a significantly higher pulse repetition rate. For example, a pulse repetition rate of 80 to 100 kc/sec is used in the present apparatus, as compared with 9 to 10 kc/sec in a typical thyratron triggered He continuum light source. The average power is approximately 3 kW, of which 1 kW is dissipated across the capillary lamp. The lamp employed in the present measurements was approximately 50 cm long. The McPherson Model 225 1m near-normal incidence monochromator was equipped with a Bausch and Lomb 1200 line/mm MgF_2 coated aluminum grating blazed for 800 Å in first order. The grating size was 114.3 mm in diameter, and the ruled area was 96 mm × 56 mm. The photon intensity as measured with an aluminum photodiode was 7×10^9 photons/sec/Å at the peak of the helium continuum. This value is reliable to ±30 percent. A factor of approximately 5 improvement is expected with such modifications as the use of purified helium for the sample gas and the use of an osmium coated grating.

POLARIZATION OF FLUORESCENCE OF $N_2^+ (B^2\Sigma_u^+)$: ALIGNMENT OF MOLECULES VIA PHOTOIONIZATION

E. D. Poliakoff, J. L. Dehmer, A. C. Parr,* K. H. Jackson,† and R. N. Zare†

The polarization of fluorescence of gas-phase atoms and molecules yields information about their state of alignment in space. Viewed classically, an excited molecule with no preferred orientation in space will radiate in random directions with random direction cosines, yielding zero polarization.[1] However, an excited molecule, when aligned, will emit dipole radiation anisotropically, and the resultant fluorescence polarization will be non-zero. Conversely, the polarization of fluorescence can be used as a measure of the degree of alignment of the molecular ion. For the case of photoionization, this degree of alignment of the excited molecular ion can be related to the photoionization dynamics in a direct way.[2]

Such a measurement has been performed, using radiation from the Synchrotron Ultraviolet Radiation Facility II (SURF II) as an excitation source. The specific reaction studied is given[3,4] by

$$N_2(X^2\Sigma_g^+) + h\nu \rightarrow N_2^+(B^2\Sigma_u^+) + e^- (\varepsilon\sigma_g, \varepsilon\pi_g)$$
$$\downarrow$$
$$N_2^+(X^2\Sigma_g^+) + h\nu' \quad . \qquad (1)$$

Here, a $2\sigma_u$ electron is removed via photoionization; dipole selection rules require that the photoelectron leave via either the σ_g or π_g continuum channels. An electron excited to the σ_g continuum wave will leave the molecular ion partially aligned with the incident radiation $\underset{\sim}{\varepsilon}$ vector. Since the transition dipole of the fluorescence is parallel with the internuclear axis, molecules excited in this way will fluoresce with a positive polarization. In contrast, when the σ_u electron is promoted into the π_g channel, there will be a negative polarization

---

*Synchrotron Ultraviolet Radiation Facility, National Bureau of Standards, Washington, D.C. 20234.

†Department of Chemistry, Stanford University, Stanford, CA 94305.

to the molecular ion fluorescence. Thus, a measurement of the polarization can yield the cross-section ratio for the σ_g and π_g continuum channels.

The experimental apparatus used to perform the measurement is illustrated schematically in Figure 1. Measurements were performed with $660.5 \leq \lambda_{ex} \leq 450$ Å. Thus, the cross-section ratio previously discussed could be determined as a function of electron kinetic energy so the dynamics of the photoionization event could be analyzed.

The results are shown in Figure 2. These results have not been corrected for a polarization bias in the optical train (whose magnitude is less than 0.01). Quantitative measurements are under way to determine and correct for any such polarization bias. Qualitatively, one notes that the polarization decreases in magnitude as the wavelength decreases. This indicates that the σ_g and π_g channels become balanced (in terms of cross section) for the outgoing electron as the electron kinetic energy increases.

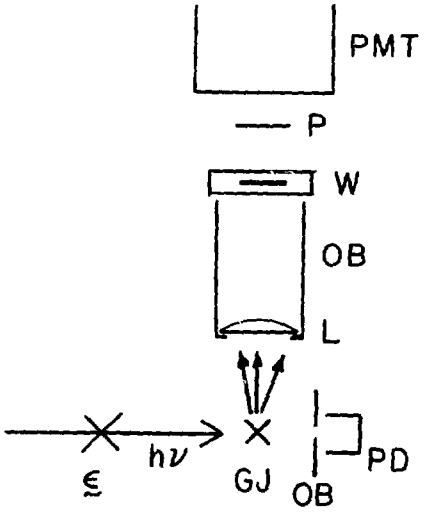

FIG. 1.--Diagram of experimental apparatus used to perform the experiment. X indicates perpendicularity to plane of paper. GJ, gas jet; OB, optical baffle; PD photodiode; L, lens; W, window; P, polarizer; PMT, photomultiplier tube.

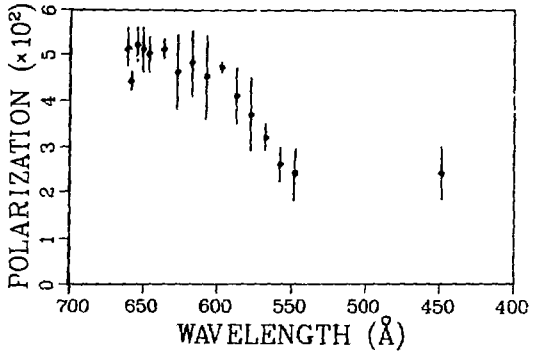

FIG. 2.--Polarization of $N_2^+(B \rightarrow X)$ fluorescence as a function of photoionization wavelength.

Although the results are preliminary, they are extremely encouraging. A detailed theoretical analysis of these results is in progress, and further studies are planned. In particular, investigations of more simple photoionization cases is planned, as well as studies of photodissociative systems, given in general terms in Eq. 2:

$$\begin{array}{l} AB + h\nu \rightarrow A^* + B \\ \qquad\qquad\quad \downarrow \\ \qquad\qquad\quad A + h\nu' \quad . \end{array} \qquad (2)$$

The alignment of A* will be measured to determine parameters (branching ratios, parent fragmentation lifetime, symmetries of dissociative surfaces) pertinent to the spectroscopy and dynamics of photodissociation.

References

1. M. McClintock, W. Demtröder, and R. N. Zare, J. Chem. Phys. 51, 5509 (1969) and references therein.
2. An atomic photoionization analog is given by C. D. Caldwell and R. N. Zare, Phys. Rev. A 16, 255 (1977); A molecular photodissociation example is given in E. D. Poliakoff, S. H. Southworth, D. A. Shirley, K. H. Jackdon, and R. N. Zare, Chem. Phys. Lett. 65, 407 (1979).
3. G. R. Cook and P. H. Metzger, J. Chem. Phys. 41, 321 (1964).
4. A. Lofthus and P. H. Krupenie, J. Phys. Chem. Ref. Data 6, 113 (1977).

PHOTOELECTRON SPECTRUM OF ALLENE USING A SUPERSONIC MOLECULAR BEAM SOURCE

P. M. Dehmer and J. L. Dehmer

Cederbaum et al.[1] have recently calculated the photoelectron spectrum of the ^2E ground electronic state of the allene ion which exhibits strong Jahn-Teller effects. The spectrum of this state, which is shown in Figure 1, shows a well-resolved progression in the torsional mode at low energy, followed by a longer

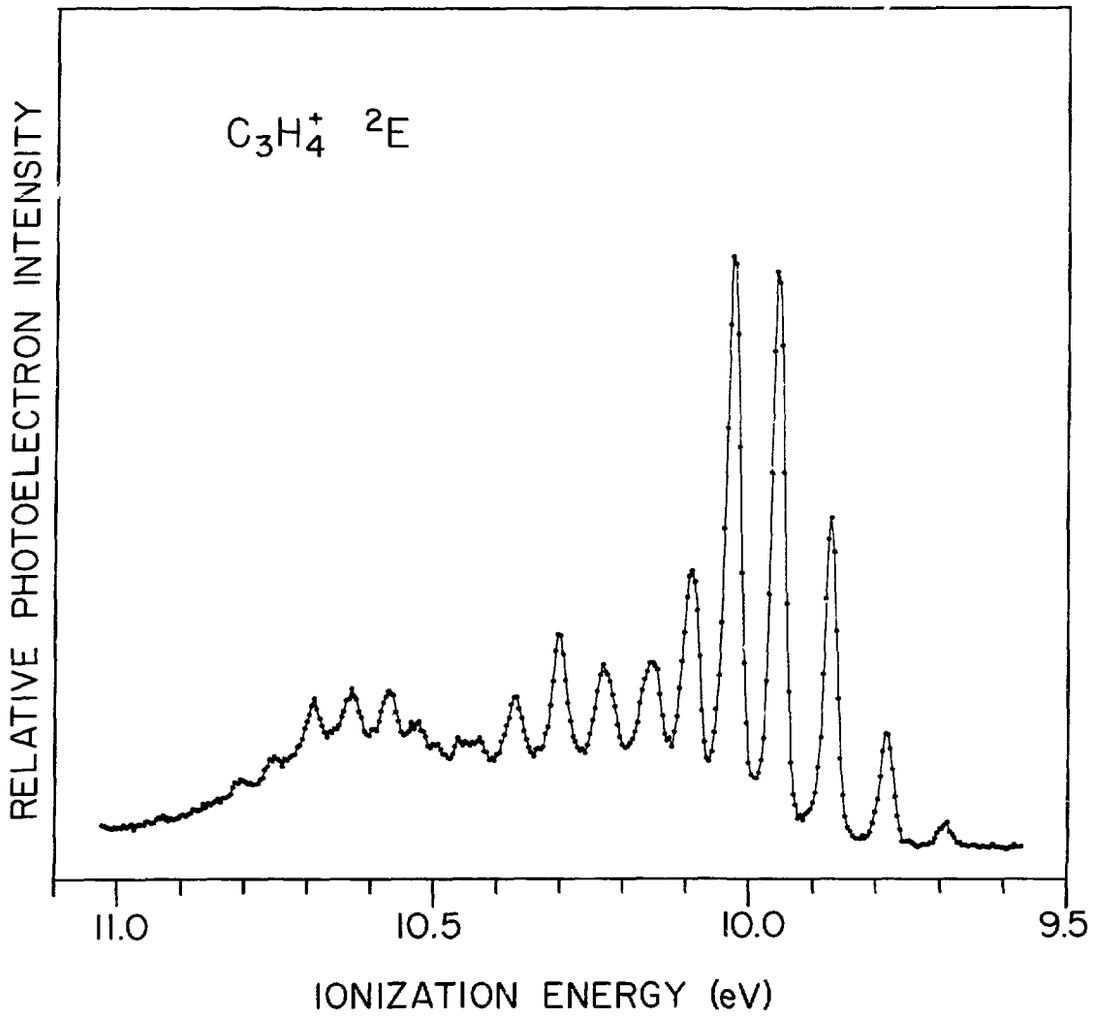

FIG. 1.--Photoelectron spectrum of the ground ionic state of allene.

region of only partially resolved structure. The present data taken at a spectrometer resolution of 22 meV using a supersonic molecular beam source to rotationally cool the target beam show considerably more detail than do the previously reported spectra, some of which were taken at higher resolution but with a room temperature sample.[2] We are presently in the process of performing a detailed comparison between the experimental and theoretical results.

References

1. L. S. Cederbaum, W. Domcke, and H. Köppel, Chem. Phys. 33, 319 (1978).
2. R. K. Thomas and H. Thompson, Proc. R. Soc. London 339, 29 (1974) and references therein.

HIGH-RESOLUTION PHOTOABSORPTION AND PHOTOIONIZATION SPECTRA OF HD AND D_2

P. M. Dehmer, P. S. Dardi,* and W. A. Chupka†

Relative photoabsorption and photoionization cross sections for D_2 and HD are reported in the wavelength region between approximately 805 Å and 735 Å. Many members of the $np\sigma\ ^1\Sigma_u^+$ and $np\pi\ ^1\Pi_u$ Rydberg series for low n and low v were identified from previous assignments. An attempt was made to extend the assignments to higher vibrational quantum numbers for n = 3-6, using previously reported spectroscopic constants. This attempt was only moderately successful because of the overlap of vibrational bands at higher v. The increasing complexity of the spectra at high v and at high n requires a more sophisticated analysis such as would be provided by multichannel quantum defect theory (MQDT).

Ionization efficiencies were calculated for all identified states. The ionization efficiency was 1 for states which can autoionize by $\Delta v = 1$, i.e., the final state of the ion has a vibrational quantum number 1 less than the autoionizing state. In general, the ionization efficiency drops rapidly with $\Delta v > 1$. The $3p\pi\ ^1\Pi_u$ state, which can autoionize only with a $\Delta v \geq 7$, has essentially an ionization efficiency of zero, so decay must proceed by predissociation or molecular fluorescence.

Introduction

The photoabsorption spectrum from the ground rotational state of molecular HD or D_2 consists of two interacting Rydberg series converging to each vibrational level of the ion core. The lower members of the series correspond to $np\sigma\ ^1\Sigma_u^+$ and $np\pi\ ^1\Pi_u$ series of states, but as n increases there is a transition from Hund's case (b) to Hund's case (d) as a result of the effects of ℓ uncoupling, and the series converge, respectively, to the N = 0 and N = 2 rotational levels of the ion core. During the course of the ℓ uncoupling the two series perturb each other strongly, resulting in large energy level shifts and intensity variations. In addition to these interactions between the series converging to the same vibrational level of the ion ($\Delta v = 0$ interactions), there may be further

*Undergraduate Research Participant from the University of Illinois, Urbana, Illinois, 1979.

†Department of Chemistry, Yale University, New Haven, Connecticut 06520.

intense perturbations from low n Rydberg states convering to higher excited vibrational states of the ion ($\Delta v \neq 0$ interactions).

The present work reports high resolution (0.016 Å, FWHM) relative absorption and photoionization cross sections for HD and D_2 at 78°K in the region from the ionization threshold to approximately 740 Å.

We were able to identify many peaks based on previous assignments made by Monfils[1,2] and by Takezawa and Tanaka[3,4] from very high resolution photoabsorption spectra. An attempt was made to extend these assignments by using (1) the vibrational and rotational term value expansion coefficients determined by the above workers and (2) the theoretical calculations of Kolos and Rychlewski[5] for the $3p\pi\ ^1\Pi_u$ state. We were aided by being able to observe the states in both absorption and ionization. For example, a state with low principal quantum number, which must autoionize with a large change in v, would be expected to have an ionization efficiency less than 1.

Experimental

A detailed description of the apparatus can be found in references 6 and 7. Only a brief summary will be given here.

The light source was the Hopfield helium continuum pulsed at 100 kc/sec. The light was monochromatized with a 3 m near-normal incidence monochromator before entering the ionization chamber. The ions were extracted from the chamber, focussed, and then passed through a quadrupole mass spectrometer for detection. Sample gas pressure was on the order of 10 μm. The resolution of the apparatus was observed to be 0.016 Å (FWHM) using 10 μm slits in 3rd order. Scanning was done in increments of 1/300 Å using a completely automated system.

Ordinary D_2 was used straight from commercial cylinders at 99.5% purity without further purification. Hydrogen deuteride was made by the hydrolysis of lithium aluminum hydride with deuterium oxide. The HD produced was about 94% pure with impurities of 5% H_2 and 1% D_2. The samples were cooled to liquid nitrogen temperature (78°K) before entering the ionization chamber.

Slippage in the wavelength drive resulted in shifts in the absolute wavelength scale of about 0.03 Å in both the positive and negative direction throughout the scanning range. Consequently, accurate absolute wavelengths are best taken from plate spectra, such as those taken by Monfils[1,2] and Takezawa and Tanaka.[3,4]

Results and Discussion

Spectra

Figures 1 and 2 show transmitted light and ionization plotted on the same wavelength scale for D_2 and HD, respectively, starting near their ionization thresholds. The data for D_2 were obtained from one continuous run. For HD, the data were collected from three separate runs. Each run was scaled, using the overlap between them, so that the final plot represents a smooth continuous spectrum.

Assignments

Our spectra were simplified because the samples were cooled to liquid nitrogen temperature, so only transitions originating in the lower rotational levels were observed. We began by using previously published assignments. First, considering D_2, we were able to identify transitions to the $3p\pi$ state for $v = 9$–15, using assignments made by Monfils.[1] Then, with the assignments of Takezawa and Tanaka,[4] all the $np\sigma$ and $np\pi$ transitions ($n = 4$–6) that they identified in our wavelength region were identified. Also, some higher lying states ($n \leq 10$) were identified from assignments by Takezawa and Tanaka.[4] For HD the $3p\pi$, $v = 7,8$ and $4p\pi$, $v = 5,6$ can be found, based on the assignments of Monfils.[1] In some cases peaks were reassigned on the basis of relative intensities in absorption and ionization.

We next extended our assignments using publishes constants. Extension of $3p\pi$ transitions was the easiest to make using our data since they distinguish themselves by negligibly autoionizing. From the expansion coefficients for the $3p\pi$ state given by Monfils[1,2] and the theoretical energy levels calculated by Kolos and Rychlewski,[5] we were able to assign the $3p\pi$ state transitions very nearly to the dissociation limit. Several other new assignments are also shown in Figures 1 and 2.

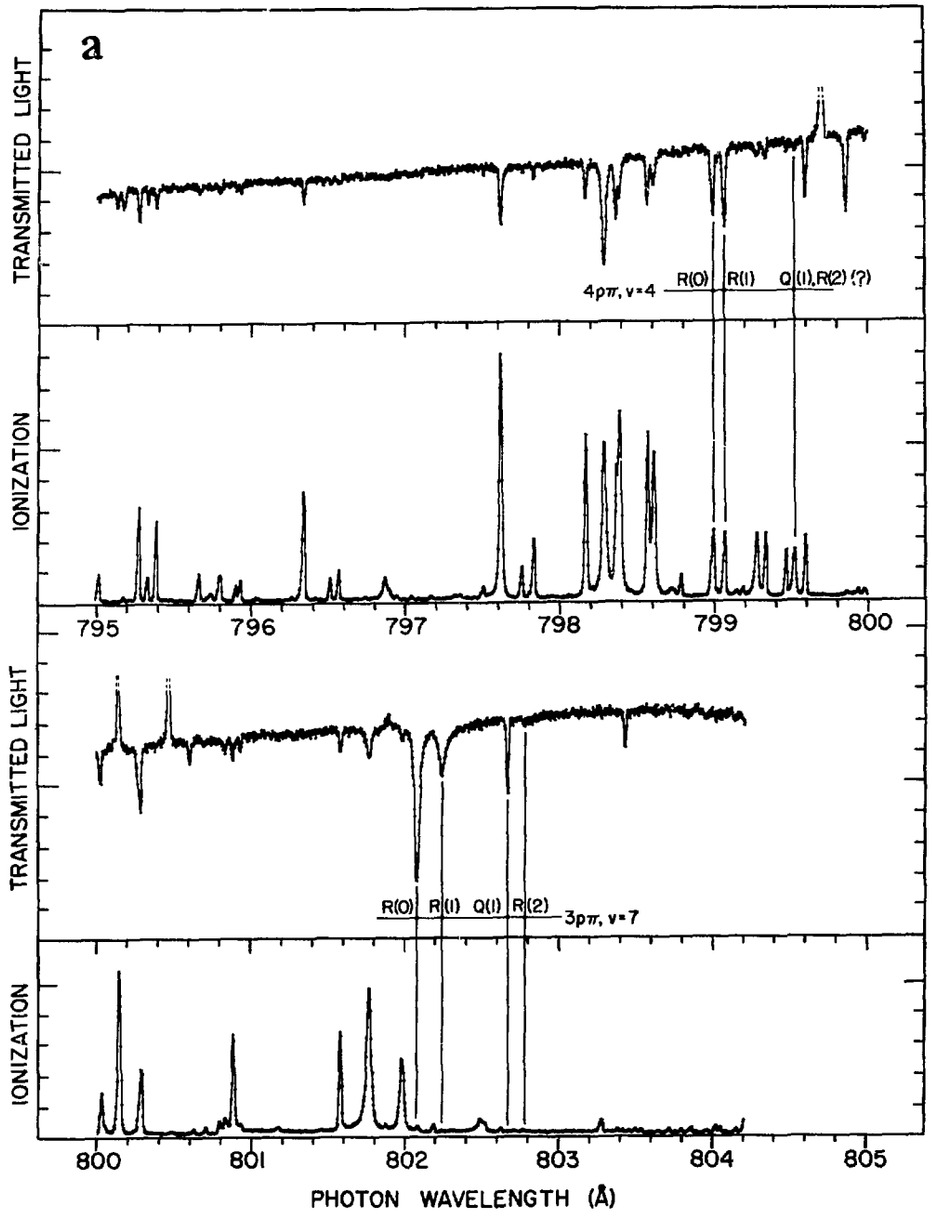

FIG. 1.--Relative photoabsorption and photoionization cross sections for HD taken at a wavelength resolution of 0.016 Å and a temperature of 78°K.

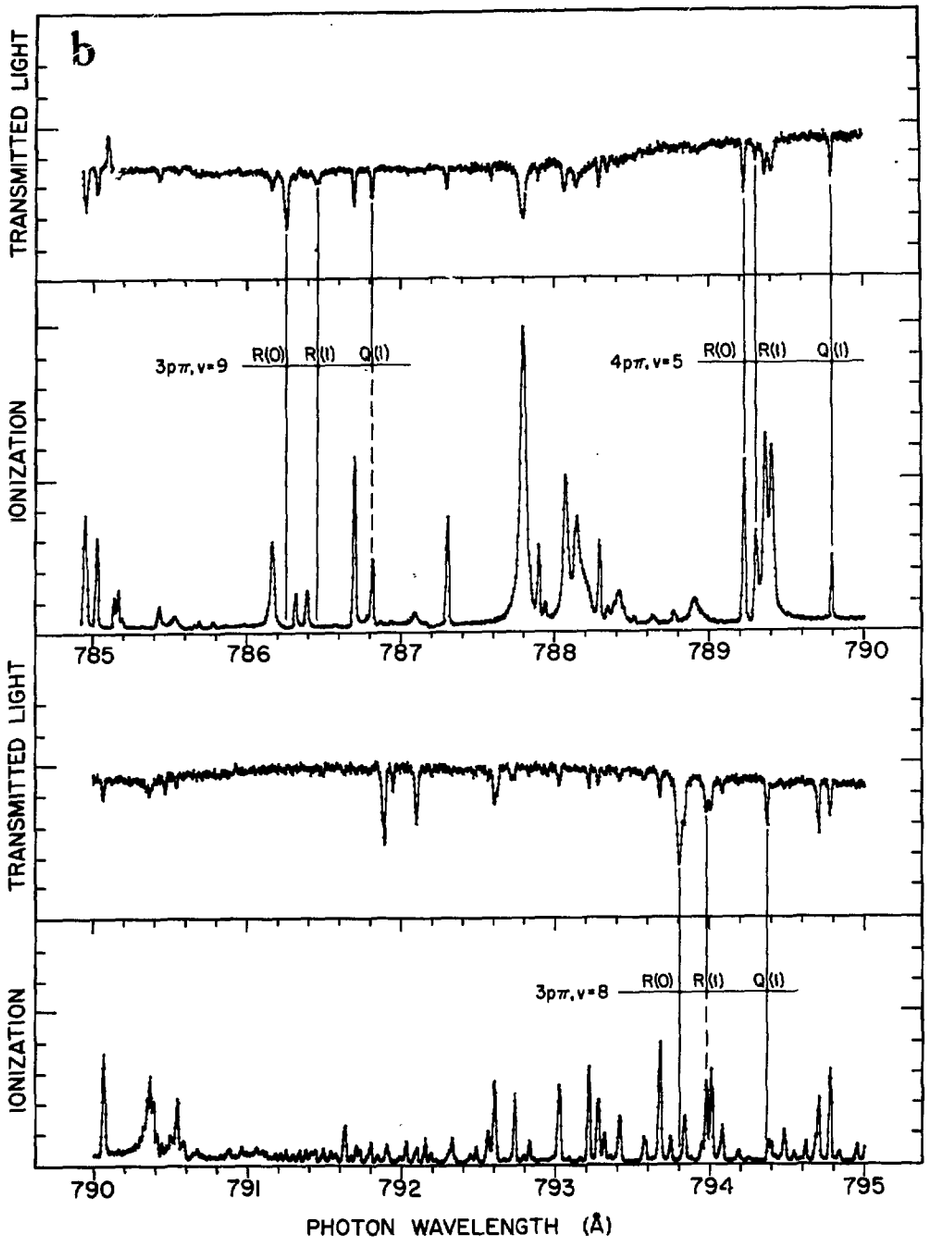

FIG. 1.--continued.

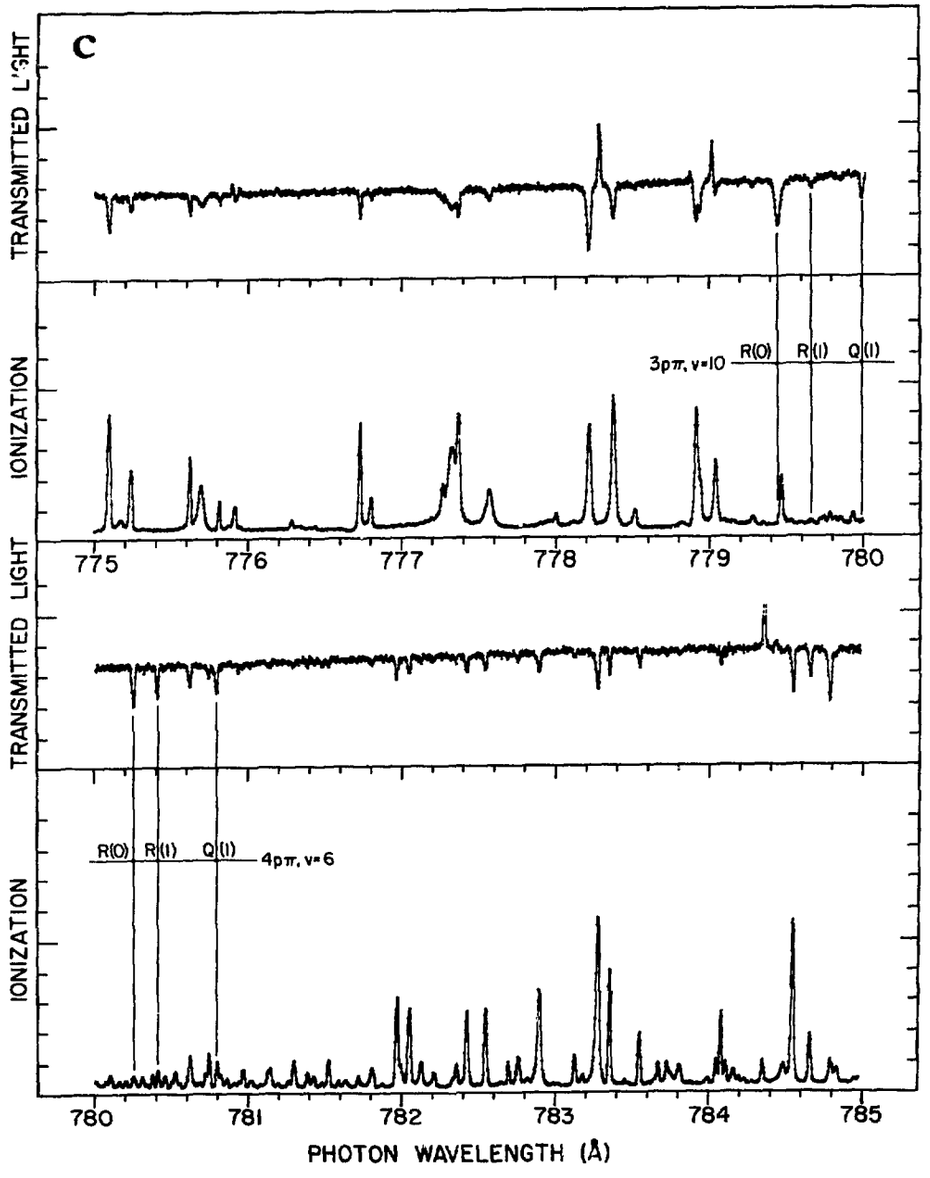

FIG. 1.--continued.

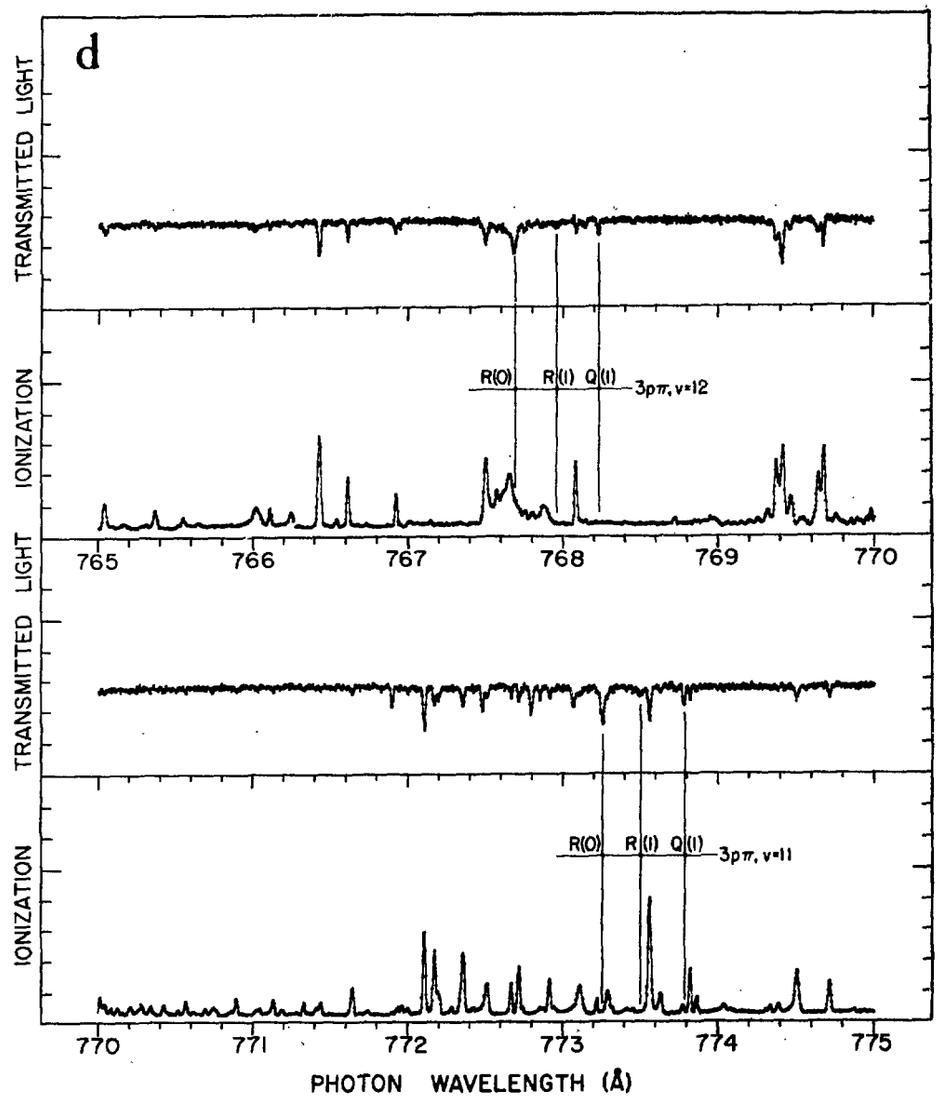

FIG. 1.--continued.

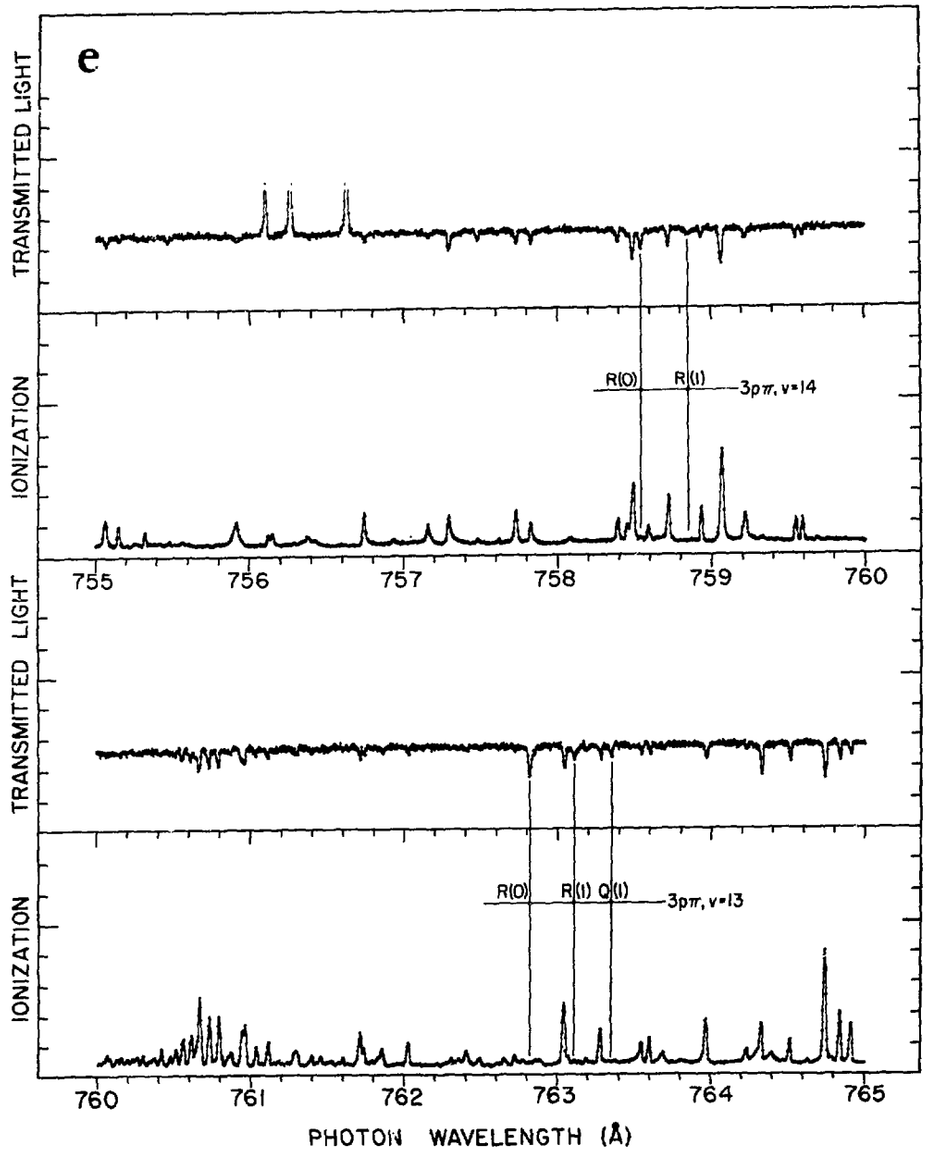

FIG. 1.--continued.

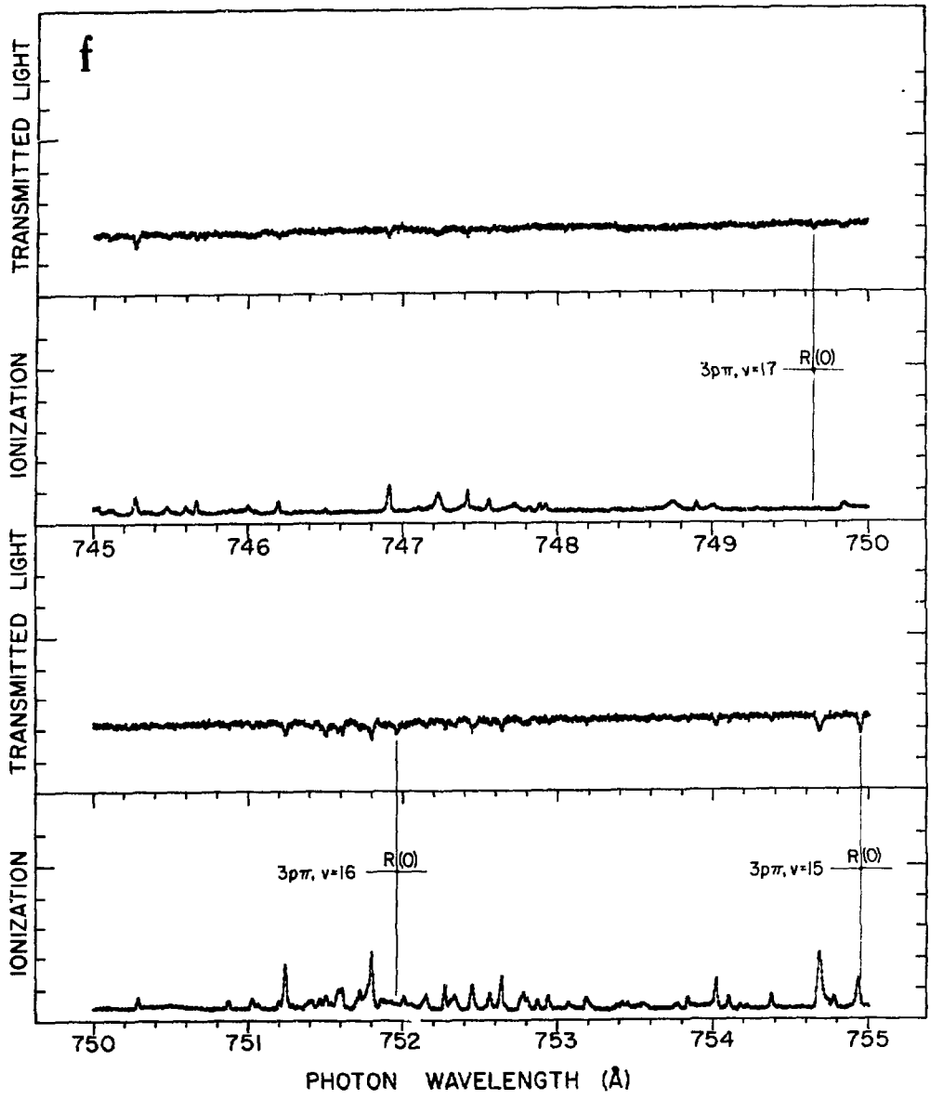

FIG. 1.--continued.

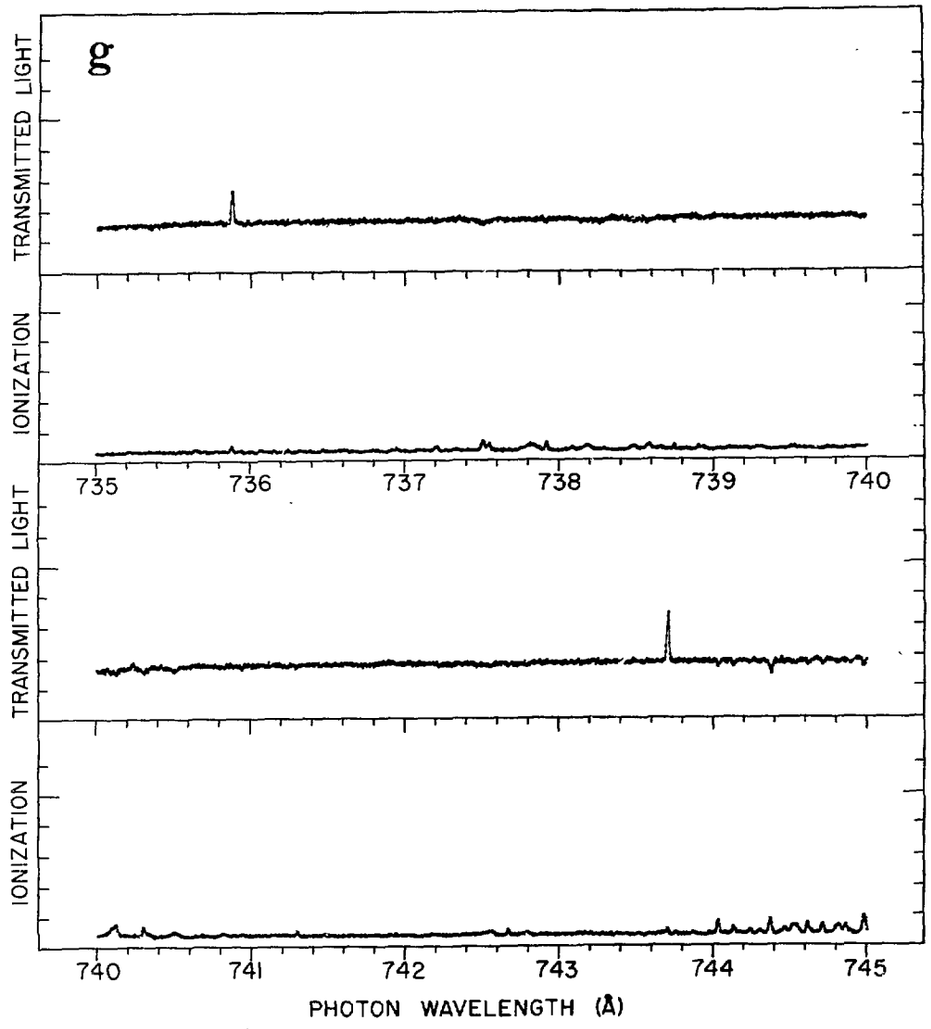

FIG. 1.--continued.

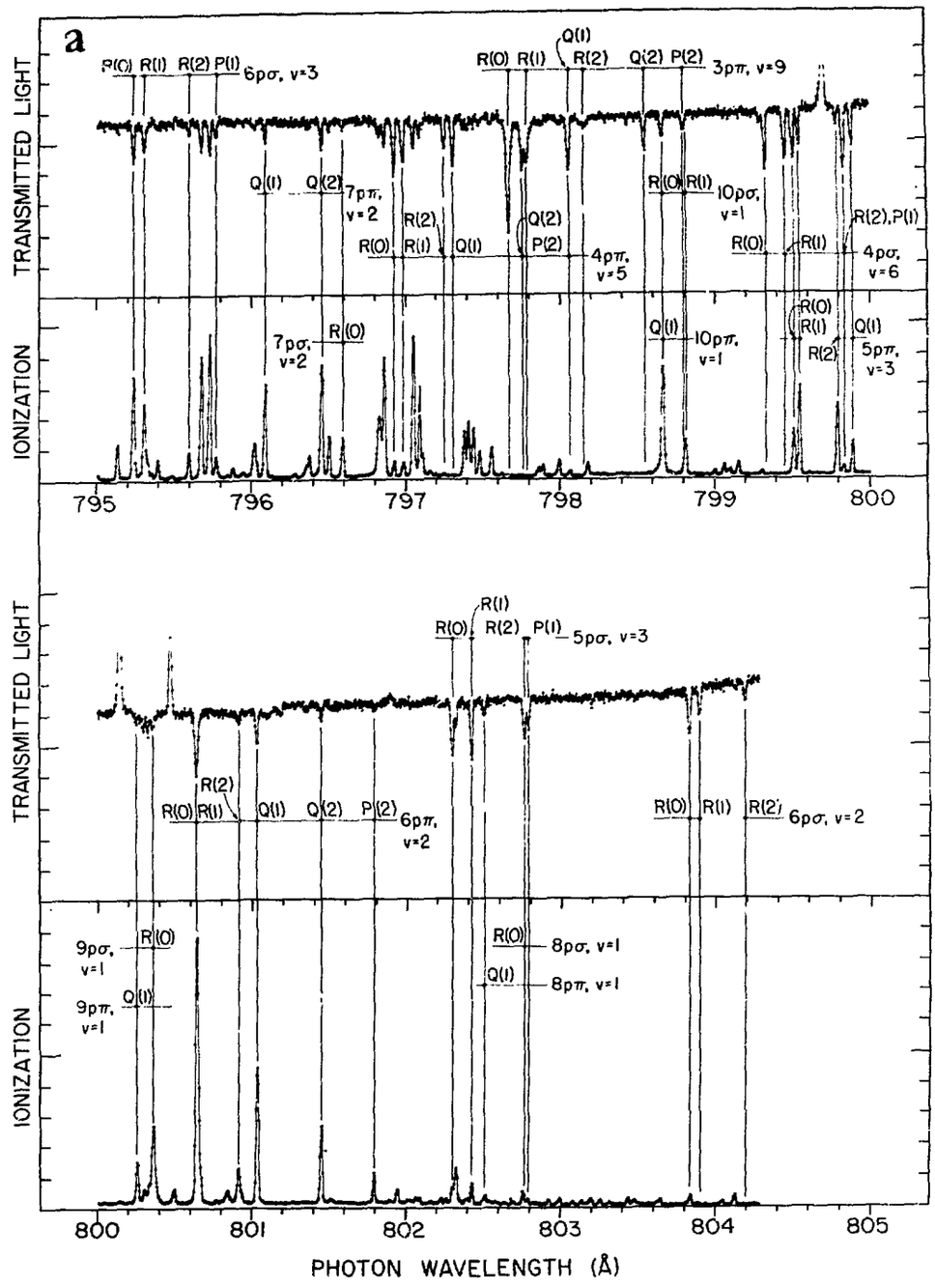

FIG. 2.--Relative photoabsorption and photoionization cross sections for D_2 taken at a wavelength resolution of 0.016 Å and a temperature of 78°K.

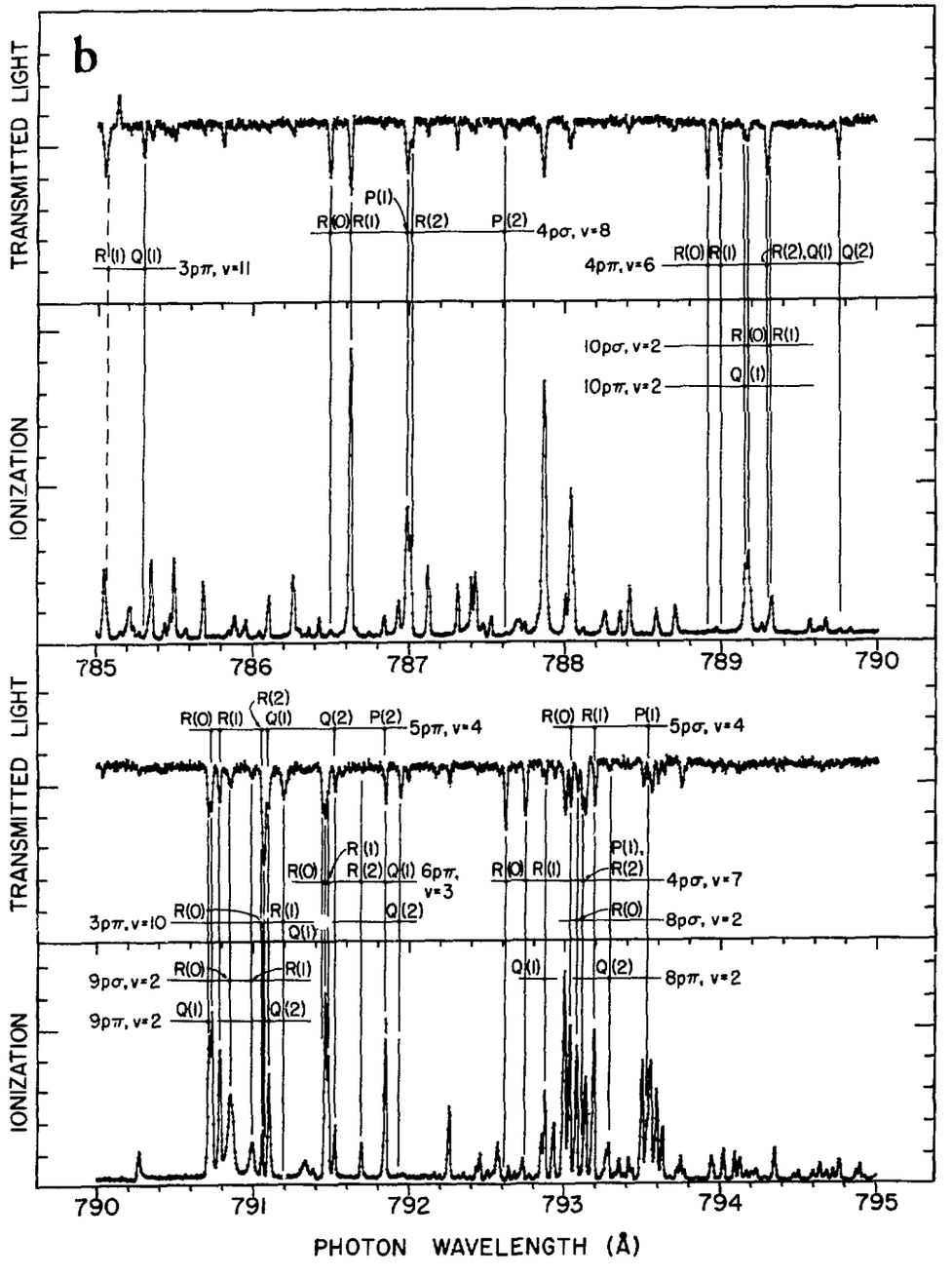

FIG. 2.--continued.

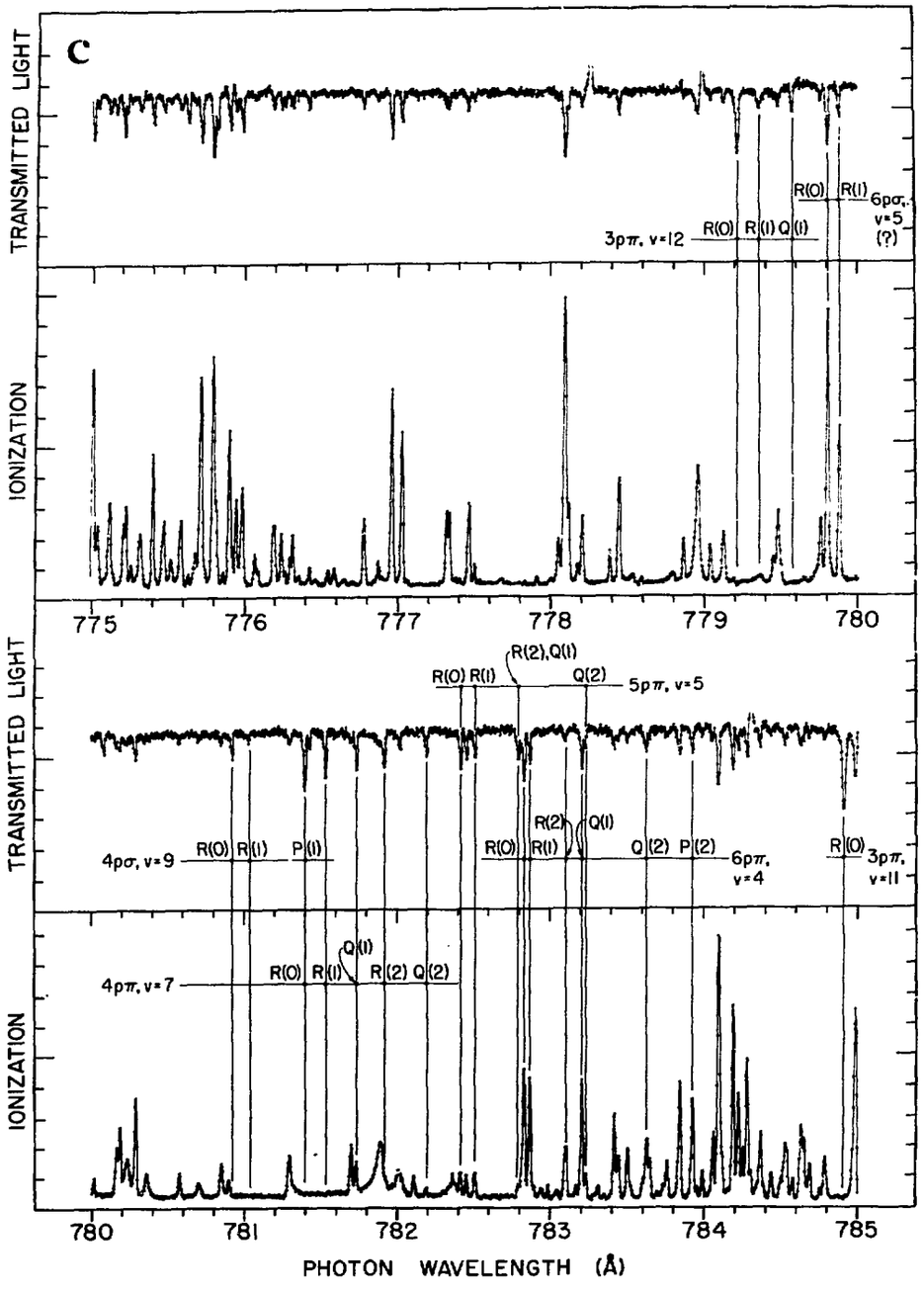

FIG. 2.--continued.

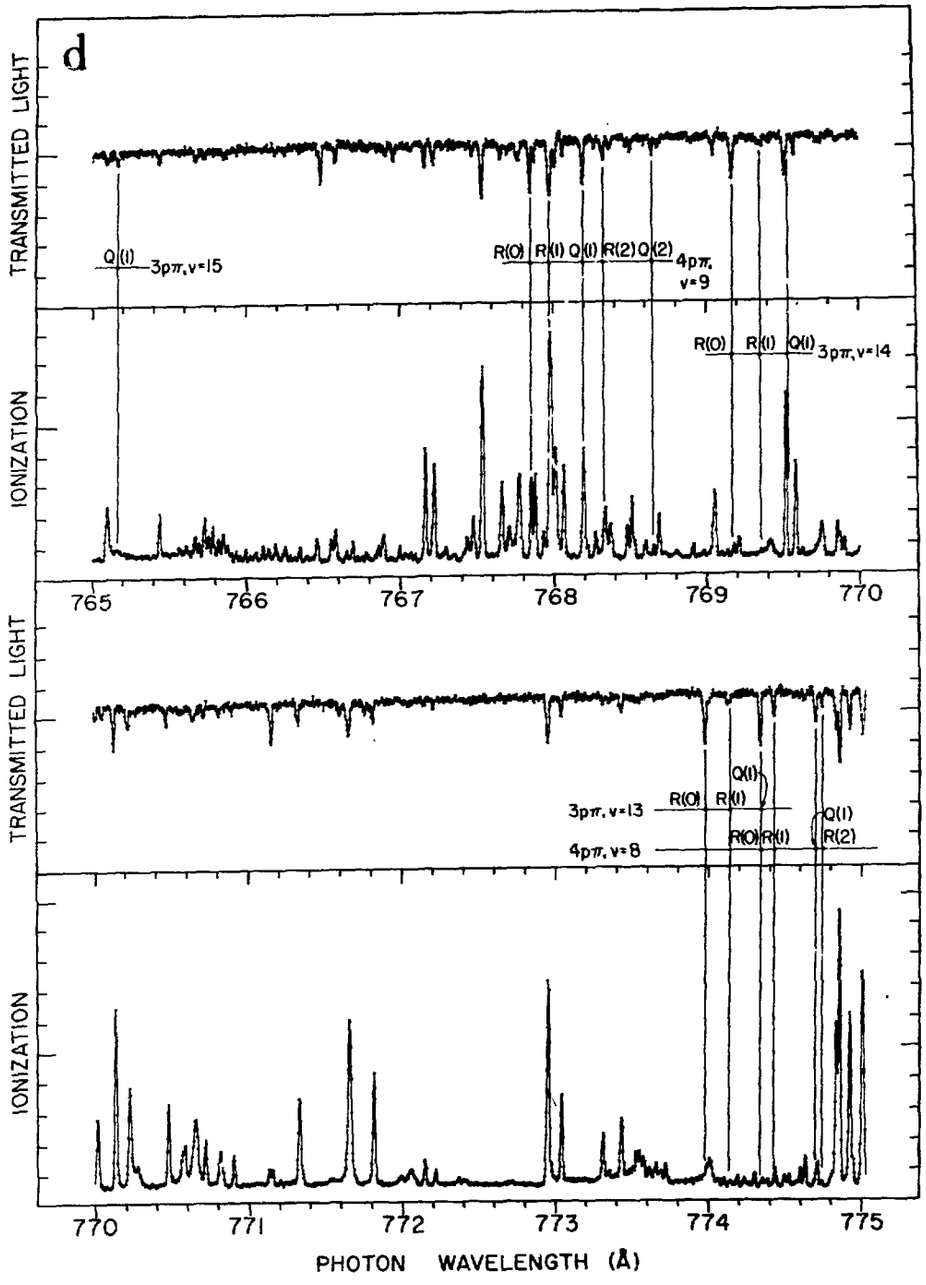

FIG. 2.--continued.

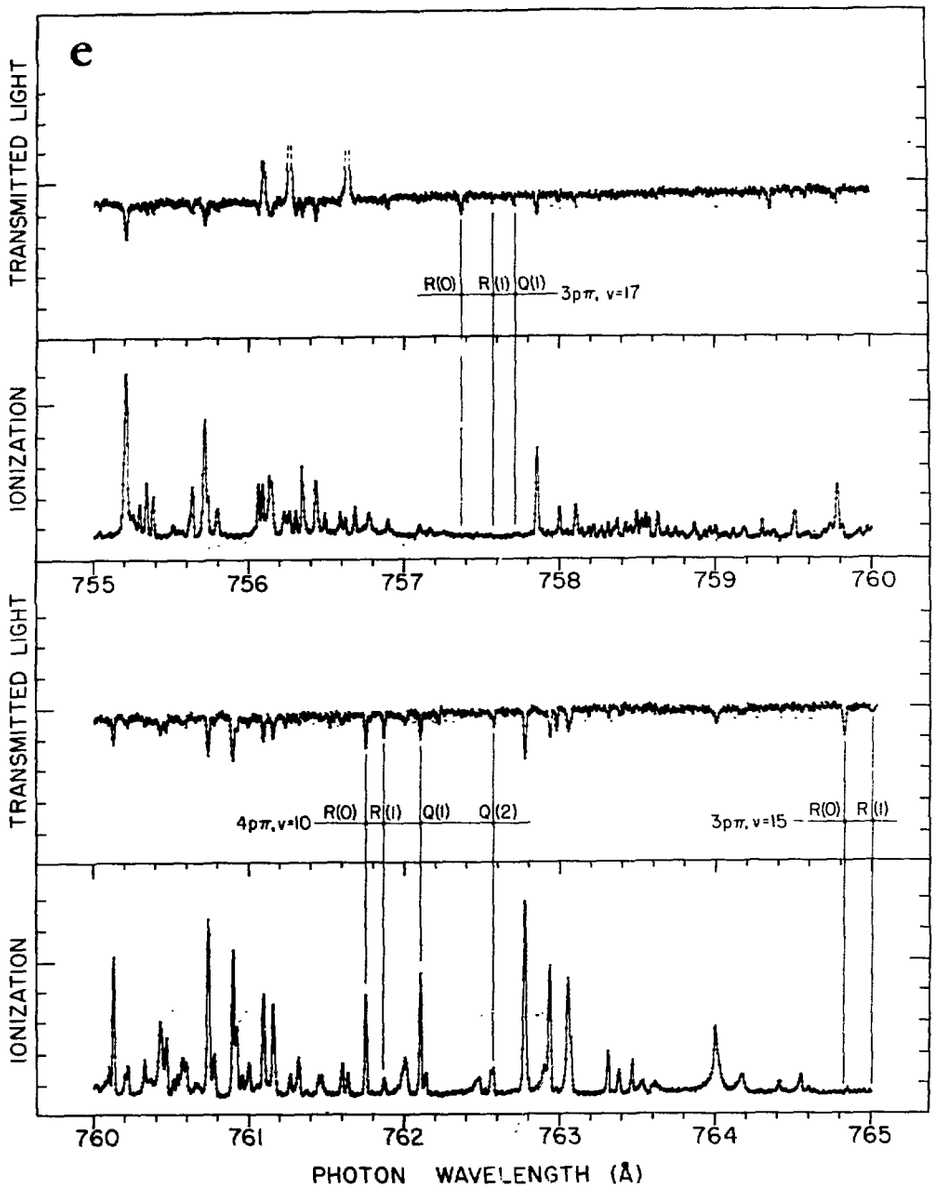

FIG. 2.--continued.

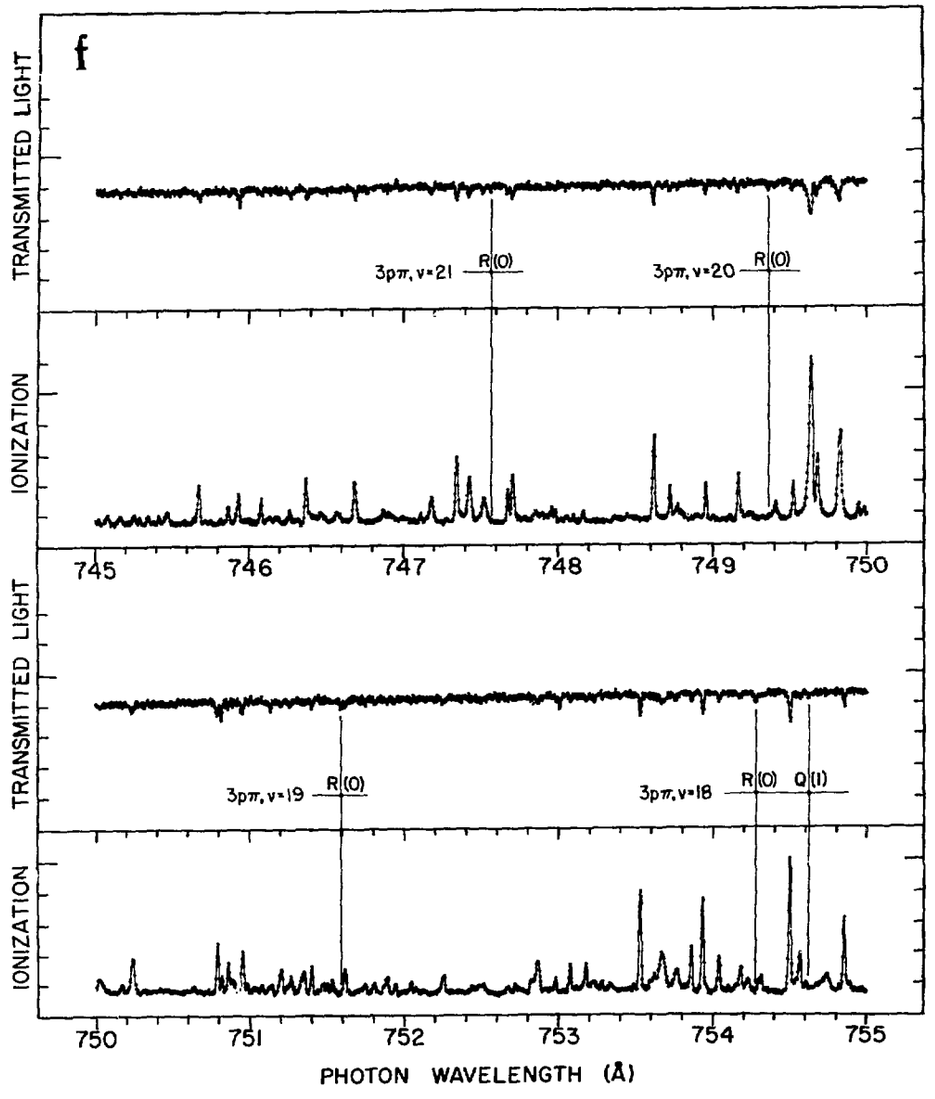

FIG. 2.--continued.

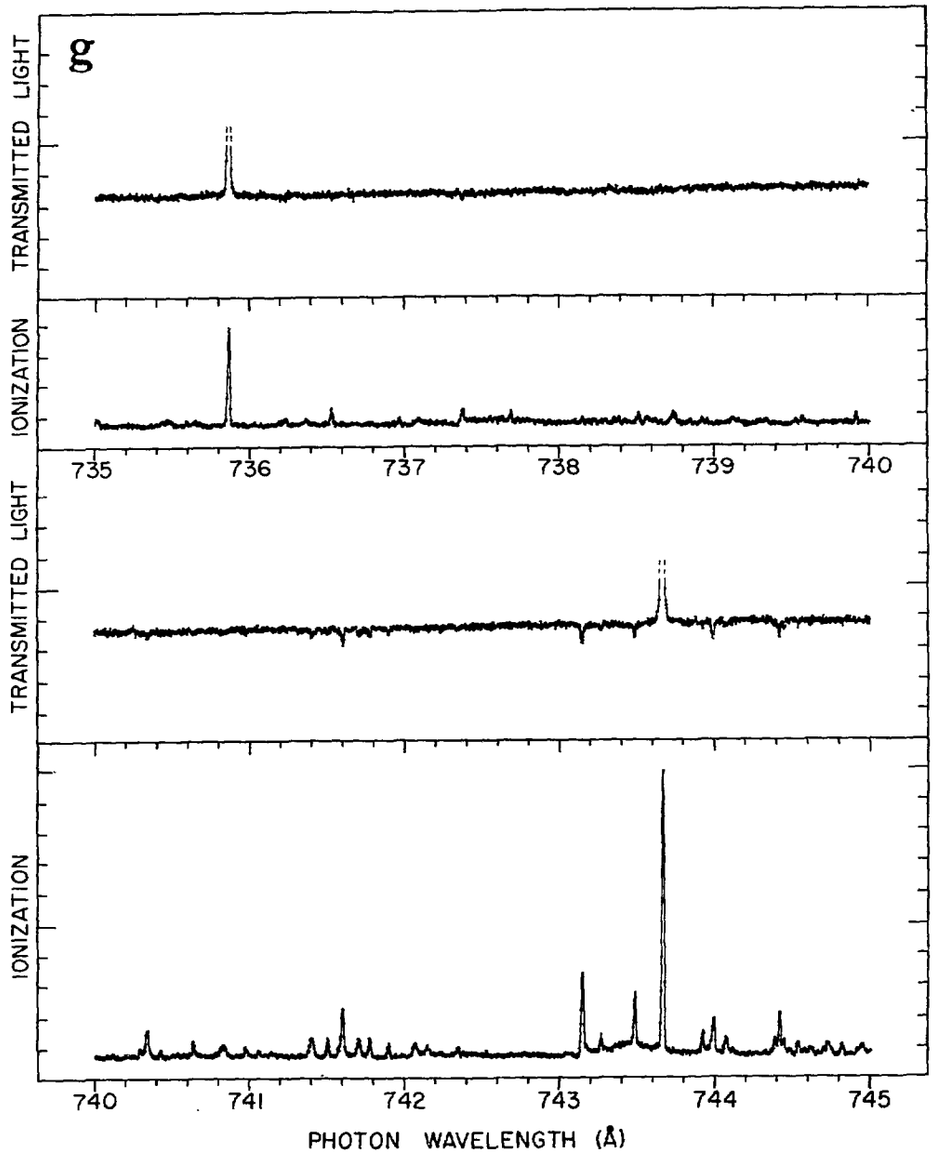

FIG. 2.--continued.

References

1. A. Monfils, J. Mol. Spectrosc. 15, 265 (1965).
2. A. Monfils, J. Mol. Spectrosc. 25, 513 (1968).
3. S. Takezawa and Y. Tanaka, J. Chem. Phys. 56, 6125 (1972).
4. S. Takezawa and Y. Tanaka, J. Mol. Spectrosc. 54, 379 (1975).
5. W. Kolos and J. Rychlewski, J. Mol. Spectrosc. 66, 428 (1977).
6. P. M. Dehmer and W. A. Chupka, J. Chem. Phys. 65, 2243 (1976).
7. W. A. Chupka, P. M. Dehmer, and W. T. Jivery, J. Chem. Phys. 63, 3929 (1975).

PREDISSOCIATION OF THE $3p\pi\ D\ ^1\Pi_u^+$ STATE IN H_2, HD, AND D_2 *

P. M. Dehmer and W. A. Chupka†

Introduction

We have recently completed a study of the predissociation linewidths and lineshapes of selected vibrational levels of the $3p\pi\ D\ ^1\Pi_u^+$ state of H_2, HD, and D_2 which lie above the ionization potential, and we report new results for the isotopic species HD and D_2. In addition, we report linewidths for rotational levels of the $B''\bar{B}\ ^1\Sigma_u^+$, v = 7, 8, and 9 vibrational levels in H_2 which lie very close to the $D\ ^1\Pi_u$, v = 9, 10, and 11 vibrational levels, respectively, and we discuss the possible consequences on the predissociation linewidths of a mixing of these electronic states.

Experimental

The relative photoabsorption and photoionization cross sections for H_2, HD, and D_2 were determined in the wavelength region between the ionization threshold and approximately 730 Å at a wavelength resolution of 0.016 Å and at a temperature of 78°K. The apparatus has been described in detail previously.[1] Since the spectra were taken at only a single pressure, some of the rotational lines of the D state (usually those originating in J" = 0) are very strongly absorbed and are not suitable for quantitative studies since saturation distorts the shape. Hence, the present analysis is limited to lines originating in J" = 1 or 2 which have values of $(I_o - I)/I_o$ of about 0.15, where I_o and I are the incident and transmitted photon intensities, respectively. As in the case of H_2, no ionization is observed corresponding to any D state absorption in HD or D_2, indicating practically complete predissociation of this state. The entire spectra of photoabsorption and photoionization for H_2 were published previously;[2] however, no quantitative analysis of linewidths in absorption was

---

* Summary of a paper published in Chem. Phys. Lett. 70, 127 (1980).

† Department of Chemistry, Yale University, New Haven, Connecticut 06520.

made at that time. The complete spectra for HD and D_2 will be published in the near future. The measured linewidths Γ for H_2, HD, and D_2 are given in Table 1.

Table 1. Linewidths of $3p\pi$ D $^1\Pi_u^+$ in H_2, HD, and D_2.

	Assignment	J	Γ, cm^{-1}	Γ, cm^{-1} (Ref. 3)
H_2	v = 7, R(1)[a]	2	11.3 ± 1.5	11.0 ± 1.0
	v = 8, R(1)[a]	2	12.3 ± 1.5	10.2 ± 0.2
	v = 9, R(1)	2	9.4 ± 1.0	9.0 ± 0.6
HD	v = 7, R(1)[a]	2	6.9 ± 0.7	
	v = 9, R(1)	2	6.9 ± 1.0	
D_2	v = 9, R(1)	2	3.9 ± 1.0	
	v = 9, R(1)	3	7.7 ± 1.5	
	v = 10, R(1)	2	3.9 ± 1.0	
	v = 12, R(1)	2	3.9 ± 1.0	

[a]Overlapped by one or more lines.

Results and Discussion

The present data for H_2 are in substantial agreement with those of Glass-Maujean et al.[3] for v = 7, 8, and 9; however, we were not able to confirm the small upturn in the linewidth for v = 10 and 11 because of poor statistics in this wavelength region. As in the case of H_2, the D_2 data show that the calculations of Fiquet-Fayard and Gallais[4] using an RKR potential for the B' state greatly overestimate the drop in linewidth as a function of vibrational quantum number. The B' potential of Julienne[5] was a considerable improvement as a result of its increased accuracy in the repulsive wall region. The next step in the calculations would be to use the recent Born-Oppenheimer potentials of Kolos and

co-workers,[6,7] corrected for the effects of nuclear motion (adiabatic corrections) and for the interaction with other electronic states (non-adiabatic corrections).[8,9] Jungen and Atabek[10] have shown that multichannel quantum defect theory (MQDT) obviates the need to calculate these corrections explicitly, and Jungen and Dill[11] recently extended MQDT to include the effects of rotational and vibrational autoionization and obtained excellent agreement with our H_2 photoionization data. The further extension of MQDT to include the effects of predissociation is now of great interest, especially with the possibility of an additional predissociation pathway through interaction with the $B''\bar{B}\,{}^1\Sigma_u^+$ state at large internuclear distances.

The $B''\bar{B}$ state is itself effectively predissociated by the B' state through a homogeneous interaction. Very little autoionization is observed corresponding to the $B''\bar{B}$ absorption in H_2, HD, and D_2, indicating that predissociation is at least 1 to 2 orders of magnitude faster than autoionization.[2,13] We felt that a comparison of the linewidths of the D state and the $B''\bar{B}$ state near the region of the curve crossing might offer some insight into the consequences of an interaction between these two states. The present resolution of 0.016 Å (which corresponds to 2.5 cm^{-1} at 800 Å) easily allows determination of linewidths as small as 3 to 4 cm^{-1}, and is sufficient to observe broadening of the J = 1 and 2 rotational levels of the $B''\bar{B}$, v = 7, 8, and 9 vibrational levels, which lie close to the D, v = 9, 10, and 11 vibrational levels, respectively. Figure 1 shows the spectra of ionization and transmitted light in the region of the D, v = 9 and $B''\bar{B}$, v = 7 states. The latter assignments are based on the recent MQDT calculations of Jungen and Atabek.[10] The widths of the J = 1 and 2 levels of the $B''\bar{B}$, v = 7 state (which correspond to the upper levels of the R(0) and R(1) transitions, respectively) are nearly identical, which is consistent with a homogeneous perturbation,[14] and are equal to approximately 4 cm^{-1}. The width of the J = 2 level of the D, v = 9 state is 9.0 to 9.4 cm^{-1} (see Table 1); however, it is not possible to determine the corresponding width of the J = 1 level from the present data because of interference from an overlapping absorption line as well as from an emission line in the He continuum light source. We may estimate the linewidth to be about 3 cm^{-1} from the pure precession model, which

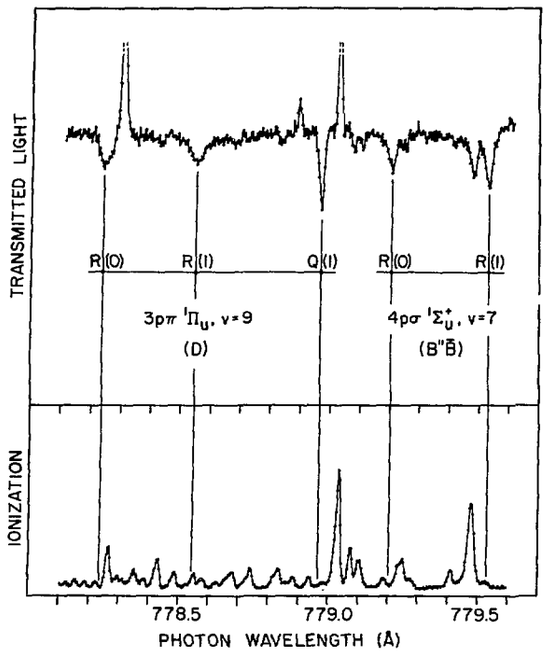

FIG. 1.--Spectra of transmitted light and ionization for ordinary H_2 (the ortho-para equilibrium mixture) at 78°K taken at a wavelength resolution of 0.016 Å. The Q(1) transition of the $D\ ^1\Pi_u,\ v' = 9 \leftarrow X\ ^1\Sigma^+_g,\ v'' = 0$ band is an example of the instrumental resolution.

predicts that the width should scale as $J(J + 1)$. Thus, the widths and the resulting predissociation rates k (where $k = 2\pi c\Gamma$) are nearly equal for the $J = 1$ level of the D, $v = 9$ and $B''\bar{B}$, $v = 7$ states, and as a consequence, a small admixture of the $B''\bar{B}$, $v = 7$ state in the D, $v = 9$ state wave function is not expected to have much effect on the predissociation rate of the latter state. A similar mixing of the states for the $J = 2$ levels could actually reduce the predissociation rate of the D, $v = 9$ state, since the $B''\bar{B}$, $v = 7$ state linewidth is only about one half that of the D, $v = 9$ state. The relative predissociation rates of the D and $B''\bar{B}$ states would have to be reversed at the point of the curve crossing in order for this mechanism to explain the upturn in the linewidths for the $J = 2$ levels of the D state observed by Glass-Maujean et al.; however, the present data do not support this reversal. We observe the R(0) transitions for the $B''\bar{B}$, $v = 8$ and 9 vibrational levels at 772.57 Å and 766.48 Å, respectively.[15] (The $B''\bar{B}$, $v = 9$ R(0) level was originally assigned $8p\sigma$, $v = 4$ R(0), Ref. 16, but has been reassigned on the basis of more recent MQDT calculations.) In both cases the $J = 1$ linewidth is approximately equal to that

observed for the v = 7 vibrational level. The J = 2 levels are either not observed or are badly overlapped with another state; however, they should have the same linewidth as the J = 1 levels, since the presidssociation is homogeneous.

References

1. W. A. Chupka, P. M. Dehmer, and W. T. Jivery, J. Chem. Phys. 63, 3929 (1975).
2. P. M. Dehmer and W. A. Chupka, J. Chem. Phys. 65, 2243 (1976).
3. M. Glass-Mujean, J. Breton, and P. M. Guyon, Chem. Phys. Lett. 63, 591 (1979).
4. F. Fiquet-Fayard and O. Gallais, Mol. Phys. 20, 527 (1971).
5. P. S. Julienne, J. Mol. Spectrosc. 48, 508 (1973).
6. W. Kolos and J. Rychlewski, J. Mol. Spectrosc. 62, 109 (1976).
7. W. Kolos, J. Mol. Spectrosc. 62, 428 (1976).
8. W. Kolos, Adv. Quantum Chem. 5, 99 (1970).
9. W. Kolos and L. Wolniewicz, J. Chem. Phys. 48, 3672 (1968).
10. Ch. Jungen and O. Atabek, J. Chem. Phys. 66, 5584 (1977).
11. Ch. Jungen and D. Dill, J. Chem. Phys., in press.
12. D. Dill and Ch. Jungen, J. Phys. Chem., in press.
13. P. M. Dehmer and W. A. Chupka, unpublished.
14. G. Herzberg, Spectra of Diatomic Molecules, Van Nostrand, New York, p. 288 (1950).
15. Ch. Jungen, private communication.
16. G. Herzberg and Ch. Jungen, J. Mol. Spectrosc. 41, 425 (1971).

OSCILLATOR-STRENGTH DISTRIBUTIONS FOR OXYGEN, CARBON DIOXIDE, WATER, METHYL CHLORIDE, AND CARBON TETRACHLORIDE

James C. Person and Paul P. Nicole

New measurements of photoabsorption give oscillator-strength values for the following gases and energy regions: O_2, 7.34 to 11.79 eV; CO_2, 7.34 to 11.77 eV; H_2O, 6.62 to 11.80 eV; CH_3CL,[2] 6.14 to 11.25 eV; and CCl_4, 6.14 to 11.49 eV. Comparisons are made with some values from the literature.

As part of a program to determine accurate oscillator-strength distributions we are measuring the absorption cross section σ over a wide range of photon energy E. We recently improved our apparatus for measuring σ at low energies,[1] and we have used the apparatus for measurements in the energy range from 5 to 11.8 eV for a number of cases. We are now in the process of improving the computer programs that process the data so as to incorporate additional corrections. This report presents preliminary data on oxygen, carbon dioxide, water vapor, methyl chloride, and carbon tetrachloride; our data are compared with representative data from the literature.

The apparatus has been described previously;[1] it consists of a hydrogen lamp, a McPherson Model 225 monochromator, an absorption cell with LiF windows and a split-beam detector system. Unless stated otherwise, the data were taken using a bandpass of 0.09 nm (FWHM). Gas pressures were measured with capacitive manometers manufactured by MKS Instruments: a Baratron Type 77H-1 was used for pressures below 1.1 torr, and a new Baratron Type 310 BH-1000 was used at higher pressures. The split-beam system uses photomultiplier detectors, and σ is determined from the transmitted light flux F_T and the incident light flux F_I by the Beer-Lambert equation

$$\sigma = \ln[F_{T0}/F_{I0})/(F_{Tn}/F_{In})]/(nL) \quad ,$$

where L is the cell length (8.486 cm), and the subscripts 0 and n refer to measurements with the cell empty and with a gas density of n, respectively. The differential oscillator strength, df/dE, in units of (1/eV) is then found by multiplying the σ values (in Mb units) by 0.0091116.

The df/dE values we present in this report are representative of a larger mass of recent data, and we are still developing the computer programs to apply corrections. The data presented here are not in final form in respect to energy scale corrections, corrections for thermal transpiration, and corrections for the effects of light that make three passes through the cell by being reflected at the windows. In addition, the scattered-light corrections are preliminary, the pressure gauges have not been calibrated, and the gas purity has not been independently verified. Also, we have not yet averaged σ values taken at different gas densities, or even verified that the Beer-Lambert equation is justified. The data are presented from scans at only two or three different gas densities, and the range of gas densities may not be large enough to provide accurate values in the peaks and valleys of the absorption spectra.

Figure 1 shows a comparison of our new data for oxygen with the relative df/dE values derived from the electron energy-loss (EEL) experiments of Huebner et al.[2] The EEL values were renormalized by multiplication by 1.02, and the fit of the Schumann-Runge continuum in the 7 to 9 eV region is remarkably close.

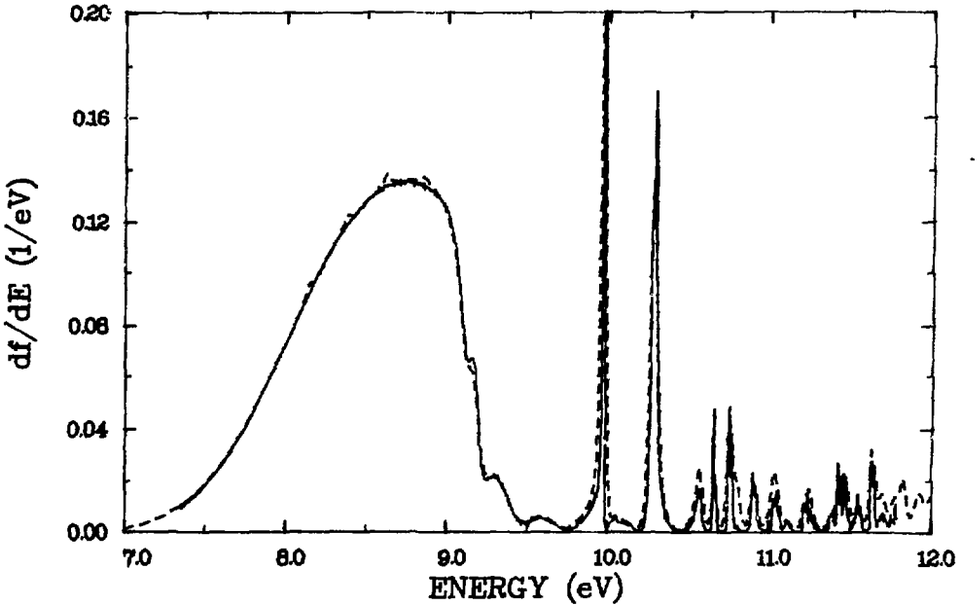

FIG. 1.--Oscillator-strength distribution for oxygen. The broken line shows data from Ref. 2 after multiplication by 1.02.

The four small peaks that are superimposed on the continuum in the EEL data at 8.14, 8.37, 8.61, and 8.84 eV are not present in our results; this indicates that these peaks result from optically-forbidden transitions, which is consistent with their assignment as the v = 0 to 3 of the $(3s\sigma_g)^3\Pi_g$ Rydberg state.[2,3] The shape of the continuum is a matter of some dispute, and the region between 8.7 and 9.0 eV is smoother in our data than in the optical data given by Watanabe,[4] or the EEL data of Geiger and Schröder.[5] Cartwright et al.[6] have discussed how the continuum is composed of several overlapping transitions, and Figure 1 shows that the shoulder near 9.15 eV shows a different behavior in the EEL data. Thus, the transition responsible for this shoulder has a shape for the generalized oscillator strength at low momentum transfer that is different from that of the $B^3\Sigma_u^-$ state responsible for the bulk of the absorption in the Schumann-Runge continuum. At energies above 9.8 eV we see more differences between our data and the EEL data. Our data in this region were taken with a bandpass of 0.044 nm, and this may not be narrow enough to avoid errors on sharp peaks, but many of the differences in relative peak areas between our data and the EEL data must be related to the different transitions having different shapes of the generalized oscillator strength at low momentum transfer.

In Figures 2 and 3 we compare our results for CO_2 with those reported by Nakata, Watanabe, and Matsunaga.[7] On the sharp peaks and valleys shown in Figure 2, our bandpass of 0.09 nm is not narrow enough to avoid errors, but our data in Figure 3, taken with a resolution of 0.044 nm, closely match the data of Nakata et al.,[7] which were taken with an even narrower bandpass. Some of the discrepancies in the match of the energy scale between our data and those of Nakata et al. are the result of small errors in our new device for deplotting, the Bit Pad, manufactured by Summagraphics Corporation. Most of the points have a position error of 0.05 cm or less in comparison with the original figures, and this corresponds to a wavelength error of about 0.05 nm (or any energy error of 0.002 to 0.006 eV) and an error of about 3% in df/dE (the original data[7] are on semi-log plots). We do find two peaks at 11.53 and 11.55 eV, where Nakata et al.[7] report one broad peak at 11.53 eV.

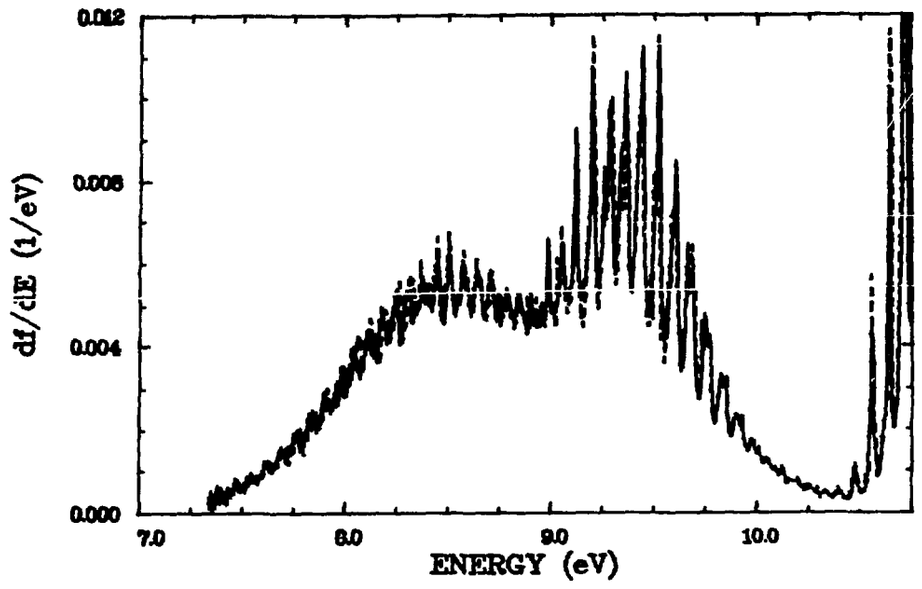

FIG. 2.--Oscillator-strength distribution for carbon dioxide at low energies The broken line shows data from Ref. 7.

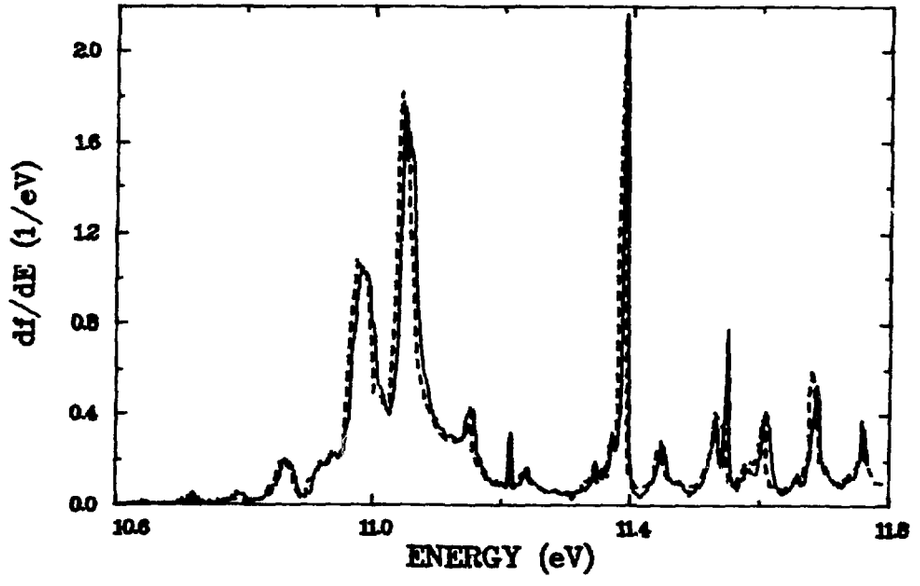

FIG. 3.--Oscillator-strength distribution for CO_2 at higher energies. The broken line shows data from Ref. 7.

We do not find such good agreement on the magnitude of df/dE with the data of Watanabe, Zelikoff, and Inn[8] for the case of water vapor. Figure 4 shows that our data are consistently higher, especially for the data below 9.9 eV; at higher energies the valleys agree fairly well, but our peaks are higher. Also, we see a peak at 11.29 eV that is not in the data of Watanabe et al.;[8] however, this peak is present in the data of Gürtler, Saile, and Koch[9] and Wang et al.[10] Figure 5 shows the better agreement with the data of Laufer and McNesby,[11] although their bandpass of 0.66 nm (0.03-0.05 eV) prevented them from resolving the structure of the 9.7 eV band, and it may have caused some error in their df/dE values for this band. Our bandpass of 0.09 nm may not be sufficiently narrow to avoid errors on the sharp features above 10 eV, but our peak values agree fairly well with the high resolution data of Gürtler, Saile and Koch.[9] This well-resolved spectrum[9] was obtained using synchrotron light as a source. As shown in Figure 5, their data show greater absorption in the valleys than do ours. Figure 6 shows a comparison of their data at higher energies with our earlier data,[12] and here their data are lower than ours. The wide energy range of the synchrotron light source makes it possible that second-order light is present in the output of their monochromator, and this could make their df/dE values low in the high-absorption region of 13 to 21 eV, and it would make their values high for the low-absorption valleys in the 10 to 12 eV region. Figure 7 shows a combination of old and new data, and a comparison with the EEL data obtained at the National Bureau of Standards.[13] For this comparison, the EEL data are renormalized by multiplication by 1.10 in order to give a better fit at lower energies. The comparison does not agree as well as for other gases;[1,2,12] the EEL data apparently have a background that increases as the energy increases.

We have also taken data for the molecules in the choromethane series, and Figures 8 and 9 show two examples. Figure 8 shows a comparison of our data for methyl chloride with that of Raymonda, Edwards, and Russell,[14] which we deplotted using the Bit Pad. Our bandpass may be too wide, or the gas density too high, to avoid errors in the region of sharp structure, and Raymonda et al. find higher peak values. Otherwise, there is good agreement except for three regions: (a) we find the intensity of the 7.76 eV peak larger; (b) Raymonda

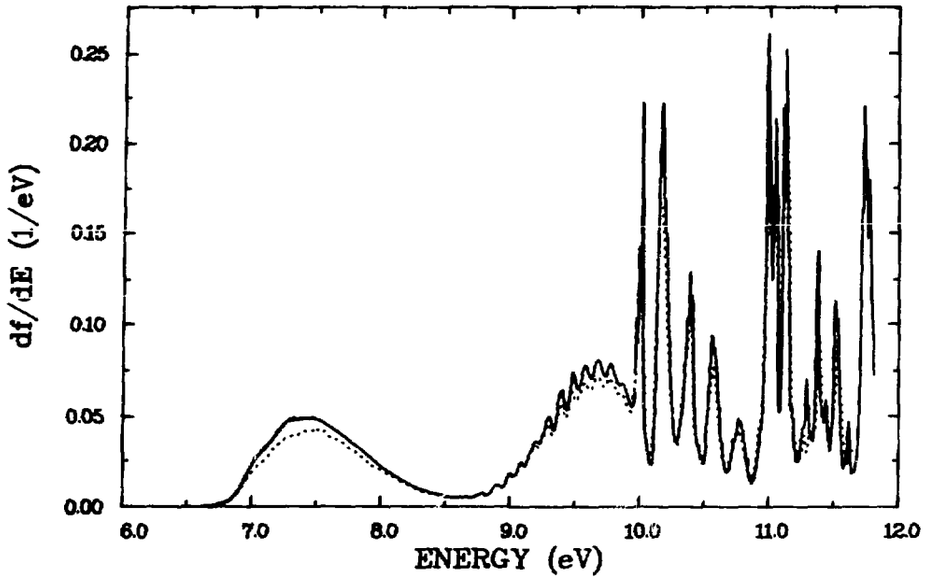

FIG. 4.--Oscillator-strength distribution for water at low energies. The dotted line shows data from Ref. 8.

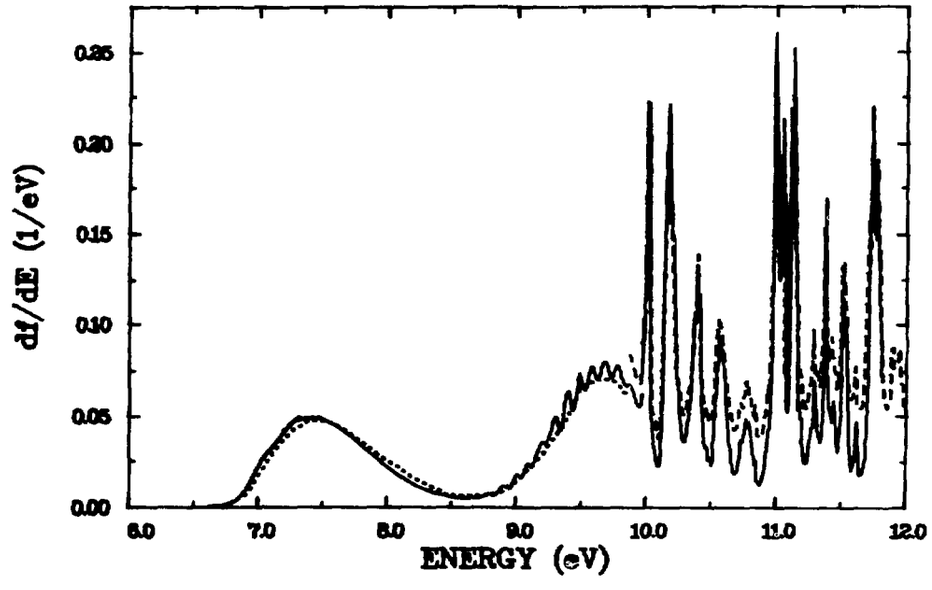

FIG. 5.--Oscillator-strength distribution for water at low energies. The dashed line above 10 eV shows data from Ref. 9, and the dotted line below 10 eV shows data from Ref. 11.

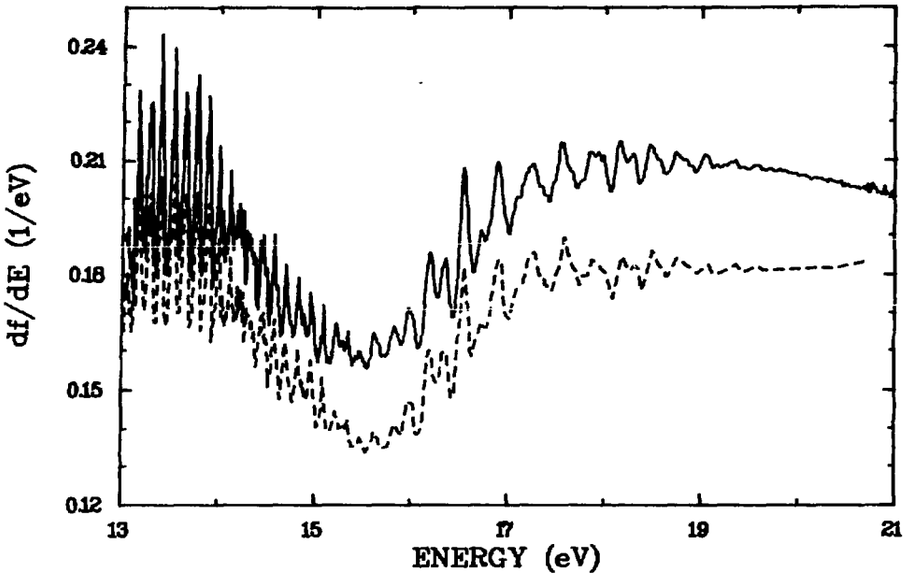

FIG. 6.--Oscillator-strength distribution for water at high energies. The solid line shows our old data (Ref. 12) and the broken line shows data from Ref. 9.

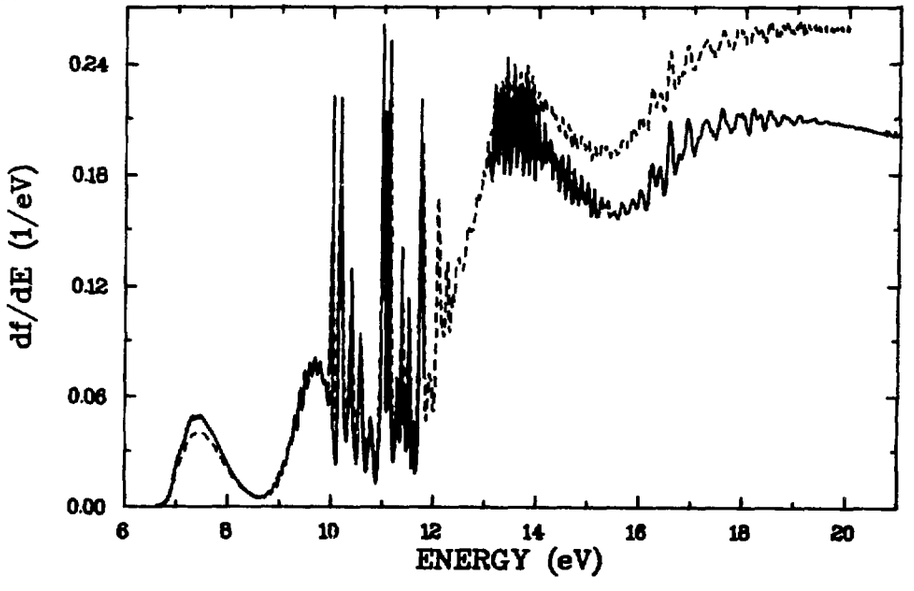

FIG. 7.--Oscillator-strength distribution for water. The solid line shows our present data below 12 eV and our earlier data (Ref. 12) above 13 eV. The broken line shows the EEL data from Ref. 13 after multiplication by 1.1.

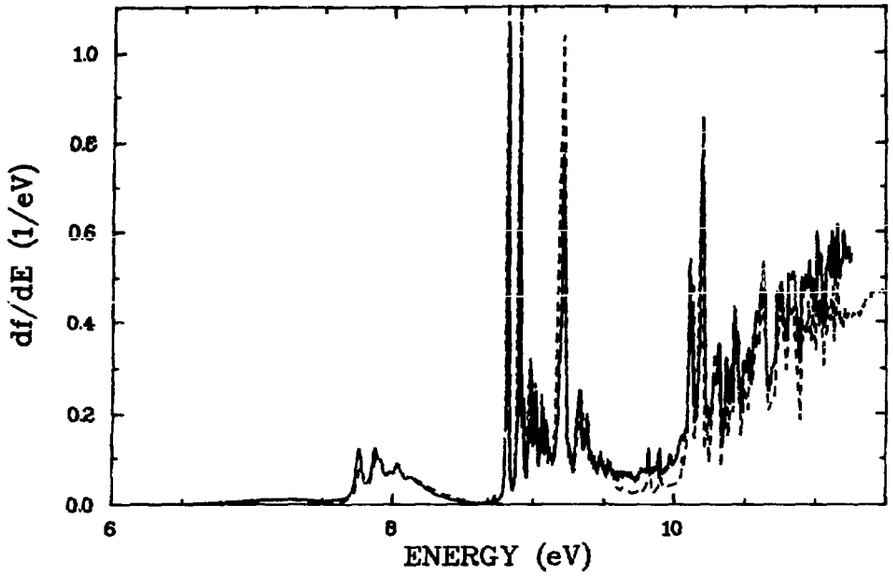

FIG. 8.--Oscillator-strength distribution for methyl chloride. The broken line shows data from Ref. 14.

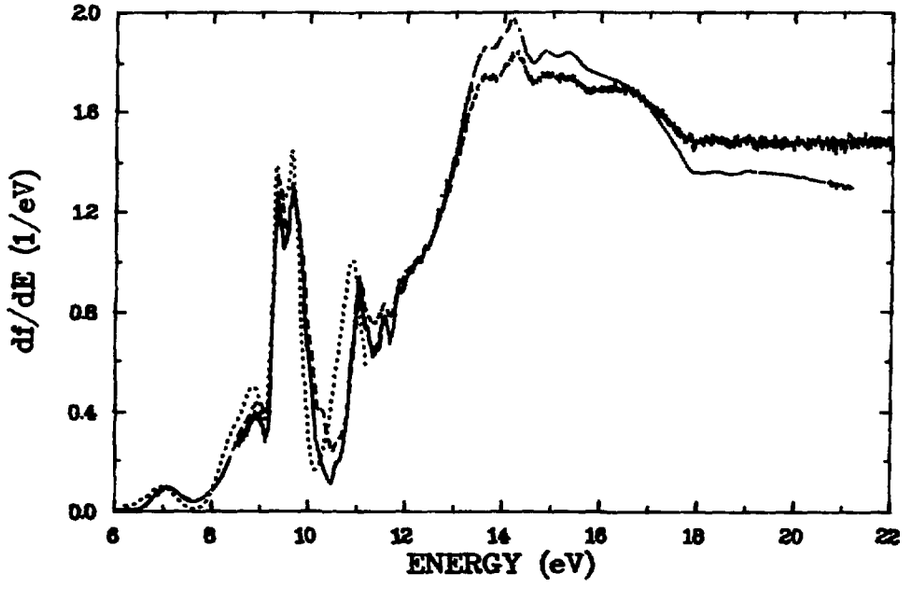

FIG. 9.--Oscillator-strength distribution for carbon tetrachloride. The solid line shows our present data below 11.5 eV and our earlier data (Ref. 12) at higher energies. The dotted line shows data from Ref. 15 and the broken line shows EEL data from Ref. 16. Our data are higher than the EEL data in the 13 to 16 eV region, and lower for E > 17 eV.

et al. find lower absorption in a region around 9 to 10 eV, and (c) our results are larger for energies above 11 eV. For the 7.76-eV peak and the 9- to 10-eV region, we agree better with the data reported earlier by the same group,[15] but the overall agreement is much better with the later data.[14] In Figure 9, we show a comparison of our present data for E < 11.49 eV and our earlier data at higher energies[12] with the data of Russell, Edwards, and Raymonda[15] for carbon tetrachloride and with EEL data of Huebner, Celotta, and Mielczarek.[16] In this case, the agreement with the EEL data is within 15% over a wide range—indeed, the shape of the EEL data for E < 13 eV agrees better than do the other optical data. Part of the disagreement with the optical data may result from our errors in deplotting their data[15] from a wavelength axis, but a comparison of the data for methyl chloride in that paper[15] with their later data[14] suggests that the data in Ref. 15 are not corrected for a drifting baseline. Further comparisons will be made after we have completed corrections on our data.

References

1. J. C. Person and P. P. Nicole, Argonne National Laboratory Radiological and Environmental Research Division Annual Report, October 1977-September 1978, ANL-78-65, Part I, p. 30.
2. R. H. Huebner, R. J. Celotta, S. R. Mielczarek, and C. E. Kuyatt, J. Chem. Phys. 63, 241 (1975).
3. D. C. Cartwright, W. J. Hunt, W. Williams, S. Trajmar, and W. A. Goddard, III, Phys. Rev. A 69, 2436 (1973).
4. K. Watanabe, Adv. Geophys. 5, 153 (1958).
5. J. Geiger and B. Schröder, J. Chem. Phys. 49, 740 (1968).
6. D. C. Cartwright, N. A. Fiamengo, W. Williams, and S. Trajmar, J. Phys. B: Atom. Molec. Phys. 9, L419 (1976).
7. R. S. Nakata, K. Watanabe, and F. M. Matsunaga, Sci. Light (Tokyo) 14, 54 (1965).
8. K. Watanabe, M. Zelikoff, and E.C.Y. Inn, Air Force Cambridge Research Center, Tech. Report No. 52-23, p. 75 (1953)
9. P. Gürtler, V. Saile, and E. E. Koch, Chem. Phys. Lett. 51, 386 (1977).
10. H.-t. Wang, W. S. Felps, and S. P. McGlynn, J. Chem. Phys. 67, 2614 (1977).
11. A. H. Laufer and J. R. McNesby, Can. J. Chem. 43, 3487 (1965).
12. J. C. Person, D. E. Fowler, and P. P. Nicole, Argonne National Laboratory Radiological and Environmental Research Division Annual Report, July 1974-June 1975, ANL-75-60, Part I, p. 26.
13. J. C. Person, R. H. Huebner, R. J. Celotta, and S. R. Mielczarek, Proc. Xth Int. Conf. on Physics of Electronic and Atomic Collisions, Paris,

Commissariat a l'Energie Atomique, Abstracts, p. 1214 (1977); Argonne National Laboratory Radiological and Environmental Research Division Annual Report, October 1976-September 1977, ANL-77-65, Part I, p. 16.
14. J. W. Raymonda, L. O. Edwards, and B. R. Russell, J. Am. Chem. Soc. 96, 1708 (1974).
15. B. R. Russell, L. O. Edwards, and J. W. Raymonda, J. Am. Chem. Soc. 95, 2129 (1973).
16. R. H. Huebner, R. J. Celotta, and S. R. Mielczarek, Argonne National Laboratory Radiological and Environmental Research Division Annual Report, July 1975-September 1976, ANL-76-88, Part I, p. 1.

SELF-CONSISTENCY AND SUM-RULE TESTS IN THE KRAMERS-KRONIG ANALYSIS OF OPTICAL DATA: APPLICATIONS TO ALUMINUM*

E. Shiles,† Taizo Sasaki,‡ Mitio Inokuti, and D. Y. Smith**

An iterative, self-consistent procedure for the Kramers-Kronig analysis of data from reflectance, ellipsometric, transmission, and electron energy-loss measurements is presented. This procedure has been developed for practical dispersion analysis since experimentally no single optical function can be readily measured over the entire range of frequencies as required by the Kramers-Kronig relations. The present technique is applied to metallic aluminum as an example. The results are then examined for internal consistency and for systematic errors by various optical sum rules. The latter provide tests of agreement with both theoretical constraints and independently measured properties such as electron density, dc conductivity and stopping power. The present procedure affords a systematic means of preparing a self-consistent set of optical functions, provided some optical or energy-loss data are available in all important spectral regions. The analysis of aluminum discloses that currently available data exhibit an excess oscillator strength, apparently in the vicinity of the L edge. A possible explanation is a systematic experimental error in the absorption-coefficient measurements resulting from surface layers—oxides present in thin-film transmission samples. A revised set of optical functions has been prepared by an ad hoc reduction of the reported absorption coefficient above the L edge by 14%. These revised data lead to a total oscillator strength consistent with the known electron density and are in agreement with dc conductivity and stopping-power measurements, as well as with absorption coefficients inferred from the cross sections of neighboring elements in the periodic table. The optical functions

---

* Abstract of a paper to appear in Phys. Rev. B.

† Solid State Science Division, ANL. Present address: IIT Research Institute, Annapolis, Maryland 21402.

‡ College of General Education, University of Tokyo, Tokyo 153, Japan.

** Solid State Science Division, ANL.

resulting from this study provide evidence for both the redistribution of oscillator strength between energy levels and the effects on real transitions of the shielding of conduction electrons by virtual processes in the core states.

AN ANGLE RESOLVED PHOTOELECTRON SPECTROMETER FOR STUDIES OF ATOMS AND MOLECULES USING SYNCHROTRON RADIATION*

A. C. Parr,† R. Stockbauer,† B. E. Cole,† D. L. Ederer,† J. L. Dehmer, and J. B. West‡

The rapid growth in the field of photoelectron spectroscopy over the past few years means that this has become a standard technique, used in studies of, for example, band structure in solids, molecular structure determinations and electron correlation effects in atoms and molecules. Now that synchrotron radiation has become more generally available, with the possibility of a continuous photon energy range and a polarized source, variable wavelength photoelectron angular and energy distribution measurements are also possible, adding a wealth of information in the fields above. Compared with a line source such as the He I resonance lamp, however, the intensity available at the exit slit of a monochromator mounted on a synchrotron radiation source has generally been one to two orders of magnitude lower. This deficiency has resulted in low resolution spectra in general, usually adequate for atomic and solid state experiments, but generally inadequate for molecular spectroscopy. The new high flux normal incidence monochromator installed at the NBS Synchrotron Storage Ring, SURF II, has sufficient intensity and resolution to permit vibrationally resolved molecular spectra to be taken. The effects of autoionization and other resonances in the ionization continuum of molecules on the vibrational intensity distributions within the electronic bands can be studied. We describe here an electron spectrometer designed specifically for the SURF II monochromator,[1] permitting measurements of both photoelectron angular distributions and partial cross sections to be made in the photon energy range 5 to 35 eV.

---

*Summary of an article to appear in Nucl. Instrum. Methods.

†National Measurement Laboratory, National Bureau of Standards, Washington, D.C. 20234.

‡Daresbury Laboratory, Science Research Council, Daresbury, Warrington WA4 4AD, England.

The basis of the photoelectron spectrometer is two copper hemispheres of 5 cm mean radius, with variable focal length lenses focussing the electron source onto a virtual entrance slit and onto the channeltron detector after energy analysis. This analyzer has been described fully elsewhere.[2] Figure 1 shows the layout of the spectrometer in its vacuum chamber, which is shielded from external magnetic fields by two layers of annealed μ-metal near the chamber walls inside the vacuum. The spectrometer rotates about an axis in the plane of Figure 1 coincident with the light beam direction, and is driven externally by a stepping motor. A 2 mm capillary tubing light guide is used to channel the photons leaving the exit slit of the monochromator into the interaction zone. Prior measurements indicated that there were negligible losses in photon intensity by using this device and thus the geometric loss involved in having the interaction region of the electron spectrometer some distance from the exit slit of the monochromator was avoided. The capillary was also found to have a negligible effect on the polarization of the light leaving the monochromator.

The use of a 1000 ℓ/s closed cycle helium cryopump permitted a high density gas jet in the interaction region, while still maintaining a vacuum of 2×10^{-4} torr in the chamber. All materials inside the chamber were compatible with a clean vacuum, and a base pressure of 2×10^{-8} torr was routinely obtained without bakeout.

The polarization of the incoming light was measured by a three-mirror polarizer similar in principle and reflection angles to the device described by Horton et al.[3] In the wavelength region of interest here, it has a rejection ratio of approximation 20:1 against the component perpendicular to the reflecting surface and is used as a polarization analyzer. This analyzer is shown in Figure 1 and rotates with the electron spectrometer. A tungsten grid was placed at its entrance to monitor the incoming photon flux. A tungsten plate was placed at its exit to monitor the beam after the three reflections. The gold coatings on the mirrors were connected to a +45 V battery to provide bias for the tungsten diodes. The resulting currents were measured by vibrating reed electrometers.

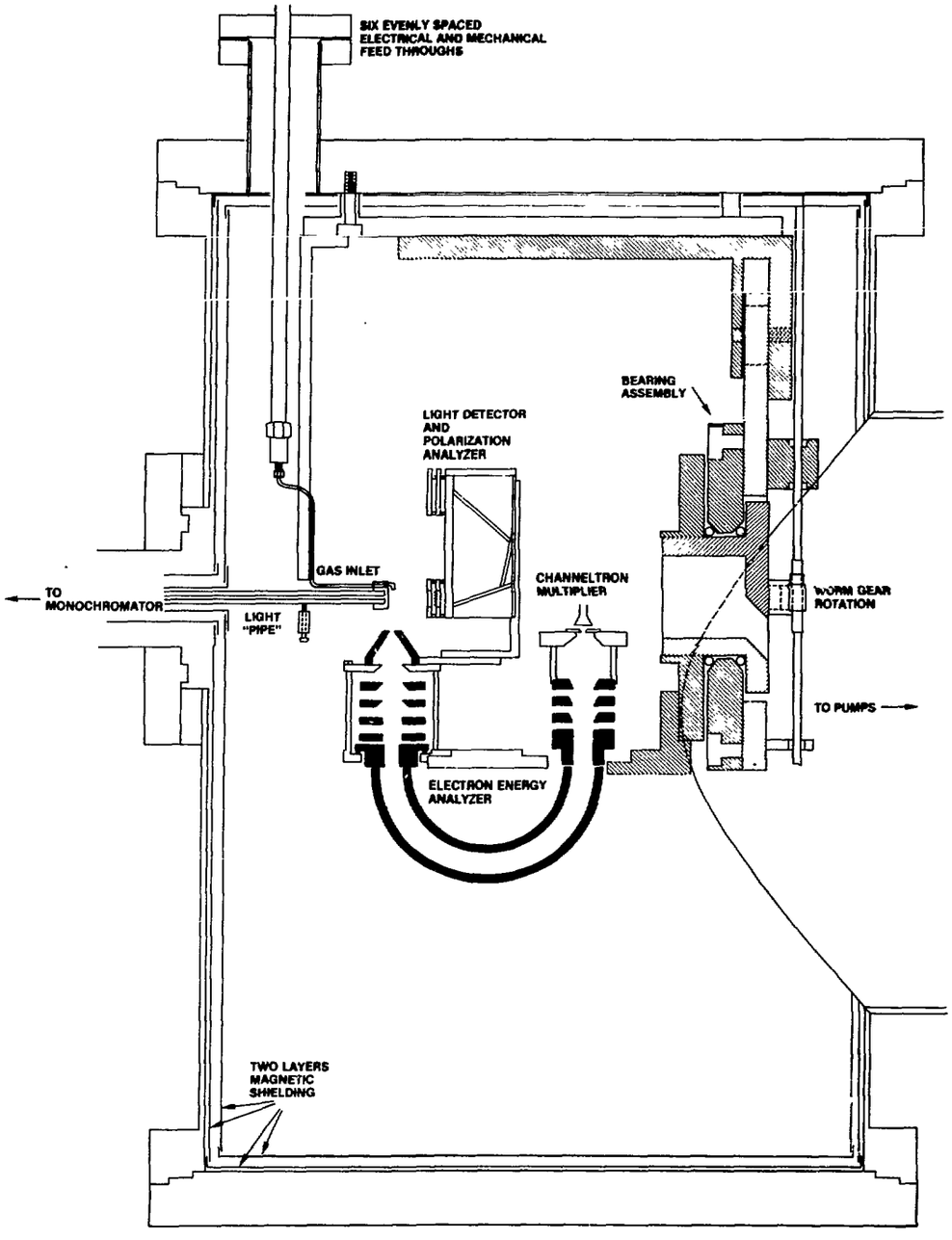

FIG. 1.--Cross section drawing of electron energy analyzer and associated mechanical components situated in the vacuum chamber. The main chamber has an inside diameter of 34.3 cm and a height of 51.5 cm. For clarity of presentation, not all the details of the devices are shown in this diagram.

The experiment runs under computer control and is based on a CAMAC system interfaced with an LSI-11 computer stationed in the CAMAC crate. The computer drives the monochromator to the desired wavelength, then sets the electron analyzer angle with respect to the E vector of the incident radiation. The user chooses these initial parameters, as well as setting the voltage range over which the electron spectrometer will scan. The electron pass energy through the analyzer is kept constant, and the voltage ramp is superimposed on a preset retarding potential, thereby maintaining constant energy resolution. A second channel on the ramp generator (CAMAC power supply controller) is used to control the focus potential on the entrance lens of the analyzer, which has to be varied with incident electron kinetic energy. The computer program scans the electron spectrometer repetitively over the voltage range selected by the user, adding each scan to the previous one until a given maximum electron count in any one voltage channel is reached. The data are then stored on a floppy disc drive and plotted on an X-Y plotter; the analyzer is moved to the next angular position and the scanning cycle repeated. The multiple scan technique avoids the effects of long-term drifts in gas jet pressure, channeltron gain, etc. The electron counts are referenced to the photon flux at each voltage using the tungsten mesh photodiode. Through the voltage-frequency converter this signal is fed to the input of one of the scaler channels, which inhibits the counting process after a preset count is reached. The data ramp voltage, electron count, photon intensity count, polarization analyzer reflected count, and time are then stored and the spectrometer repositioned at the next angle. Typically each voltage scan would take between 1 and 5 min, the total number of scans depending on sample cross section and photon intensity. The system also provides facilities via a CAMAC module to interrupt the program in a controlled way, giving the user a choice of continuing the present run, terminating it and storing the data, or abandoning the present run.

References

1. D. L. Ederer, B. E. Cole, and J. B. West, Nucl. Instrum. Methods, to be published.
2. J. L. Dehmer and D. Dill, Phys. Rev. A 18, 184 (1978).
3. V. G. Horton, E. T. Arakawa, R. N. Hamm, and M.W. Williams, Appl. Opt. 8, 667 (1969).

WAVELENGTH AND VIBRATIONAL-STATE DEPENDENCE OF PHOTOELECTRON ANGULAR DISTRIBUTIONS. RESONANCE EFFECTS IN 5σ PHOTOIONIZATION OF CO*

B. E. Cole,† D. L. Ederer,† Roger Stockbauer,† Keith Codling,‡ Albert C. Parr,† J. B. West,** E. D. Poliakoff, and J. L. Dehmer

---

The dynamics of molecular photoionization have recently been shown[1] to vary rapidly with internuclear separation in the presence of a shape resonance. In a prototype calculation[1] on the $3\sigma_g$ photoionization channel of N_2, the σ_u resonance shifted by > 10 eV and exhibited large, asymmetric variations in intensity and width over a range in R spanning the ground vibrational state of N_2. This leads to a breakdown in the Franck-Condon (FC) separation and was predicted[1] to cause non-FC vibrational intensities and v-dependent photoelectron angular distributions. The effect of shape resonances on vibrational branching ratios has been confirmed experimentally in connection with the analogous f-wave-dominated σ resonances in the 5σ channel[2] of CO and the $3\sigma_g$ channel[3] of N_2. By contrast, the available data[4-9] on vibrationally-resolved photoelectron angular distributions in shape-resonant channels is too fragmentary to establish the pattern of the shape resonance effect. Here we report measurements of vibrationally-resolved photoelectron angular distributions for the 5σ channel in CO, performed in the range 16 eV $\leqq h\nu \leqq$ 26 eV utilizing synchrotron radiation, in order to establish the gross pattern of variation of the asymmetry parameter β in the vicinity of the σ shape resonance at $h\nu \sim 24$ eV.[10-15] As discussed below, unresolved autoionization structure, also capable of producing v-dependent β's is also observed and partially masks the expected shape-resonance effect. Although mainly a compilation in this particular study, detailed studies of resolved

---

* Summary of a paper to be published in J. Chem. Phys.

† National Measurement Laboratory, National Bureau of Standards, Washington, D.C. 20234.

‡ University of Reading, Reading RG6 2AF, England.

** Daresbury Laboratory, Science Research Council, Daresbury, Warrington WA4 4AD, England.

autoionization effects are of great importance and are being pursued separately.

The wavelength dependence of the β's for the first four vibrational levels of $CO^2 X^2\Sigma^+$ is given in Figure 1. We note that the v = 0 curve is rather flat and agrees, within combined stated errors, with the vibrationally-unresolved data of Marr et al.[16] and the multiple-scattering calculations of Wallace et al.[17] and that a systematic tendency to be slightly lower than the vibrationally-unresolved data[16] reflects the small admixture of the higher vibrational levels which were resolved in this work. Also note the good agreement with the He I data of Hancock and Samson[7] for v = 0 and 1. In interpreting the gross patterns in the data, we follow the discussion of the vibrational branching ratios in Ref. 2 by tentatively defining two spectral regions with different dominant effects. Below ∿ 21 eV, we presume the main vibrational effects are caused by unresolved autoionization structure and threshold effects associated with the $B\ ^2\Sigma^+$ state of CO^+ at 19.7 eV (although shape resonance effects are also likely to extend into this region). Above 21 eV, we assume[18] the structure is caused mainly by the shape resonance centered at ∿ 24 eV.[10-15] Focussing briefly on the "autoionization" region below ∿ 21 eV, we note that a broad dip occurs in β for each vibrational level, with a successively deeper minimum centered at ∿ 19 eV. Although this is similar to the structure in the "shape resonance" region discussed below, it is significantly different in that this gross structure comprises

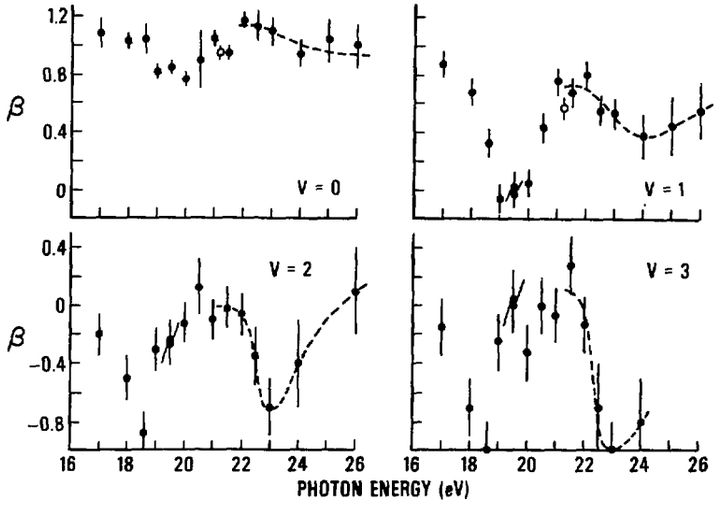

FIG. 1.--Photoelectron asymmetry parameters for the v =0-3 vibrational levels of $CO^+ X^2\Sigma^+$ in the range 16 eV ≤ hν ≤ 26 eV. The open circles are data by Hancock and Samson[7] using He I resonance radiation. The dashed lines are hand drawn to illustrate the discussion in the text.

unresolved series of autoionizing structures. Separate studies on a much finer energy mesh are being pursued to study details of individual autoionizing structures. Above $\sim$ 21 eV, we believe the present eata are the first to map the pattern of variation of v-dependent β's directly reflecting the effects of a shape resonance. The following pattern emerges, as illustrated by the hand-drawn dashed lines in Figure 1: First, the v = 0 curve is relatively flat at $\beta \sim 1$. The vibrationally unresolved data[16] (dominated by the v = 0 component) exhibit a broad, shallow dip at $\sim$ 28 to 30 eV, in agreement with theory.[17] Second, the v = 1 curve is substantially lower above 22 eV and exhibits a discernible minimum at $\sim$ 24 eV, the position of the shape resonance. Third, the v = 2 curve continues the pattern of a deeper dip (note the ordinate scale change on the lower part of Figure 1) centered at lower photon energy. Finally, the v = 3 curve, although of marginal statistical significatnce owing to the vanishingly small branching ratio, appears to indicate a deeper plunge. We emphasize that our interpretation of this pattern as a shape resonance effect is tentative, as we cannot definitely rule out influence by weak autoionization structure in this spectral range.[18] (As noted in Ref. 2, a number of autoionizing structures have been observed[18] throughout the 20 to 23 eV region; however, these are extremely weak, doubly-excited features and are assumed not to significantly interfere with the dominant one-electron character of the process discussed here.) However, the interpretation is plausible in view of related definitive work on vibrational branching ratios, particularly Refs. 1 and 3, and qualitative agreement of the present results with recent multiple-scattering model calculations[19] further supports this interpretation.

References

1. J. L. Dehmer, D. Dill, and S. Wallace, Phys. Rev. Lett. 43, 1005 (1979).
2. R. Stockbauer, B. E. Cole, D. L. Ederer, J. B. West, A. C. Parr, and J. L. Dehmer, Phys. Rev. Lett. 34, 757 (1979).
3. J. B. West, A. C. Parr, B. E. Cole, D. L. Ederer, R. Stockbauer, and J. L. Dehmer, J. Phys. B, in press.
4. T. A. Carlson and A. E. Jonas, J. Chem. Phys. 55, 4913 (1971).
5. T. A. Carlson, Chem. Phys. Lett. 9, 23 (1971).
6. R. Morgenstern, A. Niehaus, and M. W. Ruf, Proc. Seventh Int. Conf. on the Physics of Electronic and Atomic Collisions, Amsterdam, 26-30

July 1971, Abstracts of Papers, L. Branscomb et al., Eds., North-Holland Publ. Co., Amsterdam, p. 167 (1971).
7. W. H. Hancock and J.A.R. Samson, J. Electron Spectrosc. 9, 211 (1976).
8. D. M. Mintz and A. Kuppermann, J. Chem. Phys. 69, 3953 (1978).
9. R. M. Holmes and G. V. Marr, to be published.
10. J. W. Davenport, Phys. Rev. Lett. 36, 945 (1976).
11. A. Hammett, W. Stoll, and C. E. Brion, J. Electron Spectrosc. 8, 367 (1976).
12. J.A.R. Samson and J. L. Gardner, J. Electron Spectrosc. 8, 35 (1976).
13. E. W. Plummer, T. Gustafsson, W. Gudat, and D. E. Eastman, Phys. Rev. A 15, 2339 (1977).
14. N. Padial, G. Csanak, B. V. McKoy, P. W. Langhoff, J. Chem. Phys. 69, 2992 (1978).
15. R. S. Wallace, Ph.D. Thesis, Boston University (1979).
16. G. V. Marr, J. M. Morton, R. M. Holmes, and D. G. McCoy, J. Phys. B 12, 43 (1979).
17. S. Wallace, D. Dill, and J. L. Dehmer, J. Phys. B 12, L417 (1979).
18. K. Codling and A. W. Potts, J. Phys. B 7, 163 (1974) and references therein.
19. J. Stephens, D. Dill, and J. L. Dehmer, to be published.

MEASUREMENT OF THE EFFECTS OF SHAPE RESONANCES ON VIBRATIONAL INTENSITY DISTRIBUTION IN MOLECULAR PHOTOIONIZATION*

R. Stockbauer,† B. E. Cole,† D. L. Ederer,† J. B. West,‡ A. C. Parr,† and J. L. Dehmer

---

We report striking non-Franck-Condon vibrational intensity distributions associated with the shape resonance in the 5σ photoionization channel of CO. This example confirms the recent theoretical prediction[1] that shape resonances are very sensitive to internuclear separation, leading to different resonance energies and profiles, and non-Franck-Condon intensities in alternative

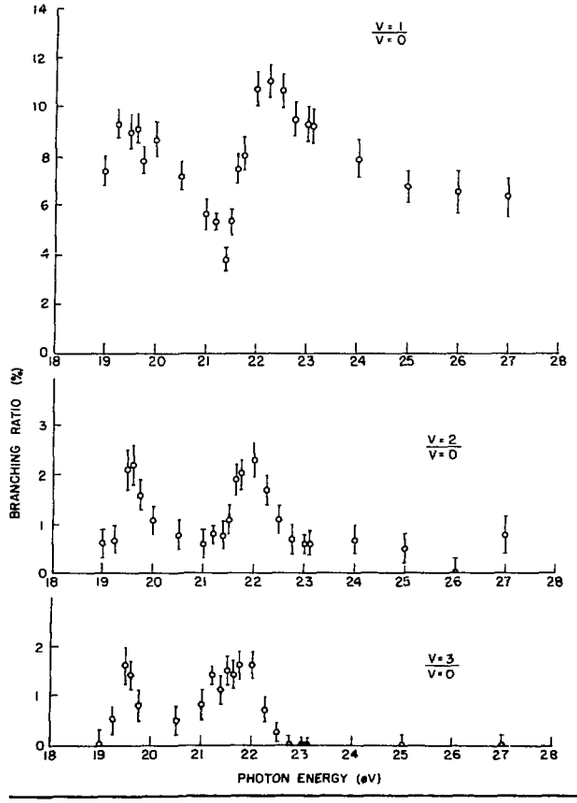

FIG. 1.--Photoionization branching ratios for the v = 0-3levels of $CO^+ X^2\Sigma^+$.

---

*Summary of a paper appearing in Phys. Rev. Lett. 43, 757 (1979).

†National Bureau of Standards, Washington, D.C. 20234.

‡Daresbury Laboratory, Science Research Council, Daresbury, Warrington WA4 4AD, England.

vibrational channels. Analogous effects are expected in connection with the widespread occurrence of shape resonances in both inner- and outer-shell molecular photoionization spectra.

The results are presented in Figure 1 as ratios of intensities of the $v = 1$, 2, and 3 levels of $CO^+ X^2\Sigma^+$ to that of the ground vibrational state of the ion, as functions of incident photon energy. Immediately apparent in Figure 1 is that, aside from the structures at $\sim$ 19.5 eV, attributable to unresolved autoionization structure, the gross pattern of spectral variation of these ratios strongly resembles that predicted[1] for the analogous states in N_2. Specifically, the $(v = 1)/(v = 0)$ curve shows an oscillation with a minimum at $\sim$ 22.3 eV and a peak-to-trough ratio of $\sim$ 3. The $(v = 2)/(v = 0)$ curves are less well defined but clearly show successively greater enhancement at $\sim$ 22 eV, relative to their weak background levels. Accordingly, we interpret the present results as the direct observation of the effects of shape resonances on vibrational intensity distributions.

Reference

1. J. L. Dehmer, D. Dill, and S. Wallace, Phys. Rev. Lett. 43, 1005 (1979).

SHAPE-RESONANCE-INDUCED NON-FRANCK-CONDON VIBRATIONAL INTENSITIES IN $3\sigma_g$ PHOTOIONIZATION OF N_2

John B. West,[†] A. C. Parr,[‡] B. E. Cole,[†] D. L. Ederer,[‡] Roger Stockbauer,[‡] and J. L. Dehmer

---

We report a broad pattern of non-Franck-Condon (FC) vibrational intensities extending over $\sim$ 25 eV of the $3\sigma_g$ photoionization continuum of N_2. The effect was recently predicted[1] theoretically to arise from shape-resonance-induced breakdown of the FC separation of electronic and nuclear motion. Here experiment and theory are directly compared for the first time. Qualitative agreement verifies the basic theoretical concept, yet significant quantitative differences indicate the need for further work.

Branching ratios for the v = 0, 1 levels of $N_2^+ X^2\Sigma_g^+$ are given as a function of photon energy in Figure 1. The present data are denoted by solid dots with error bars indicative of the precision of the computer fit to the v = 0, 1 peaks in the experimental spectrum. The theoretical prediction[1] is given by the solid line. Other points of reference include the FCF = 9.3%,[2] which would apply if nuclear and electronic motion were completely separable, and data (▲) in the 16 to 23 eV region and at 40.8 eV taken by Gardner and Samson[3] using laboratory line sources.

The central message in Figure 1 is that, as predicted by theory,[1] the vibrational branching ratio exhibits a gross oscillation relative to the FCF over a broad $\sim$ 30 eV spectral range. This verifies, by direct comparison between experiment and theory, that shape resonances invalidate the Franck-Condon separation and that the resulting vibrational effects can extend far beyond the resonance half-width, $\sim$ 5 eV in this case. Several secondary points also stand out in Figure 1. First, the branching ratio exhibits a seemingly erratic behavior

---

*Summary of a paper published in J. Phys. B 13, L105 (1980).

[†]Daresbury Laboratory, Science Research Council, Daresbury, Warrington WA4 4 AD, England.

[‡]National Measurement Laboratory, National Bureau of Standards, Washington, D.C. 20234.

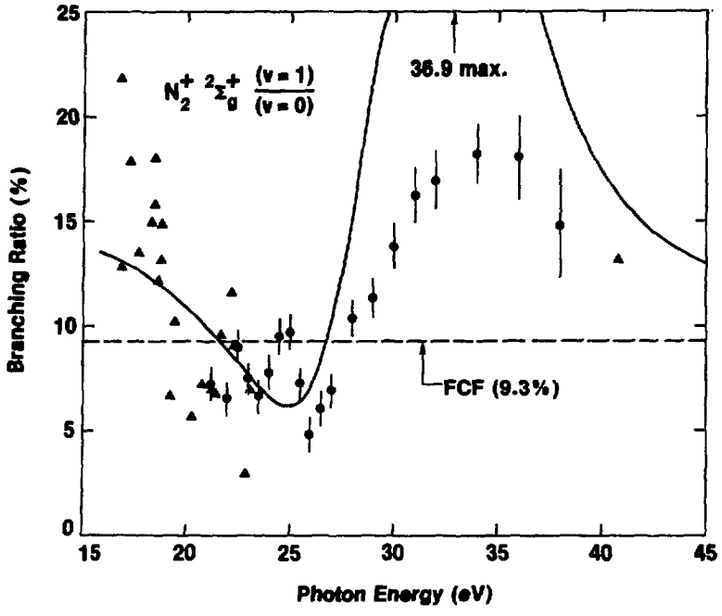

FIG. 1.--Branching ratios as a function of photon energy for production of the v =0, 1 levels of $N_2^+ X^2\Sigma_g^+$ by photoionization of N_2: ●, present results; ▲, data from Gardner and Samson;[3] —, theory from Ref. 1; ---, the Franck-Condon factor, Albritton.[2]

in the 16 to 26 eV region (several data points from Gardner and Samson[3] are out of the frame of Figure 1). We attribute this to effects of incompletely resolved autoionizing states which are populated in this wavelength range. In this case, autoionization effects obscure the mapping of the shape resonance effect, but are the primary focus of parallel studies performed on a much finer energy mesh. Second, experiment and theory agree rather well in magnitude at the lower and higher energies in Figure 1 and in the location of the maxima and minima; however, theoretical results overestimate the branching ratio by about a factor of two at the maximum. Thus, while the qualitative basis for this effect has been firmly established, future work is needed to achieve a quantitative theory.

References

1. J. L. Dehmer, D. Dill, and S. Wallace, Phys. Rev. Lett. 43, 1005 (1979).
1. D. L. Albritton, private communication.
3. J. L. Gardner and J.A.R. Samson, J. Electron Spectrosc. 13, 7 (1978).

NUCLEAR-MOTION EFFECTS IN THE PHOTOIONIZATION OF CO_2 *

J. R. Swanson,† D. Dill,†‡ and J. L. Dehmer

A calculation of the photoionization cross section of CO_2 reveals that the σ_u shape resonance at approximation 19 eV, accessed by the $1\pi_g$ and $4\sigma_g$ valence levels, is reduced and broadened by coupling to the ground state vibrational motion. Off resonance the effect of nuclear motion is negligible. Results are compared with experimental branching ratios.

Both fixed-R and R-averaged cross sections for the $1\pi_g$ and $4\sigma_g$ levels are shown in Figures 1 and 2. For both levels the nonresonant channels are unaffected by averaging, while the resonant peak in the $\varepsilon\sigma_u$ channel is reduced and broadened. For $1\pi_g$ the effect of R-averaging leaves the resonance barely discernible in the total cross section dominated by the non-resonant $\varepsilon\delta_u$ channel. For $4\sigma_g$ the resonant cross section is reduced by 70%. In Figure 3 (top) we compare our fixed-R results with the experimental branching ratios measured by Gustaffson et al.[1] Figure 3 (bottom) compares the same experimental results with an R-averaged calculation. The theoretical cross sections have been multiplied by $(1-0.16\beta)$, where β is the photoelectron asymmetry parameter, to account for the experimental geometry.[1] We find that R-averaging has only a slight effect on the $1\pi_u$ and $3\sigma_u$ levels, since they do not access the resonant continuum channel.

Although it is apparent that the vibrationally averaged results are in substantially better agreement with experiment, it is equally apparent that a discrepancy remains in the $4\sigma_u$ channel. There are several possible explanations for this disparity. Calculations of analogous resonances in atoms show that models, such as the Hartree-Slater or the MSM, which use a statistical exchange approximation, yield cross sections which may be several times larger than those

---

*Summary of a paper to be publsihed in J. Phys. B.

†Department of Chemistry, Boston University, Boston, MA 02215.

‡Consultant, RER Division.

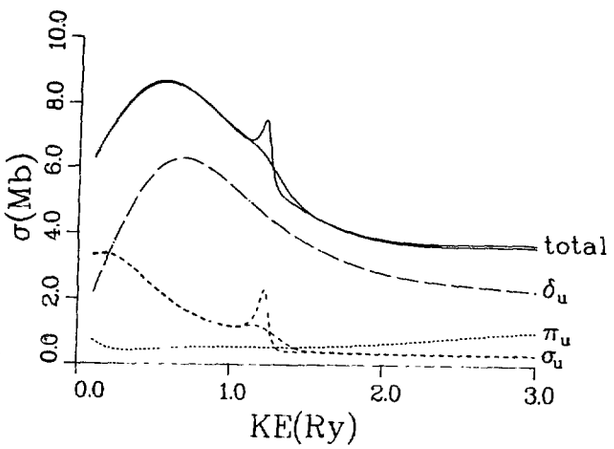

FIG. 1.--R =R_e and R-averaged cross sections for $1\pi_g$ photoionization. The peak at 1.2 Ry is prominent in the R =R_e cross section.

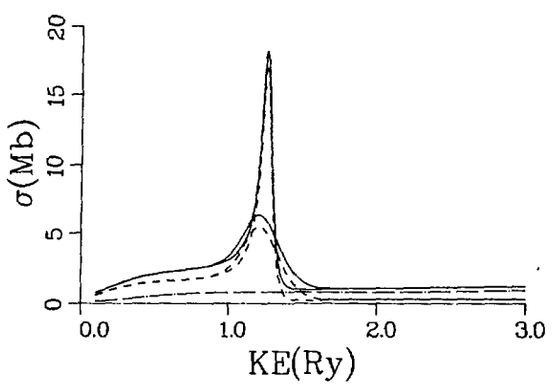

FIG. 2.--R =R_e and R-averaged cross sections for $4\sigma_g$ photoionization. Dashed lines are $\varepsilon\sigma_u$ channel; dash-dot lines are $\varepsilon\pi_u$ channel; solid lines are total cross section. The sharper peaked curves are for R =R_e.

calculated with an exact treatment of exchange.[2] Another possibility is the presence of strong interchannel coupling. The shape resonance would then behave as though it were a bound state imbedded in the continuum of another channel and oscillator strength would be transferred to the other channel by interelectron Coulomb interactions. A third possibility is that the vibrational modes we have neglected play a larger role than suspected. Resolution of these problems will be facilitated by experimental results on vibrationally-resolved cross sections and photoelectron angular distributions. Vibrationally-resolved CO_2 spectra have been calculated and will be reported elsewhere.

This work illustrates that nuclear motion cannot be neglected in the vicinity of shape resonances. Their energy and width are sensitive to nuclear

motion, because the potential barriers which support them depend on the nuclear configuration. On the other hand, regions of the spectrum not affected by shape resonances can be realistically treated by calculations at the equilibrium nuclear configuration.

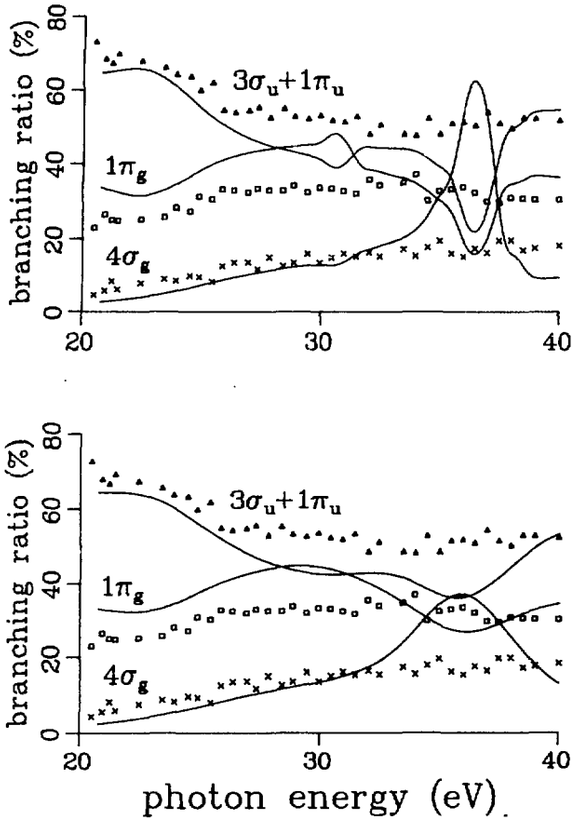

FIG. 3.--Comparison of calculated branching ratios with the experimental data of Gustaffson et al.[1] Top, $R = R_e$ results; bottom, R-averaged results.

References

1. T. Gustaffson, E. W. Plummer, and W. Gudat, Phys. Rev. A 17, 175 (1978).
2. D. J. Kennedy and S. T. Manson, Phys. Rev. A 5, 227 (1972).

EFFECTS OF VIBRONIC INTERACTION AND AUTOIONIZATION ON THE PHOTOELECTRON SPECTRUM OF N_2O *

P. M. Dehmer, J. L. Dehmer, and W. A. Chupka†

Introduction

Recently, Frey et al.[1] reported the high resolution threshold photoelectron spectra (TPES) of the X $^2\Pi$ and A $^2\Sigma^+$ states of N_2O^+. In contrast to the more familiar fixed-wavelength photoelectron spectra (PES) in which ejected photoelectrons are energy analyzed using a dispersive analyzer, TPES uses a variable wavelength photon source and detects only zero energy photoelectrons. The TPES often show non-Franck-Condon intensity distributions as a result of autoionization of intermediate neutral states that are nearly degenerate with the molecular ion state to which they decay; in fact, Frey et al. observed very intense peaks in the TPES of the X $^2\Pi$ state of N_2O^+, corresponding to excitation of one and two quanta of the bending mode. These transitions, which had not been observed in earlier HeI 584 Å fixed-wavelength PES,[2] are normally very weak or absent in linear-linear transitions. Symmetry selection rules forbid the excitation of a single quantum of bending vibration,[3] although this mode may be induced through vibronic coupling.[4,5] In addition to the appearance of the bending mode of the X $^2\Pi$ state, the TPES also gave intensities for the symmetric stretch in the X $^2\Pi$ and A $^2\Sigma^+$ states which are significantly different from those observed in previous HeI PES.[2]

In order to explore in more detail the occurrence of weak bands corresponding to excitation of the bending mode and the differences in relative intensities in the HeI PES and the TPES of N_2O, we have measured HeI PES of N_2O at a spectrometer resolution of 12 to 16 meV, using both effusive and supersonic (rotationally cooled) molecular beam sources.

---

*Summary of a paper to appear in J. Chem. Phys.

†Department of Chemistry, Yale University, New Haven, Connecticut 06520.

In order to help interpret the differences in the relative intensities in the TPES and the HeI PES, we also measured the high resolution photoionization mass spectra of N_2O^+ and its fragments in the regions of the X $^2\Pi$ and A $^2\Sigma^+$ convergence limits. The observation of autoionization structure that is nearly degenerate with ionic convergence limits helps to explain many of the observations.

Experimental

Photoelectron Spectra

Photoelectron spectra of the X $^2\Pi$, A $^2\Sigma^+$, B $^2\Pi$, and C $^2\Sigma^+$ states of N_2O were measured at a resolution of 16 meV or better with a rotatable hemispherical photoelectron spectrometer. The details of the analyzer and the hollow cathode lamp used to produce the HeI 584 Å ionizing radiation have been given previously.[6,7] In the present experiments, photoelectrons were sampled at 90° relative to the incident light beam in order to maximize the counting rate. With $\sim$ 0.05 cm diameter entrance and exit apertures on the analyzer, and a photoelectron analysis energy of 2 eV, the observed photoelectron resolution was 16 meV on atomic xenon using an effusive molecular beam source. A portion of the spectrum due to the X $^2\Pi$ state was measured at even higher resolution (12 to 13 meV) in order to resolve the Renner-Teller splitting in the (0,1,0) band. A supersonic molecular beam source was used for this measurement in order to reduce both Doppler and rotational broadening in the target gas.

Photoionization Mass Spectra

Relative photoionization cross sections were measured in the wavelength region of the X $^2\Pi$ vibrational convergence limits (965 Å to 940 Å) for N_2O^+ and in the wavelength region of A $^2\Sigma^+$ vibrational convergence limits (760 Å to 730 Å) for N_2O^+, NO^+, and O^+, using an ionization chamber that was cooled to approximately 130°K. The wavelength resolution was 0.07 Å for the parent ion and 0.14 Å for the fragment ions. The apparatus, which consisted of a He continuum light source, a 3 m near-normal incidence monochromator, and a quadrupole mass spectrometer for ion detection, has been described in detail previously.[8]

Results and Discussion

The data for the X $^2\Pi$ state will be discussed here as an example of the results of the present measurements. Figure 1 shows the photoelectron spectrum of the X $^2\Pi$ state of N_2O^+ taken at a resolution of 16 meV using an effusive molecular beam source. Several features are evident that were not observed in the lower resolution spectrum of Brundle and Turner,[2] most notably the appearance of the (0,2,0) band, corresponding to 2 quanta of bending. The present assignments for the higher vibrations are revised slightly from the earlier work, and are in accord with the N_2O^+ A $^2\Sigma^+ \rightarrow$ X $^2\Pi$ emission studies of Callomon and Creutzberg.[9] The asymmetric appearance of the (2,0,0) band is the result of one of a number of weak impurity lines in the undispersed light source, in this case the HeI 591.4117 Å line photoionizing the (0,0,0) level.

Figure 2 shows a portion of the spectrum taken at a resolution of 12 to 13 meV using a supersonic molecular beam source to reduce Doppler and rotational broadening. The position of the (0,1,0), (0,2,0), and (1,0,0) levels referenced to the (0,0,0) level were drawn on Figure 2 from the spectroscopic data of Callomon and Creutzberg,[9] i.e., the lines were <u>not</u> forced to match the observed structure. The weak features definitely correspond to three of the

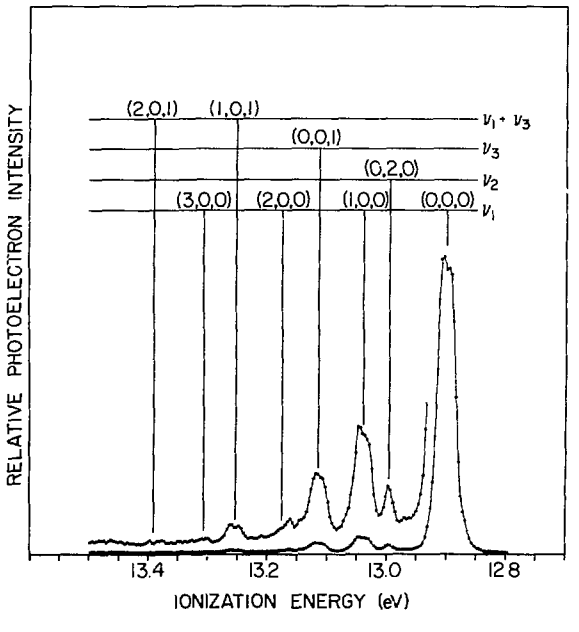

FIG. 1.--The HeI 584 Å photoelectron spectrum of the X $^2\Pi$ state of N_2O^+, taken with a spectrometer resolution of 16 meV using an effusive molecular beam source.

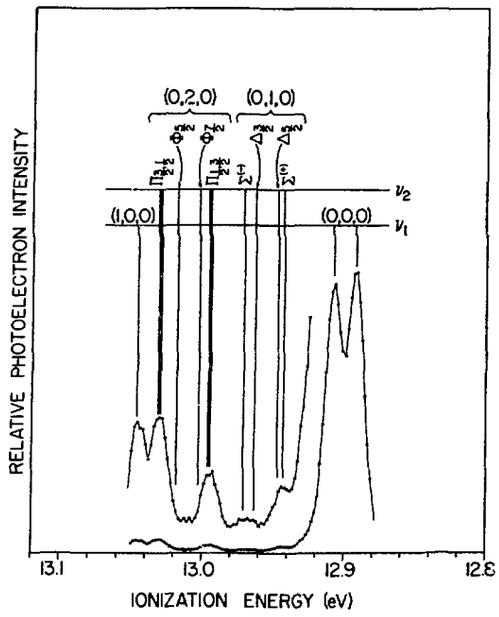

FIG. 2.--The HeI 584 Å photoelectron spectrum of the X $^2\Pi$ state of N_2O^+, taken with a spectrometer resolution of 12 to 13 meV using a supersonic molecular beam source.

components of the (0,1,0) level, which are labeled in Figure 2 with their vibronic term symbols.

The $^2\Sigma^+_{1/2}$, $^2\Delta_{3/2}$, and $^2\Sigma^-_{1/2}$ vibronic components are observed, and of these, the $^2\Sigma^+_{1/2}$ component is the most intense, almost certainly because it gains intensity as a result of a mixing of the X $^2\Pi$ and the A $^2\Sigma^+$ electronic states.

In Table 1, the relative intensities from the present HeI PES are compared with those from the TPES. (The TPES intensities for the X $^2\Pi$ and A $^2\Sigma^+$ states are obtained from Figures 1 and 2, respectively, of Ref. 1.) Each set of data has been normalized on the (0,0,0) band. Two things are immediately apparent: (1) the $^2\Sigma^+$ component of the (0,1,0) band is enormously enhanced in the TPES and (2) the remaining bands, and in particular, the (1,0,0) and (2,0,0) bands are all slightly more intense in the TPES than in the HeI PES. In a recent study of photoionization processes in N_2O using both variable wavelength PES and TPES, Baer et al.[10] determined that, in the energy region between the X $^2\Pi$ and $^2\Sigma^+$ states, about 10% of the Rydberg state autoionization produces vibrationally excited X $^2\Pi$ ions. The ejected electrons associated with this process, which the authors termed resonant autoionization, have a distribution beaking at zero energy and have a width of about 40 meV. The high-resolution photoionization

Table 1. Comparison of intensities in the HeI PES and TPES for the N_2O^+ X $^2\Pi$ and A $^2\Sigma^+$ states.

State	Band (ν_1, ν_2, ν_3)	Relative intensities HeI PES	TPES[a]	Ratio
X $^2\Pi$	(0,0,0)	100.0	100.0	1.00
	(0,1,0) $^2\Sigma^+_{1/2}$	0.3	11.8	42.1
	(0,1,0) $^2\Delta_{3/2}$ $^2\Sigma^-_{1/2}$	0.1_5		
	(0,2,0)[b] $^2\Pi$	1.0	3.1	3.0
	(1,0,0)	4.2	22.0	5.3
	(0,0,1)	2.8	4.9	1.8
	(2,0,0)	(0.7)[c]	6.0	9.2
	(1,0,1)	0.7		
	(3,0,0)	0.1		

[a] Ref. 1.

[b] Lower $^2\Pi$ components at 12.996 eV.

[c] Overlapped with HeI 591.4117 Å on (0,0,0) band.

mass spectrum of N_2O^+ in the energy region of the X $^2\Pi$ convergence limits determined in the present work is shown in Figure 3 and reveals weak autoionization structure not previously observed throughout the region. This structure has not been identified, but is near several low-lying Rydberg states converging to the A $^2\Sigma^+$ state of N_2O^+.[11] The most intense autoionizing peak in this region is nearly coincident with the (0,1,0) $^2\Sigma^+$ convergence limit, and almost certainly accounts for the unusually large intensity in the TPES.

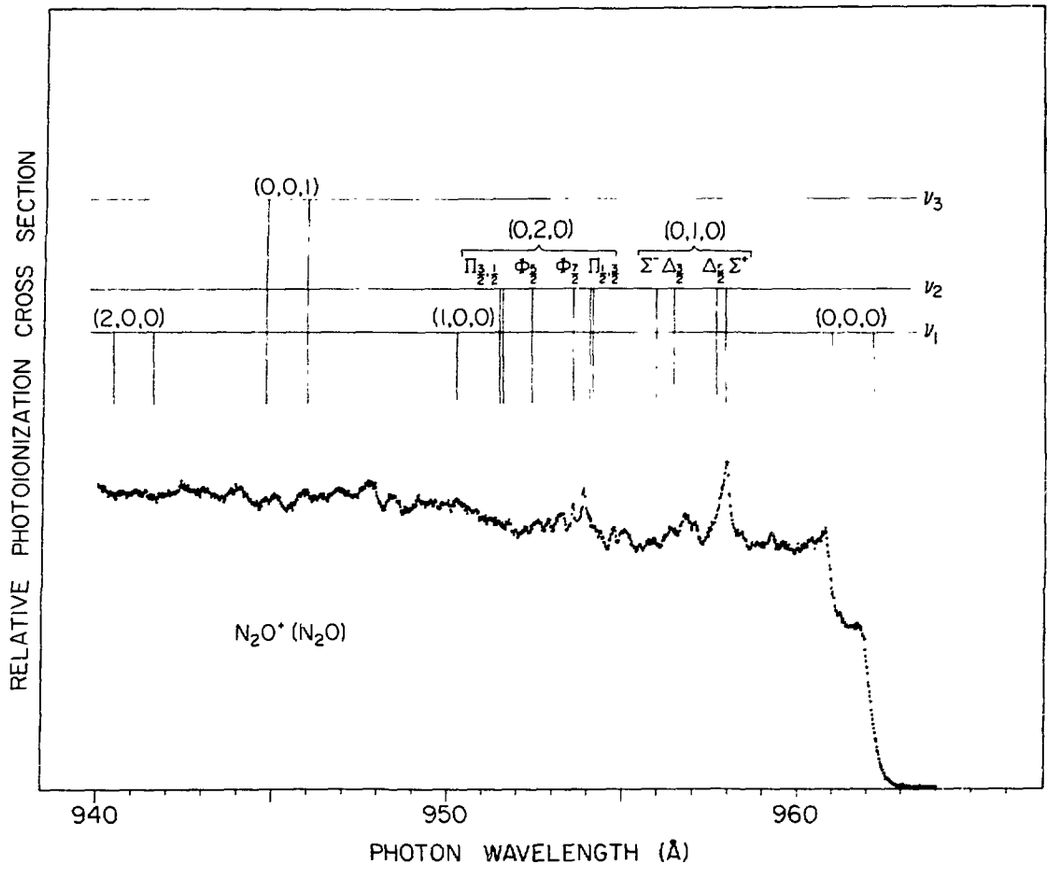

FIG. 3.--The relative photoionization cross section for N_2O^+ from the N_2O in the region of the X $^2\Pi$ vibrational limits, taken at a wavelength resolution of 0.07 Å using an ionization chamber that was cooled to approximately 130°K.

References

1. R. Frey, B. Gotchev, W. B. Peatman, H. Pollak, and E. W. Schlag, Chem. Phys. Lett. 54, 411 (1978).
2. C. R. Brundle and D. W. Turner, Int. J. Mass Spectry. Ion Phys. 2, 195 (1969).
3. G. Herzberg, Electronic Spectra and Electronic Structure of Polyatomic Molecules, Van Nostrand, New York, pp. 23-26; 150-159 (1966).
4. Ch. Jungen and A. J. Merer, Molecular Spectroscopy: Modern Research, Vol. 2, K. N. Rao, Ed., Academic Press, New York, pp. 127-164 (1976).

5. H. Köppel, L. S. Cederbaum, W. Domcke, and W. von Niessen, Chem. Phys. 37, 303 (1979).
6. J. L. Dehmer, Argonne National Laboratory Radiological and Environmental Research Division Annual Report, July 1974-June 1975, ANL-75-60, Part I, pp. 61-63.
7. J. L. Dehmer and D. Dill, Phys. Rev. A 18, 164 (1978).
8. W. A. Chupka, P. M. Dehmer, and W. T. Jivery, J. Chem. Phys. 63, 3929 (1975).
9. J. H. Callomon and F. Creutzberg, Phil. Trans. Roy. Soc. London A277, 157 (1974).
10. T. Baer, P.-M. Guyon, I. Nenner, A. Tabche-Fouhaille, R. Botter, L.F.A. Ferreira, and T. R. Govers, J. Chem. Phys. 70, 1585 (1979).
11. Y. Tanaka, A. S. Jursa, and F. J. LeBlanc, J. Chem. Phys. 32, 1205 (1959).

THEORETICAL PREDICTION OF SHAPE-RESONANCE-ENHANCED NUCLEAR MOTION EFFECTS IN MOLECULAR PHOTOIONIZATION*

J. L. Dehmer, D. Dill,[†] and Scott Wallace[‡]

Shape resonances in molecular photoionization are predicted to induce strong non-Franck-Condon effects over a spectral range several times broader than the resonance half-width. This is manifested by large deviations from Franck-Condon vibrational intensity distributions and strong dependence of photoelectron angular distributions on the vibrational state of the residual ion. These effects are illustrated for the $3\sigma_g$ photoionization channel of N_2 in Figures 1 and 2, using the multiple-scattering model and the adiabatic nuclei approximation.

Of central importance in Figure 1 is the clear demonstration that resonance positions, strengths, and widths are sensitive functions of R. In particular, for larger separations, the effective potential acting on the $\ell = 3$ components of the σ_u wave function is more attractive and the shape resonance shifts to lower kinetic energy, becoming narrower and higher. Conversely, for lower values of R, the resonance is pushed to higher kinetic energy and is weakened. This indicates that nuclear motion exercises great leverage on the spectral behavior of shape resonance, since small variations in R can significantly shift the delicate balance between attractive (mainly Coulomb) and repulsive (mainly centrifugal) forces which combine to form the barrier. In the present case, variations in R corresponding to the ground state vibration in N_2 produce significant resonant behavior over a spectral range several times the FWHM of the resonance calculated at $R = R_e$.

---

*Summary of both a paper appearing in Phys. Rev. Letters 43, 1005 (1979) and part of a paper presented at the XIth ICPEAC, Kyoto, Japan, Aug. 29-Sept. 5, 1979 [J. L. Dehmer and Dan Dill, Electronic and Atomic Collisions, N. Oda and K. Takayanagi, Eds., North-Holland Publ. Co., Amsterdam, pp. 195-208 (1980)].

[†]Consultant, Radiological and Environmental Research Division. Permanent address: Department of Chemistry, Boston University, Boston, MA 02215.

[‡]Center for Materials Science and Engineering, M.I.T., Cambridge, MA 02139.

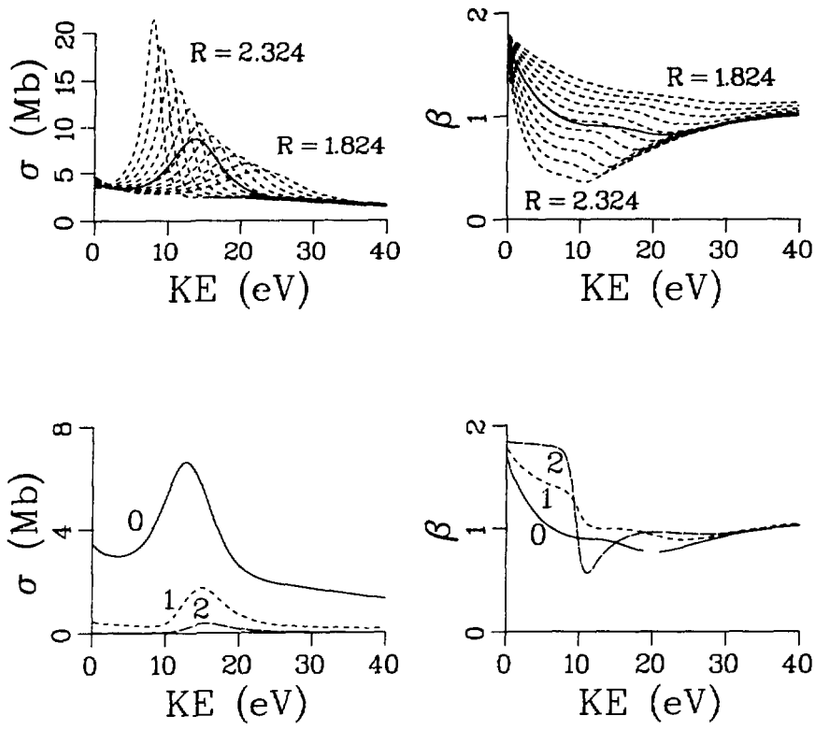

FIG. 1.--Cross sections σ and asymmetry parameters β for photoionization of the $3\sigma_g$ (v_i = 0) level of N_2. Top, fixed R (----) and R-averaged, vibrationally unresolved (——) results. Bottom, results for resolved final-state vibrational levels, v_f = 0-2.

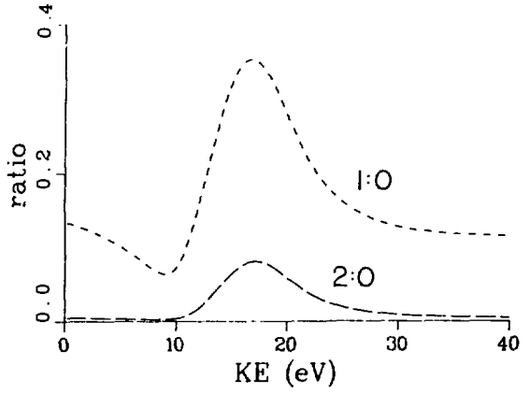

FIG. 2.--Vibrational state branching ratios $\sigma(v_f)/\sigma(v_f=0)$ for photoionization of the $3\sigma_g$ level of N_2.

Effects of nuclear motion on individual vibrational levels are shown in the bottom half of Figure 1. Looking first at the partial cross sections, we see that the resonance position varies over a few volts depending on the final vibrational state, and that higher levels are relatively more enhanced at their resonance position than is $v_f = 0$. This sensitivity to v_f arises because transitions to alternative final vibrational states preferentially sample different regions of R. In particular, $v_f = 1,2$ sample successively smaller R, governed by the maximum overlap with the ground vibrational state, causing the resonance in those vibrational channels to peak at higher energy than that for $v_f = 0$. The impact of these effects on branching ratios is clearly seen in Figure 2, where the ratio of the higher v_f intensities to that of $v_f = 0$ is plotted in the resonance region. There we see the ratios are slightly above the FC factors[1] (9.3%, $v_f = 1$; 0.6%, $v_f = 2$) at zero kinetic energy, go through a minimum just below the resonance energy in $v_f = 0$, then increase to a maximum as individual $v_f > 0$ vibrational intensities peak, finally approaching the FC factors again at high kinetic energy. Note the maximum enhancement over the FCF's is progressively more pronounced for higher v_f, i.e., 340% and 1300% for $v_f = 1,2$, respectively.

Equally dramatic are the effects on $\beta(v_f)$ shown in the lower right-hand portion of Figure 1. Especially at and below the resonance position, the β's vary greatly for different final vibrational levels. The $v_f = 0$ curve agrees well with the solid curve in the upper half, since the gross behavior of the virationally unresolved electronic band will be governed by the β of the most intense component.

Reference

1. D. L. Albritton, private communication.

SHAPE-RESONANCE-ENHANCED VIBRATIONAL EXCITATION AT INTERMEDIATE ENERGIES (10 to 40 eV) IN ELECTRON-MOLECULE SCATTERING*

D. Dill,† J. Welch,† J. L. Dehmer, and J. Siegel

The importance of shape resonances in the low energy portion (< 10 eV) of the electron-molecule scattering spectrum is widely appreciated (see, for example, Ref. 1). The π_g d-wave (ℓ=2) resonance at 2.4 eV in e^--N_2 scattering is perhaps the most thoroughly studied example.[2,3] Such resonances stand out clearly above the nonresonant background, have widths on the order of an eV, and are usually dominated by a single asymptotic angular momentum, which imposes a well-defined angular distribution characteristic of that ℓ. Here we emphasize a new class of shape resonances, falling in the intermediate-energy range (10 to 40 eV), which have emerged in the course of our current survey studies of electron-molecule scattering, using the multiple-scattering method (MSM).[4,5] Compared with their low-energy counterparts, these resonances are broader, are usually barely detectable in the elastic or total scattering cross sections, and often are composed of significant contributions from several asymptotic angular momenta, whose mixture can vary significantly within the resonance. These properties are consistent with the picture of a quasi-bound state lying near the top of its centrifugal barrier. These weak resonances are, however, very sensitive to changes in the molecular geometry and can, therefore, couple significantly to nuclear motion. We have found that these features are thereby enhanced in vibrational excitation and appear prominently, all the more so because the nonresonant background is negligible in the vibrationally inelastic channels.

To illustrate these ideas, the spectrum for the excitation of the symmetric-stretch vibrational mode in CO_2 is shown in Figure 1. Here the π_u resonance

---

*Summary of a paper published in Phys. Rev. Lett. 43, 1236 (1979).

†Consultant, Radiological and Environmental Research Division. Permanent address: Dept. of Chemistry, Boston University, Boston, MA 02215.

‡Department of Chemistry, Harvard University, Cambridge, MA 02138.

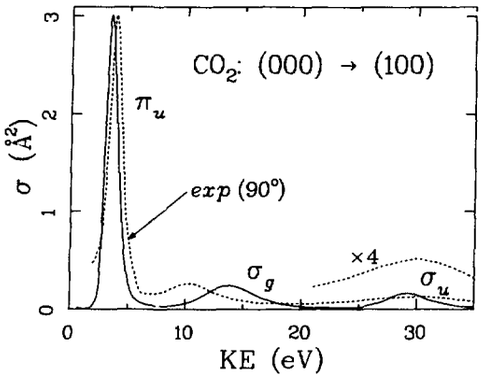

FIG. 1.--Cross section for excitation of the symmetric-stretch mode in CO_2 by electron impact. Experimental data taken from Ref. 6.

is very strong, as it is in the vibrationally elastic spectrum, but in addition, the σ_g and σ_u resonances stand out clearly as well. The δ_g resonance does not contribute appreciably since it is oriented perpendicular to the symmetric stretch and therefore is coupled weakly to it. Tronc et al.[6] observe the strong π_u induced excitation and two much weaker and broader excitations at 11 eV and 29.5 eV, with no evidence of a third (δ_g) weak feature, thus confirming our results.

References

1. G. J. Schulz, in Principles of Laser Plasmas, G. Bekefi, Ed., John Wiley and Sons, p. 33 (1976) and references therein; J. N. Bardsley and F. Mandl, Reports on Progress in Physics 31, 471 (1968).
2. M. Krauss and F. H. Mies, Phys. Rev. A 1, 1592 (1970); D. T. Birtwistle and A. Herzenberg, J. Phys. B 4, 53 (1971); P. G. Burke and N. Chandra, J. Phys. B 5, 1696 (1972); B. D. Budkley and P. G. Burke, J. Phys. B 10, 725 (1977); M. A. Morrison and B. I. Schneider, Phys. Rev. A 16, 1003 (1977); M. A. Morrison and L. A. Collins, Phys. Rev. A 17, 918 (1978); A. W. Fliflet, D. A. Levine, M. Ma, and V. McKoy, Phys. Rev. A 17, 160 (1978).
3. D. Dill and J. L. Dehmer, Phys. Rev. A 16, 1423 (1977); J. Siegel, D. Dill, and J. L. Dehmer, Phys. Rev. A 17, 2106 (1978); and J. Siegel, J. L. Dehmer, and D. Dill, Phys. Rev. A, to be published.
4. D. Dill and J. L. Dehmer, J. Chem. Phys. 61, 692 (1974).
5. J. L. Dehmer and D. Dill, Electron and Photon Molecule Collisions, T. Rescigno, V. McKoy, and B. Schneider, Eds., Plenum Publ. Corp., New York (1979).
6. M. Tronc, R. Azria, and R. Paineau, J. de Physique Lettres, in press.

SPECTRAL VARIATION OF MOLECULAR PHOTOELECTRON ANGULAR DISTRIBUTIONS: VALENCE SHELLS OF N_2 AND CO *

Scott Wallace,† Dan Dill,‡ and J. L. Dehmer

Angular distribution measurements probe the interference between alternative angular momentum components of the wave function of electrons ejected from a given subshell. Accurate description of these measurements requires a detailed knowledge of the relative phases of these components. These so-called phaseshifts measure the deviation of the molecular ion from a unit positive point charge. The calculation of these phaseshifts requires a realistic description of the interaction of the photoelectron with the molecular core, especially at short range where deviations from a pure Coulomb field are most pronounced. When the resulting forces affect alternative angular momenta differently, i.e., are anisotropic, then effects on the angular distribution will be most pronounced. While the main sources of anisotropic forces in atoms are many-electron interactions, anisotropic forces in molecules are considerable even at the one-electron level, because while atoms are spherical, molecules are not.

Photoelectron angular distributions have been calculated, with the multiple-scattering method[1,2] for electrons ejected from the outer shells $2\sigma_g$, $1\pi_u$, and $3\sigma_g$ of N_2, and 4σ, 1π, and 5σ of CO from threshold to 10 rydbergs electron kinetic energy. Results are given in Figure 1. Clear evidence of the σ f-wave ($\ell = 3$) shape resonance is seen in the $3\sigma_g$ spectrum of N_2 and in all three spectra of CO. Agreement with very recent wavelength-dependent measurements made at the Bonn synchrotron by Marr and Holmes[3] is generally good, but more detailed measurements and further theoretical work are needed to eliminate remaining discrepancies.

---

*Summary of an article which appeared in J. Phys. B 12, L417 (1979).

†Center for Materials Science and Engineering, M.I.T., Cambridge, MA 02139.

‡Consultant, Radiological and Environmental Research Division. Permanent address: Department of Chemistry, Boston University, Boston, MA 02215.

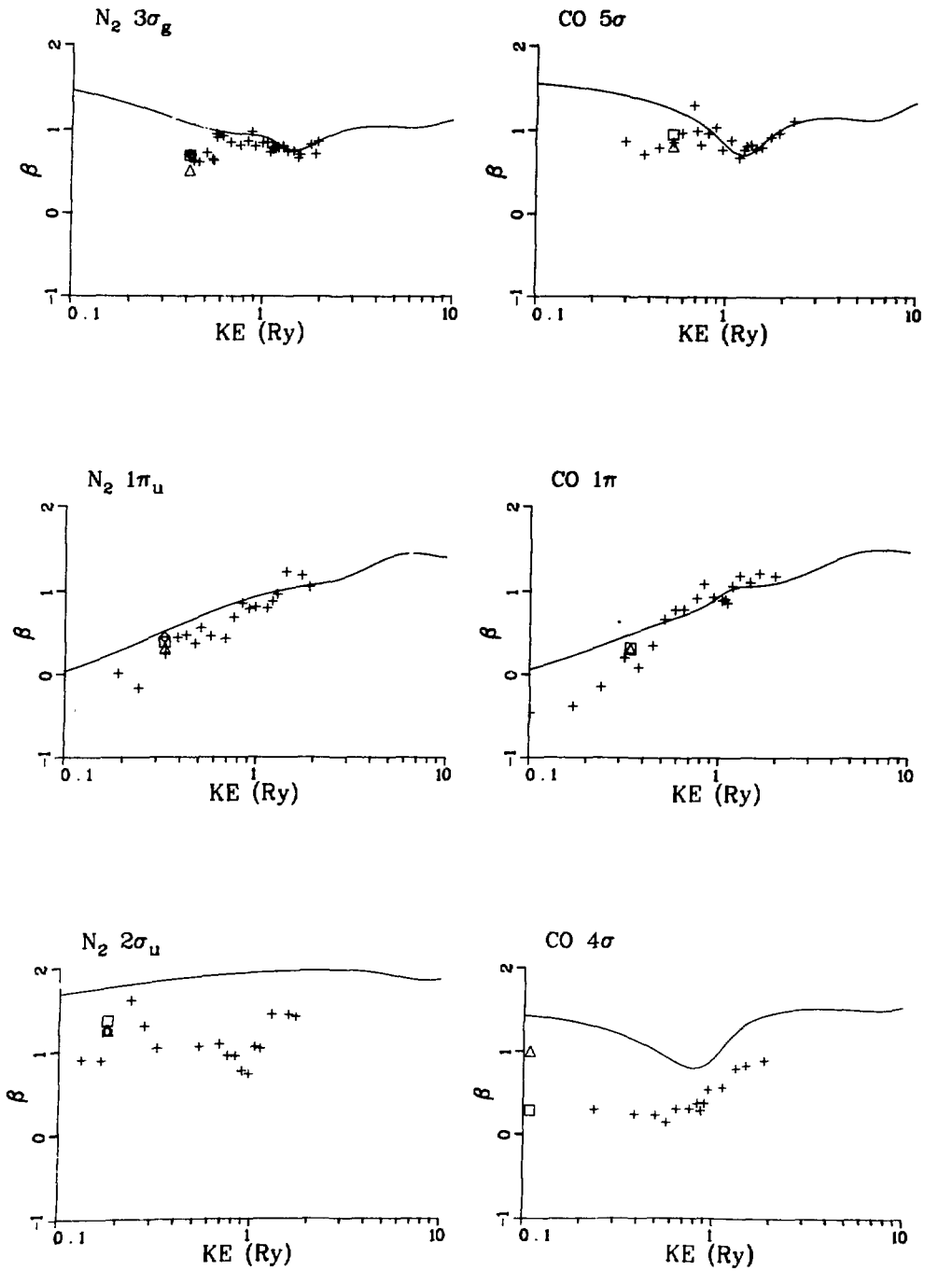

FIG. 1.--The photoelectron asymmetry parameter β as a function of electron kinetic energy for photoionization of the levels $2\sigma_g$, $1\pi_u$, and $3\sigma_g$ of N_2, and 4σ, 1π, and 5σ of CO; ——, calculation. Experimental values: +, Marr et al.;[3] □, Hancock and Sampson;[4] ◇, Morgenstern et al.[5] and Niehaus and Ruf;[6] Δ, Carlson and co-workers.[7]

References

1. D. Dill and J. L. Dehmer, J. Chem. Phys. 61, 692 (1974).
2. J. L. Dehmer and D. Dill, Electron and Photon Molecule Collisions, T. Rescigno, V. McKoy, and B. Schneider, Eds., Plenum Publ. Corp., New York, p. 225 (1979).
3. G. V. Marr, J. M. Morton, R. M. Holmes, and D. G. McCoy, J. Phys. B 12, 43 (1979).
4. W. H. Hancock and J.A.R. Samson, J. Electron Spectrosc. 9, 211 (1976).
5. R. Morgenstern, A. Niehaus, and M. W. Ruf, Electronic and Atomic Collisions, L. M. Branscomb, Ed., North Holland Publ. Co., Amsterdam, p. 167 (1971).
6. A. Niehaus and M. W. Ruf, Z. Phys. 252, 84 (1971).
7. T. A. Carlson and A. E. Jonas, J. Chem. Phys. 55, 4913 (1971); T. A. Carlson et al., Electron Spectroscopy, D. A. Shirley, Ed., North Holland Publ. Co., Amsterdam, p. 307 (1971); T. A. Carlson and G. E. McGuire, J. Electron Spectrosc. 1, 209 (1972).

ANGULAR DISTRIBUTION OF MOLECULAR K-SHELL AUGER ELECTRONS: SPECTROSCOPY OF PHOTOABSORPTION ANISOTROPY *

D. Dill,† J. R. Swanson,‡ S. Wallace,** and J. L. Dehmer

Atomic K-shell vacancies are isotropic, and hence electrons emitted by Auger decay of such vacancies have an isotropic angular distribution.[1-4] Molecules are different, however, for two reasons. First, molecular photoabsorption is highly anisotropic, both in the discrete, because excited states have definite symmetries but generally different energies, and in the continuum, where shape resonances can enhance photoabsorption along characteristic directions of the molecule.[5-9] As a result, molecular photoabsorption produces neutral molecular excited states with definite, characteristic orientations, and shape-resonant photoionization produces molecular ions with energy-dependent orientations characteristic of each resonance. Second, subsequent decay of the K-shell vacancy is a fast process compared to molecular rotation, so that the orientation of the molecular excited state/ion will be reflected in the angular distribution of the emtted Auger electrons. For example, in CO and N_2 there is a very intense discrete absorption of π symmetry about 1 Ry below the K-shell ionization threshold and a broad σ-symmetry shape resonance centered about 1 Ry above threshold.[6,7,10,11] Thus photoabsorption to the π excited states preferentially creates excited molecules perpendicular to the electric vector of the light while photoionization within the σ shape resonance yields molecular ions preferentially parallel. The angular distribution of a particular Auger electron will mirror these alternative orientations produced as one scans through the photoabsorption spectrum. Thus, molecular Auger-electron angular distributions, as a function of photoexcitation energy, provide us with a spectroscopy

---

* Summary of a paper submitted for publication.

† Consultant, Radiological and Environmental Research Division. Permanent address: Department of Chemistry, Boston University, Boston, MA 02215.

‡ Department of Chemistry, Boston University, Boston, MA 02215.

** Center for Materials Science and Engineering, MIT, Cambridge, MA 02139.

of the anisotropy of molecular photoabsorption spectra, whereby they can be decomposed into their component symmetries.

References

1. W. Mehlhorn, Phys. Lett. 26A, 166 (1968).
2. B. Cleff and W. Mehlhorn, Phys. Lett. 37A, 3 (1971).
3. S. Flugge, W. Mehlhorn, and V. Schmidt, Phys. Rev. Lett. 29, 7 (1972).
4. B. Cleff and W. Mehlhorn, J. Phys. B 7, 593 (1974).
5. J. L. Dehmer, J. Chem. Phys. 56, 4496 (1972) and references therein.
6. J. L. Dehmer and D. Dill, Phys. Rev. Lett. 35, 213(1975).
7. J. L. Dehmer and D. Dill, J. Chem. Phys. 65, 5327 (1976).
8. D. Dill, S. Wallace, J. Siegel, and J. L. Dehmer, Phys. Rev. Lett. 41, 1230 (1978); 42, 411 (1979).
9. S. Wallace, Ph.D. thesis, Boston University (1979).
10. G. R. Wight, C. E. Brion, and M. J. van der Wiel, J. Electron Spectrosc. 1, 457 (1973).
11. R. B. Kay, Ph. E. van der Leeuw, and M. J. van der Wiel, J. Phys. B 10, 2513 (1977).

CONNECTIONS BETWEEN MOLECULAR PHOTOIONIZATION AND ELECTRON-MOLECULE SCATTERING WITH EMPHASIS ON SHAPE RESONANCES*

J. L. Dehmer and Dan Dill†

Most of our detailed information on the spectroscopy and dynamics of the electronic continuum of molecules is based on the complementary probes—photoionization and electron scattering. Though usually studied separately, it is most useful to appreciate the connections between these two processes since our understanding of one is often the key to interpreting or even generating any new results in the other. We approach this subject in two steps. First, we very briefly outline the well-established connections, e.g., the Bethe-Born theory and comparisons of isoelectronic systems. Then we focus on a point of contact—the role of shape resonances in molecular photoionization and electron-molecule scattering—for which a substantial amount of new information has become available. Specific topics include mapping of resonances from the neutral ($h\nu$ + molecule) to the negative ion (e + molecule) system, angular distributions, and interaction with vibration.

* Abstract of an article published in Proc. Symp. Electron-Molecule Collision—Invited Papers, I. Shimamura and M. Matsuzawa, Eds., University of Tokyo, p. 95 (1979).

† Consultant, Radiological and Environmental Research Division. Permanent address: Department of Chemistry, Boston University, Boston, MA 02215.

ELECTRON-POLAR MOLECULE SCATTERING AT INTERMEDIATE VALUES OF J: A CLOSED-FORM TREATMENT*

Jon Siegel and C. W. Clark†

The bulk of the total cross section for electron-polar molecule scattering results from small angle scattering at large impact parameter, for which perturbative treatments (e.g., the first Born approximation[1,2]) or semiclassical mechanics[3,4] are adequate. Scattering into intermediate and large angles from closer collisions; calculation of accurate differential and momentum-transfer cross sections therefore requires that the short- and intermediate-range dynamics be represented realistically in the context of an overall quantum mechanical calculation (Siegel, Dill, and Dehmer, Ref. 5, to be referred to as SDD; Collins and Norcross, Ref. 6, to be referred to as CN). As this analysis suggests, the dipole scattering problem naturally subdivides, by geometry and dynamics, into three parts: (1) the core region, where the multicenter molecular potential determines the electron's motion; (2) the intermediate region, where the essentially pure fixed dipole field is still strong enough to couple the electronic motion to the molecular axis, and (3) the outermost region, where rotational dynamics dominate as the electron can no longer follow the molecule's rotation. Clark[7] took advantage of this quasi-separability in applying frame transformation theory[8] to dipole scattering, but his final formulation still required propagation of a large array of coupled differential equations through all three regions of space, matching function and derivative at two boundaries.

Although the influence of the outermost region on the total cross section is large, its effects on each individual partial wave is so small that it may be neglected for partial waves which penetrate into the inner two regions (SDD, CN). The effects of rotational dynamics on the higher-ℓ (and therefore non-penetrating) partial waves, necessary to converge the forward-scattering cross section,[9] may be taken into account analytically[10] so that no solution need be

---

*Excerpt from a letter published in J. Phys. B 13, L31 (1980).

†Daresbury Laboratory, Daresbury, Warrington WA4 4AD, England.

propagated through the boundary between the outermost and intermediate regions. By further exploiting centrifugal barrier effects, one can construct (SDD, CN) an accurate hybrid S matrix in which the lowest-ℓ partial waves are calculated using a conventional body-frame expansion including an explicit representation of the molecular core; intermediate-ℓ partial waves, excluded from the core by their centrifugal barriers, are calculated using a point-dipole potential; and the highest-ℓ S matrix elements are obtained using the first Born approximation[1,2] in which rotational dynamics are included explicitly. Here, we present results of closed-form expressions for the S and K (reactance) matrices for fixed (i.e., body frame) point-dipole scattering, and show that these results are equivalent to the close-coupling results for rotationally adiabatic scattering (e.g., $E > 0.2$ eV for LiF), when transformed geometrically to the laboratory frame. Furthermore, the closed-form S and K matrices are energy-independent, and need be calculated only once for application to the entire energy range for which the scattering process is adiabatic with respect to rotation. We illustrate the ranges of equivalence of these various approaches through Figure 1, which depicts the integrated cross section $\sigma^{J}_{j=0\to1}$ as a function of the total angular momentum J for e-LiF scattering at 5.44 eV.

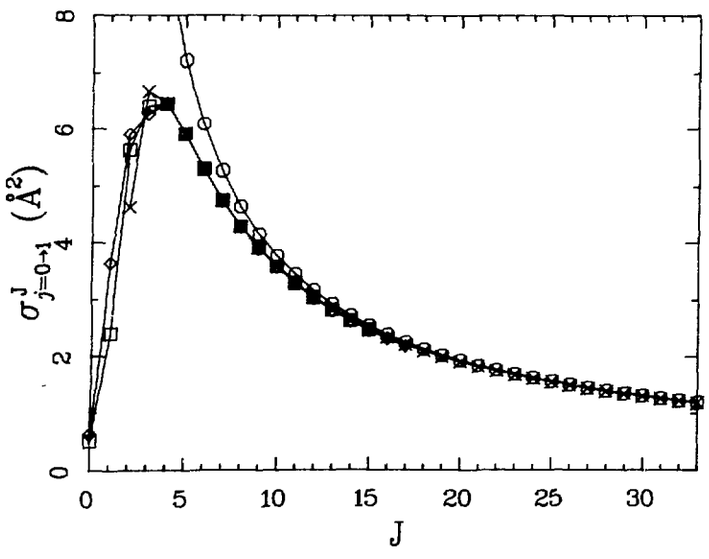

FIG. 1.--Rotational cross sections $\sigma^{J}_{j=0\to1}$ for e-LiF scattering at 5.44 eV: X, closed-form treatment, J =2-33; □ , body-frame close-coupling molecular core potential, J =0-17; ◇ , laboratory frame close coupling, cut-off dipole potential, J =0-15;0, the first Born approximation, J =0-33 although J =0-4 fall off scale. (The first three Born cross sections are 19.7, 29.5, and 16.4 Å^2, respectively. The lower value for J =0 reflects the lack of an $\ell\to\ell$-1 component.)

Since $\ell \approx J$ for the $j = 0 \rightarrow 1$ transition, the figure illustrates the validity of treating separate ranges of ℓ by different approximations. By $J \sim 25$ to 30, all approximations yield equivalent results. The Born results behave as $\sigma^{J(\text{Born})} \propto 1/(J+1)$ in the adiabatic range. This formula overestimates the cross section as J decreases, reflecting the incipient violation of unitarity. For $J \geq 5$, the equivalence of the closed-form, laboratory-frame, close-coupling, and body-frame molecular core results demonstrates the validity of the adiabatic approximation as well as the unimportance of the core region. Finally, the differences in the results for $J \leq 4$ reflect differences in the approximate representations of the core. Note that the few low-ℓ partial waves which penetrate to the core region have profound impact on the differential and momentum-transfer cross sections (SDD,CN), especially at large scattering angle θ.

In summary, we stress two points: (1) The plot of σ^J vs J brings out, in a manner easily understood, how a given range of J may be associated with a specific region of configuration space. Because the source of this effect is the centrifugal barrier, the association is strongest for low j,j' (as in Figure 1), so that $\ell \approx J$: The adiabatic recoupling (Refs. 11 and CN) necessary to calculate scattering from higher initial or final rotatonal states, where each J has contributions from a larger range of ℓ, may obscure the association. Since many phenomena of interest in electron collision studies (e.g., vibrational or electronic excitation processes) occur in well-defined regions of configuration space, similar plots may bring out the range of J where these phenomena have effect. (2) Finally, the key point of this work is that the closed-form point-dipole method provides extremely accurate S matrix elements for dipolar scattering, and should become the method of choice in the applicable ranges of J and energy due to the economy, accuracy, and physical insight which it brings to the problem.

Acknowledgements

We wish to thank Ugo Fano, Joseph Dehmer, and Dan Dill for valuable discussions and critical reading of the manuscript. In addition, we thank Y. Itikawa for providing the computer code used to generate the laboratory-frame results of Figure 1.

References

1. Y. Itikawa, J. Phys. Soc. Japan 27, 444 (1969).
2. Y. Itikawa and K. Takayanagi, J. Phys. Soc. Japan 26, 1254 (1969).
3. A. S. Dickinson and D. Richards, J. Phys. B 8, 2846 (1975).
4. D. Mukherjee and F. T. Smith, Phys. Rev. A 17, 954 (1978).
5. J. Siegel, J. L. Dehmer, and D. Dill, XIth Annual ICPEAC Abstracts of Contributed Papers, K. Takayanagi and N. Oda, Eds., The Society for Atomic Collision Research, Kyoto, p. 300 (1979); J. Siegel, J. L. Dehmer, and D. Dill, J. Phys. B, in press; J. Siegel, J. L. Dehmer, and D. Dill, to be published.
6. L. Collins and D. W. Norcross, Phys. Rev. A 18, 467 (1978).
7. C. W. Clark, Phys. Rev. A 20, 1875 (1979).
8. E. S. Chang and U. Fano, Phys. Rev. A 6, 173 (1972).
9. W. R. Garrett, Mol. Phys. 24, 465 (1972).
10. O. H. Crawford and A. Dalgarno, J. Phys. B 4, 494 (1971).
11. I. Shimamura, U. of Tokyo Institute of Space and Aeronautical Science Research Note RN83 (1979).

DIFFERENTIAL CROSS SECTIONS FOR e-LiF SCATTERING*

Jon Siegel, J. L. Dehmer, and Dan Dill†

Here we present differential cross sections (DCS's) for (vibrationally and electronically) elastic electron-LiF scattering from 1 to 20 eV and compare them to experiment and other theory. They were calculated using the hybrid method described by Clark and Siegel.[1] The lowest-ℓ partial waves, which penetrate to the interior of the molecule, are calculated by a model which includes an explicit representation of the molecular core potential. Intermediate-ℓ partial waves, excluded from the core by their centrifugal barrier, are calculated using a point-dipole model potential. Finally, the highest-ℓ partial waves are calculated in the first Born approximation which includes dynamic effects of molecular rotation.

Although similar in general strategy to the hybrid approach of Collins and Norcross,[2] the present calculation treated the low-ℓ and intermediate-ℓ ranges differently. For the former, where they used a single-center expansion of the molecular core potential, we employed the multiple-scattering method[3,4] (MSM), including the dipole potential[5] in the outer sphere. For the latter, where Collins and Norcross[2] performed a laboratory-frame-close-coupling calculation at each energy, we used the closed-form point-dipole method detailed by Clark and Siegel.[1] This economical and accurate method yields an energy-independent dipole scattering S matrix based on a single matrix diagonalization.

At each energy, a body-frame hybrid S matrix was constructed of MSM elements $S^{\lambda}_{\ell\ell'}$ for ℓ and $\ell' \leq \ell_{mol}$, and closed-form elements for ℓ or $\ell' > \ell_{mol}$, where ℓ_{mol} is a convergence parameter determined empirically. This matrix was transformed to the laboratory frame using, e.g., Eq. (3.15) of Collins and Norcross,[2] and, for transitions having $\Delta j \neq 1$, that portion of it

---

*Summary of a paper to be published in J. Phys. B.

†Consultant, RER Division. Permanent address: Department of Chemistry, Boston University, Boston, MA 02215.

having $J \leq J_{jj'}^{(ft)}$ was used to calculate DCS's.[6,7] For the $j = 0 \rightarrow 1$ transition, this matrix was supplemented with elements calculated in the first Born approximation[8,9] up to $J_{jj'}^{(B)}$, and then the closure formula[8,10] was used to obtain effective convergence to infinite J. Convergence of ℓ_{mol}, and $J_{jj'}^{(B)}$, was based on the DCS and is discussed in detail in the full paper we are publishing in J. Phys. B.

Figure 1 shows the differential cross sections from 1 to 20 eV, plotted as a surface. Note that no resonance structure interrupts the smooth spectral variation of the DCS within this energy range. At the lowest energies, where only s and possibly p waves penetrate to the core, the shape is Born-like although the magnitude is much smaller (see Figure 2). At 3 or 4 eV, the DCS passes through a minimum and starts a slow rise, except at very small θ (not shown) where the monotonic decline from threshold continues. This rise, a deviation from the k^{-2} behavior at lower energies, reflects the increasing effect of the molecular core. Above 5 eV this effect is seen even more emphatically in the structure at $\sim 40°$ and $\sim 100°$: Both the shape and the angle at which this structure appears confirm its non-dipolar origin. Thus, although only a few partial waves penetrate to the molecular core, their effect on scattering dynamics is significant at all except small angles. Both the DCS and the momentum-transfer cross sections,[11] therefore, require a realistic core potential for their accurate evaluation.

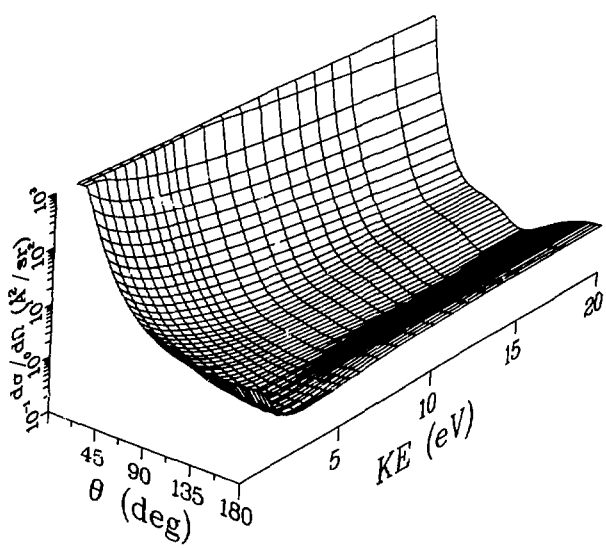

FIG. 1.--Differential cross section spectrum for e-LiF scattering from 1 to 20 eV.

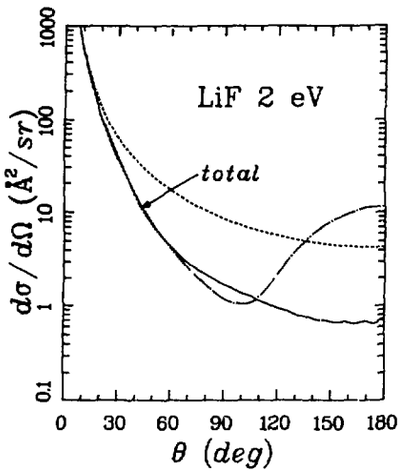

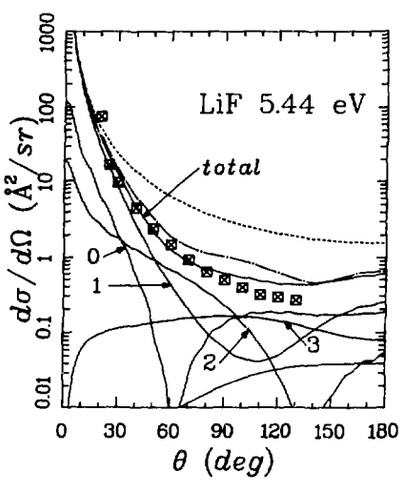

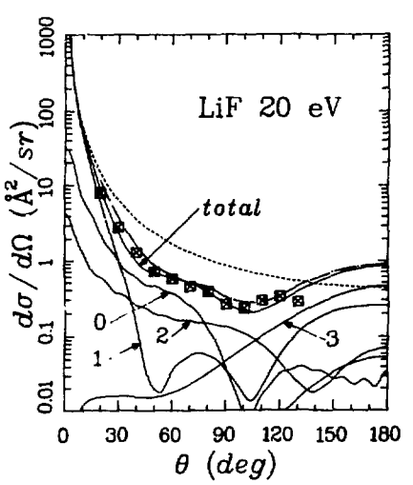

FIG. 2.--e-LiF scattering differential cross sections at selected energies: —, this work, showing transitions from initial j = 0 to indicated final j, plus total; ----, first Born approximation; -.-.-, Collins snd Norcross;[2] ▪, experimental results of Vuškovič et al.,[12] using their normalization.

In Figure 2 we compare some of these results to experiment[12] at 5.44 and 20 eV as well as to the theoretical results of Collins and Norcross[2] and the first Born approximation. Note especially the good agreement with experiment, as well as the failure of the Born approximation to reproduce the intermediate and large angle behavior of the $j = 0 \rightarrow 1$ partial cross section at these low energies.

In summary, the good agreement demonstrated here between cut results and experiment confirms the accuracy of the three models employed in this study, as well as the suitability of the hybrid S matrix approach used to combine them. The calculations are economically feasible, requiring only $\sim$ 3 minutes/energy on an IBM 370/3033 computer from the core MSM calculation through the total DCS. This allows the economical production of detailed spectral surfaces such as Figure 1, which bring out subtle variation of the DCS better than calculation at a small number of widely-spaced energies. In addition, use of the MSM for the molecular core means that a wide range of molecules, of arbitrary symmetry and complexity, may be treated. Extension of this work to polyatomic molecules (e.g., HCN, KOH) and vibrational excitation (e.g., HCl), plus a more detailed description of the LiF calculation,[11] will be reported elsewhere.

References

1. C. W. Clark and J. Siegel, J. Phys. B 13, L31 (1980).
2. L. Collins and D. W. Norcross, Phys. Rev. A 18, 467 (1978).
3. D. Dill and J. L. Dehmer, J. Chem. Phys. 61, 692 (1974).
4. J. L. Dehmer and D. Dill, Electron-Molecule and Photon-Molecule Collisions, T. Rescigno, V. McKoy, and B. Schneider, Eds., Plenum Publ. Corp., New York, 1979.
5. J. Siegel, D. Dill, and J. L. Dehmer, J. Chem. Phys. 64, 3204 (1976).
6. J. M. Blatt and L. C. Biedenharn, Rev. Mod. Phys. 24, 258 (1952).
7. M. A. Brandt, D. G. Truhlar, and R. C. Smith, Comput. Phys. Commun. 5, 456 (1973).
8. Y. Itikawa, J. Phys. Soc. Japan 27, 444 (1969).
9. Y. Itikawa and K. Takayanagi, J. Phys. Soc. Japan 26, 1254 (1969).
10. O. H. Crawford and A. Dalgarno, J. Phys. B 4, 494 (1971).
11. J. Siegel, J. L. Dehmer, and D. Dill, to be published.
12. L. Vušković, S. K. Srivastava, and S. Trajmar, J. Phys. B 11, 1643 (1978).

CLOSURE FORMULA FOR VIBRATIONAL EXCITATION IN ELECTRON-POLAR MOLECULE SCATTERING

Jon Siegel, J. L. Dehmer, and Dan Dill*

Application of the closure formula to electron-dipolar molecule scattering is straightforward if the nuclei are frozen at $R = R_e$. Here we apply it to vibrationally inelastic scattering, focussing particularly on the R dependence of exact and Born approximation T matrix elements. This R-dependence must be the same for the two levels of approximation if the closure formula is to be applied.

In our hybrid treatment[1-3] of electron-polar molecule scattering, S-matrix elements are combined from three sources: (1) Low-ℓ elements are calculated in the body frame using a potential which incorporates the molecular core interaction;[4,5] (2) intermediate-ℓ elements are calculated in the body frame using an exact formulation with a point-dipole potential;[1] and (3) high-ℓ elements are obtained in the laboratory frame using the first Born approximation with a point-dipole potential.[6,7] In the calculation of rotational transitions having $\Delta j \equiv j' - j = \pm 1$, elements from sources 1 and 2 are combined into a matrix which is transformed geometrically[8] into the laboratory frame before being combined with the Born elements, source 3. In order to calculate converged cross sections from this matrix, a closure formula[1-3,7,9,10] must be applied in the final step of the calculation, due to the large number of partial waves (> several hundred) which would otherwise be required for convergence.

Here we present the extension of the hybrid method to vibrational excitation within the constraints of the adiabatic approximation,[11] with emphasis on the validity of the closure formula. The S matrix in the vibrational adiabatic approximation is given by[12]

$$S^{v_i v_f}_{n_i n_f} = \int d\,R\, \chi_{v_f}(R)\, S_{n_i n_f}(R)\, \chi_{v_i}(R) \quad , \qquad (1)$$

*Consultant, RER Division. Permanent address: Department of Chemistry, Boston University, Boston, Mass. 02215.

where χ_v is the Hermite polynomial of order v; R is the internuclear distance coordinate; and n represents all quantum numbers besides v necessary to specify a particular (body- or laboratory-frame) molecular state so that $S_{n_i n_f}(R)$ may represent an S-matrix element from any of the three sources just mentioned, specified now as a function of internuclear distance R. In order to apply the closure formula to vibrational excitation, it is necessary to establish that matrix elements from all three sources share the same functional dependence on R. Reference 1 established this connection between sources 1 and 2, and here we will establish it between sources 2 and 3. To do this, we will first examine matrix elements in the first Born approximation (in both laboratory and body frames), whose dependence on the dipole moment is simple and analytic. Then, using exact body-frame point dipole matrix elements obtained using the closed-form point-dipole formulation,[1] we will show graphically that they approach the Born elements for sufficiently high ℓ, ℓ' and thus share the same functional dependence on the dipole moment and internuclear distance.

Assuming separability of rotational, vibrational, and electronic motion, the complete molecular wave function in the Born approximation may be written

$$\psi^{(\text{Born})}_{v,j,m_j}(\vec{R},\vec{r};\vec{k}) = \frac{1}{\sqrt{2\pi}} e^{i\vec{k}\cdot\vec{r}} \mathcal{R}_v(R)\, Y_{jm_j}(\hat{R}) \quad , \qquad (2)$$

where $(2\pi)^{-1} e^{i\vec{k}\cdot\vec{r}}$ is the electronic wave function,

$$\mathcal{R}_v(R) = R^{-1}\chi_v(R) \qquad (3)$$

is the rotational wave function, and the spherical harmonic $Y_{jm_j}(\hat{R}=\Theta_R,\phi_R)$ is the rotational wave function for a linear molecule in a Σ electronic state. $\vec{R}$ and $\vec{r}$ represent internuclear and electronic coordinates, respectively; $\vec{k}$ represents the momentum of the electron so that k^2 is its kinetic energy in Rydberg units.

Using Eq. (2), the amplitude for dipole scattering in the first Born approximation may be written

$$F(\vec{k}_i, v_i, j_i, m_{j_i} \longrightarrow \vec{k}_f, v_f, j_f, m_{j_f}) =$$

$$\frac{1}{2\pi}\iint d\vec{R}\, d\vec{r}\; \psi^{*(\mathrm{Born})}_{v_f j_f m_{j_f}}(\vec{R},\vec{r};\vec{k}_f)\; V(\vec{R},\vec{r})\, \psi^{(\mathrm{Born})}_{v_i, j_i, m_{j_i}}(\vec{R},\vec{r};\vec{k}_i) \quad , \tag{4}$$

$$V(\vec{R},\vec{r}) = -\frac{D(R)}{r^2} P_1(\hat{R}\cdot\hat{r}) \quad , \tag{5}$$

where $D(R)$ is the molecular dipole moment in a.u. as a function of internuclear distance, P_1 is the first order Legendre polynomial, and $\cos^{-1}(\hat{R}\cdot\hat{r})$ is the angle between internuclear and electronic axes.

Defining the usual coupled rotational basis functions

$$\mathcal{Y}^{LM}_{j\ell}(\hat{R},\hat{r}) \equiv \sum_{\substack{m \\ m_j}} (\ell m, j m_j | LM)\, Y_{\ell m}(\hat{r}) Y_{j m_j}(\hat{R}) \tag{6}$$

gives for the scattering amplitude, in parallel with Itikawa,[7]

$$F(\vec{k}_i, v_i, j_i, m_{j_i} \to \vec{k}_f, v_f, j_f, m_{j_f}) = 4\sqrt{\pi}$$

$$\times \sum_J \sum_{\ell_i \ell_f} i^{\ell_i - \ell_f} (\ell_f m_{j_i} - m_{j_f}, j_f m_{j_f} | J m_{j_i})$$

$$\times (\ell_i 0, j_i m_{j_i} | J m_{j_i}) (2\ell_i + 1)^{\frac{1}{2}} Y_{\ell_f m_{j_i} - m_{j_f}}(\hat{k}_f)$$

$$\times \int dr\, j_{\ell_f}(k_f r) j_{\ell_i}(k_i r) \int dR\, \chi_{v_f}(R)\, D(R)\, \chi_{v_i}(R)$$

$$\times \left\langle j_f \ell_f | P_1(\hat{R}\cdot\hat{r}) | j_i \ell_i \right\rangle_L \quad , \tag{7}$$

where

$$\left\langle j_f \ell_f | P_1(\hat{R}\cdot\hat{r}) | j_i \ell_i \right\rangle_L = \iint d\hat{R}\, d\hat{r}\; \mathcal{Y}^{*JM}_{j_f \ell_f}(\hat{R},\hat{r})$$

$$\times P_1(\hat{R}\cdot\hat{r})\, \mathcal{Y}^{JM}_{j_i \ell_i}(\hat{R},\hat{r}) \quad . \tag{8}$$

Note that if D is independent of R and $v_f = v_i$, then Eq. (7) reduces to Eq. (A.3) of Itikawa,[7] as it should. We may take advantage of the parallel with Itikawa's Eq. (A.3) to immediately write the T-matrix element in the Born approximation

$$T^{Jvv'(\mathrm{Born})}_{j\ell,j'\ell'} = \int dR\, \chi_{v_f}(R)\, T(R)\, \chi_{v_i}(R) \quad , \tag{9}$$

$$T(R) = C^{J(\mathrm{Born})}_{j\ell,j'\ell'} D(R) \quad , \tag{10}$$

$$C^{J(\mathrm{Born})}_{j\ell,j'\ell'} = -\, 4i\sqrt{k_i k_f} \int_0^\infty dr\, j_{\ell_f}(k_f r)\, j_{\ell_i}(k_i r)$$

$$\times \left\langle j_f \ell_f \left| P_1(\hat{R}\cdot\hat{r}) \right| j_i \ell_i \right\rangle \quad . \tag{11}$$

Equation (10) shows that the T-matrix element depends linearly on the dipole moment, and (9) confirms that the vibrational excitation is properly treated with the adiabatic approximation [cf. Eq. (11)]. Matrix elements (9) comprise the highest-ℓ part of the hybrid T matrix.

In order to use the closure formula to calculate vibrational excitation, it is necessary to establish that, for sufficiently high ℓ and ℓ', the exact body frame point dipole S or T matrix may be factored analogously to Eq. (10), i.e., that

$$\lim_{\ell,\ell'\to\infty} T^{\lambda}_{\ell\ell'}(D) \sim C^{\lambda}_{\ell\ell'} D \quad , \tag{12}$$

where we have suppressed the R dependence implicit in the expressed dependence on D. The closed-form point-dipole formulation[1] allows straightforward calculation of the exact T matrix, but does not furnish a simple analytic formulation for the individual elements because a matrix inversion must be performed during their calculation. Therefore, to establish the relationship (12) we turn to the Born approximation in the body frame.

Chandra[13] has shown that, for scattering from a fixed point dipole in the Born approximation, the T matrix is given by

$$T^{\lambda(\mathrm{Born})}_{\ell\ell'} = C^{\lambda(\mathrm{Born})}_{\ell\ell'} D \quad , \tag{13}$$

$$C^{\lambda(\mathrm{Born})}_{\ell\ell'} = (-)^m \, i \, 4[(2\ell+1)(2\ell'+1)]^{\frac{1}{2}} \times \begin{pmatrix} \ell & \ell' & 1 \\ \lambda & \lambda & 0 \end{pmatrix} \begin{pmatrix} \ell & \ell' & 1 \\ 0 & 0 & 0 \end{pmatrix} \frac{\sin(\ell-\ell')\pi/2}{\ell(\ell+1) - \ell'(\ell'+1)} \quad . \tag{14}$$

Because (13) clearly exhibits the desired factorization, it will be sufficient for us to establish that the exact T matrix elements approach the Born elements for high enough ℓ, ℓ'.

We show this graphically in Figure 1 for several values of λ and D. The quantity plotted is $C^{\lambda}_{\ell\ell'}/C^{\lambda(\mathrm{Born})}_{\ell\ell'}$, where [cf. Eq. (12)]

$$C^{\lambda}_{\ell\ell'} = T^{\lambda}_{\ell\ell'}(D)/D \quad , \tag{15}$$

and the exact matrix elements $T^{\lambda}_{\ell\ell'}(D)$ were obtained using the closed-form point-dipole formulation. The most striking aspect of the graph is how close the ratios are to unity, even for relatively low ℓ: The graph displays only the limited range from 0.980 to 1.002. At low ℓ, deviation from unity is greatest for small λ. As ℓ increases, the effects of λ become subordinate to the effects of D so that by $\ell = 25$, the lines are grouped in threes by dipole moment. At $\ell = 28$, all values of λ and D shown in the figure exhibit ratios close to or greater than 0.998, with those for D = 0.5 and 1.0 a.u. being treater than 0.999.

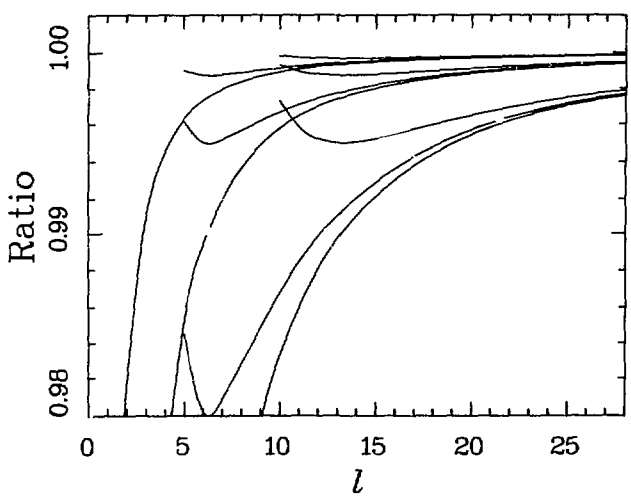

FIG. 1.--The ratio $C^{\lambda}_{\ell\ell'}/C^{\lambda(\mathrm{Born})}_{\ell\ell'}$ as a function of ℓ for $\ell' = \ell+1$, λ = 0, 5, 10 and D = 0.5, 1.0, and 2.0 a.u. Lines for λ = 0 enter from the bottom of the graph; lines for λ = 5 and 10 start at ℓ = 5 and 10, respectively. Within each λ-triplet of lines, the highest represents D = 0.5 a.u., underneath which are D = 1.0 and 2.0 in that order.

In our calculations[1-3] of differential cross sections from hybrid T matrices, we have found the ratios of 0.995 to 0.998 are sufficient for large matrix elements, with proportionately larger deviation being permissible for smaller (higher-ℓ) elements, which contribute less to the cross section.

Because Eq. (13) displays the same dependence on dipole moment (and therefore on R) as Eq. (10), this confirms graphically that the body frame vibrational matrix elements

$$T^{\lambda}_{\ell v, \ell' v'} = C^{\lambda}_{\ell \ell'} \int d\,R\, \chi_{v'}(R)\, D(R)\, \chi_{v}(R) \quad , \tag{16}$$

after geometric transformation to the laboratory frame, will join smoothly to the Born elements so long as the requirement of vibrational adiabaticity is met. The closure formula which may then be applied is (cf. Ref. 10)

$$\frac{d\sigma_{vj,v'j'}}{d\Omega} = \frac{d\sigma^{(Born)}_{vj,v'j'}}{d\Omega} - \sum_{L} (A_L^{(Born)} - A_L) P_L(\cos\phi) \quad , \tag{17}$$

$$d\sigma^{(Born)}_{vj,v'j'} = \frac{4}{3} \left(\int d\,R\, \chi_{v'}(R)\, D(R)\, \chi_{v}(R) \right)^2 \times \frac{j_>}{(2j+1)} \frac{k'}{k} (k^2 + k'^2 - 2kk' \cos\theta)^{-1} \quad , \tag{18}$$

$$k'^2 = k^2 - 2B[j'(j'+1) - j(j+1)] - \omega_e (v' - v) \quad , \tag{19}$$

where the coefficients A_L and $A_L^{(Born)}$ were calculated from the hybrid and Born T matrices, respectively, using the general formalism of Blatt and Biedenharn.[14,15]

Proper application of this formula requires that the scattering be adiabatic with respect to vibration as well as rotation. Because vibrational spacings may be as large as a few tenths of an eV, it cannot be used to as low energies as the pure rotational closure formula. Deviations from adiabaticity may be seen in the 5 to 10 eV range, and become much larger below 5 eV. However, because of the extreme economy of the overall hybrid method as described here (the intermediate-ℓ T matrix is <u>energy-independent</u>,[1] requiring calculation <u>only once</u> by a method which avoids all integration of radial equations and requires only a single matrix inversion), we have found it useful[16] to

extend our calculations as low as a few eV to investigate, e.g., gross features in e-HX (X = halogen) vibrational excitation. While such calculations cannot provide a definitive treatment of, e.g., resonance mechanisms, they can be qualitatively reliable and point the way for future calculations by more sophisticated methods which take vibrational dynamics into account.

References

1. C. Clark and J. Siegel, J. Phys. B 13, L31 (1980).
2. J. Siegel, J. L. Dehmer, and D. Dill, J. Phys. B, in press.
3. J. Siegel, J. L. Dehmer, and D. Dill, to be published.
4. J. L. Dehmer and D. Dill, Electron-molecule and photon-molecule collisions, T. Rescigno, V. McKoy, and B. Schneider, Eds., Plenum Publ. Corp., New York, p. 225 (1979).
5. D. Dill and J. L. Dehmer, J. Chem. Phys. 61, 692 (1974); J. Siegel, D. Dill, and J. L. Dehmer, J. Chem. Phys. 64, 3204 (1976).
6. Y. Itikawa and K. Takayanagi, J. Phys. Soc. Japan 26, 1254 (1969).
7 Y. Itikawa, J. Phys. Soc. Japan 27, 444 (1969).
8. See, e.g., L. Collins and D. W. Norcross, Phys. Rev. A 18, 467 (1978), Eq. (3.15).
9. O. H. Crawford and A. Dalgarno, J. Phys. B 4, 494 (1971).
10. Y. Itikawa, J. Phys. Soc. Japan 28, 1062 (1970).
11. D. M. Chase, Phys. Rev. 104, 838 (1956).
12. J. L. Dehmer, J. Siegel, J. Welch, and D. Dill, Phys. Rev. A 21, 101 (1980).
13. N. Chandra, Phys. Rev. A 12, 2342 (1975).
14. J. M. Blatt and L. C. Biedenharn, Rev. Mod. Phys. 24, 258 (1952).
15. M. A. Brandt, D. G. Truhlar, and R. C. Smith, Comp. Phys. Comm. 5, 456 (1973).
16. J. Siegel, J. L. Dehmer, and D. Dill, Vibrational Excitation in Electron-DCl Scattering, this report.

VIBRATIONAL EXCITATION IN ELECTRON-DCl SCATTERING

Jon Siegel, J. L. Dehmer, and Dan Dill*

Experimental measurements[1] of low-energy, vibrationally elastic ($v = 0 \rightarrow 0$) and inelastic ($v = 0 \rightarrow 1,2$) electron-HCl scattering show two prominent features: (1) a sharp rise at each threshold, and (2) a broader peak starting at $\sim$ 3 eV above threshold. Several contradictory explanations[2,3] of the threshold feature have been suggested, although none has been confirmed by a full ab initio calculation. Gianturco and Thompson[3] have performed fixed-nuclei, single-center calculations in the vicinity of the second feature which indicate that it is a σ shape resonance, followed at slightly higher energy by a similar resonance in the π channel.

We have initiated fixed-nuclei and adiabatic calculations of the e-HCl and e-DCl systems, which will address both of these problems directly. To our knowledge, this is the first calculation of electron impact vibrational excitation of a polar molecule to incorporate simultaneously both short-range core and longer-range dipolar vibrational effects. Our calculations are performed in the rotational[4] and vibrational[5] adiabatic approximation:[6] the use of DCl rather than HCl therefore allows calculation to substantially lower energy owing to its smaller B_e and ω_e (Table 1). However, the results presented here should still be regarded as somewhat schematic because of partial breakdown of the adiabatic approximation at the near-threshold energies involved. This paper is a preliminary report of our results; the computational methods have been detailed elsewhere[4,5] and the full tabulation of the calculational conditions will be postponed until the full report.

Eigenphase sums for the energy range 0.01 to 8 eV are shown in Figure 1. These reflect body-frame dynamics only, and are restricted to partial waves $\ell \leq 7$. The σ channel shows evidence of activity at threshold, and again starting at $\sim$ 3 eV. However, in neither case could these slight rises be

*Consultant, RER Division. Permanent address: Department of Chemistry, Boston University, Boston, Mass. 02215.

Table 1. Comparison of Spectroscopic Constants in HCl and DCl.[7]

	B_e, cm^{-1}	ω_e, cm^{-1}
HCl	10.59	2989.74
DCl	5.45	2090.78

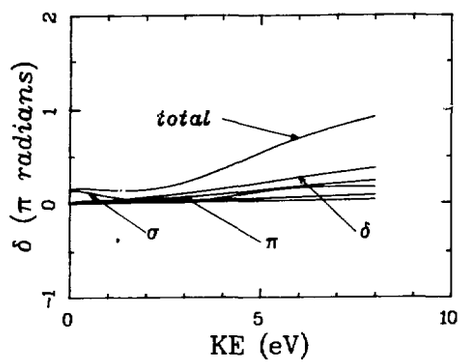

FIG. 1.--Electron-DCl scattering eigenphase sums from 0.01 to 8 eV. Note the activity in the σ channel threshold, and again starting at ∿ 3eV. However, no true resonances are present.

termed resonances in a strict sense. In contrast, Gianturco and Thompson's[3] single-center result displays very suggestive evidence of a σ resonance centered at ∿ 2.7 eV (showing a sharp rise by ∿ π/2 in the eigenphase sum), and indicates the presence of a π resonance as well. At the current stage of our investigation, we do not have an explanation for the differences between the two calculations.

In Figure 2 we present differential cross section (DCS) spectra at several angles, comparing our calculation with the experimental data of Rohr et al.[1] This comparison suggests strongly that both the threshold and higher-energy features are modeled reasonably well by our model. The threshold rise is clearly seen especially at 10° and 20°, while the later rise is seen at all angles. Further investigation is planned into the nature of these two features as revealed by, e.g., individual components of the eigenphase sums.

For the calculation of vibrational excitation, fixed-nuclei calculations were performed at nine internuclear distances and the resulting S matrices were

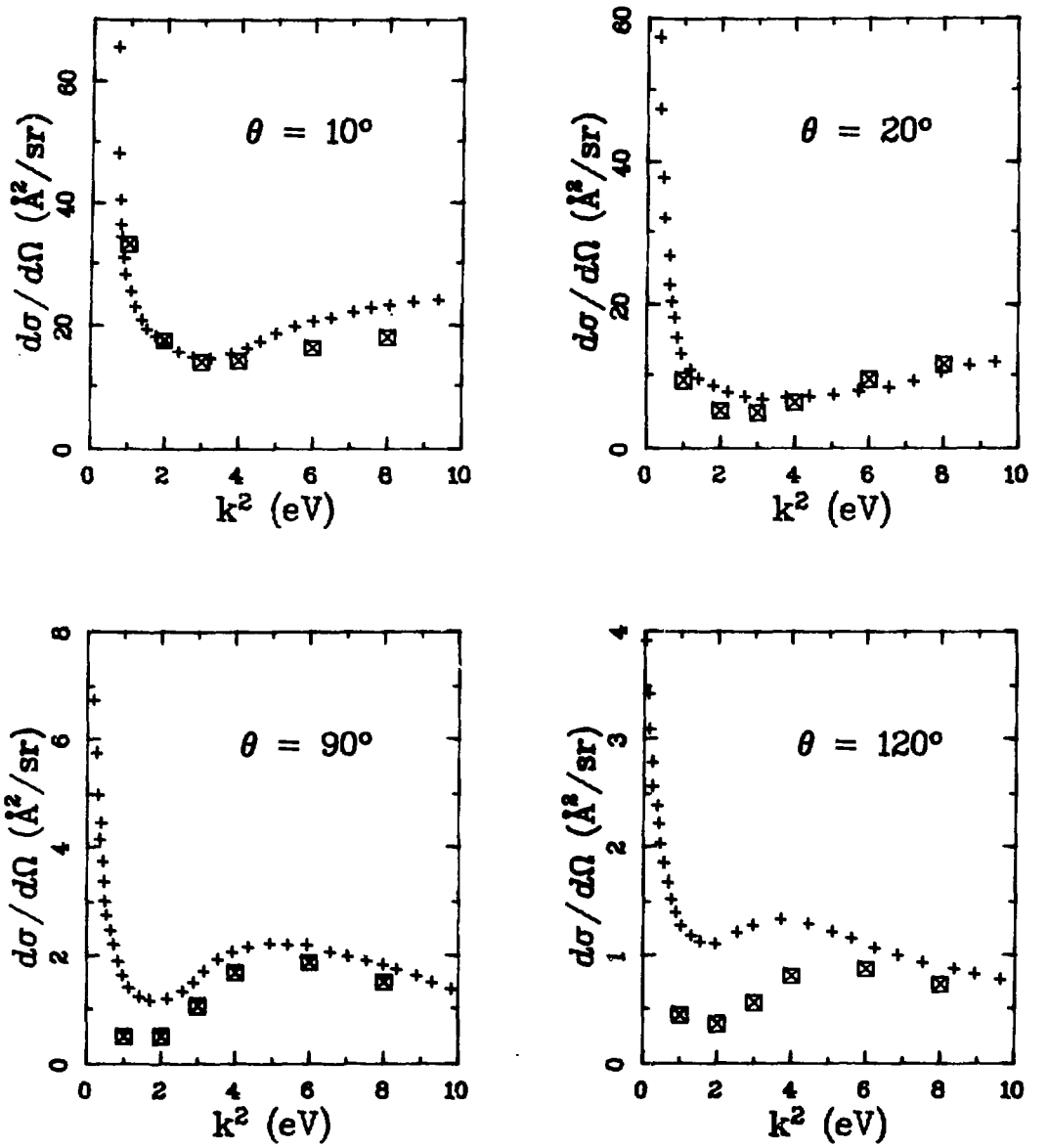

FIG. 2.--Differential cross section spectra for e-DCl scattering, presented at several angles as a function of energy. ■ , this work; +, from the experimental results of Rohr et al.[1] Results calculated at the fixed equilibrium internuclear distance $R = R_e$.

treated using the method detailed in the preceding report.[5] At present, this calculation has been performed at only one energy, 3 eV, chosen to permit the comparison with published experimental results shown in Figure 3 for both $v = 0 \rightarrow 0$ and $0 \rightarrow 1$ transitions. As is evident from the figure, the elastic DCS

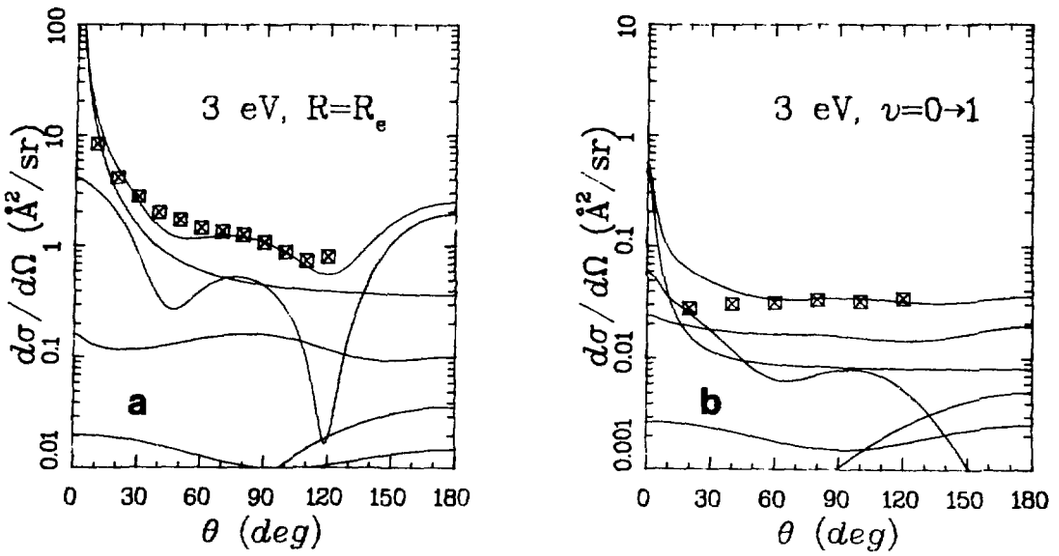

FIG. 3.--Vibrational DCS's for e-DCl scattering at 3 eV, showing rotational transition from j = 0 and total. Solid line, this work; ■ , experimental results of Rohr et al.[1] normalized at 90°. Figure 3a, vibrationally elastic as calculated at fixed R = R_e; Figure 3b, v =0 →1.

displays good agteement in basic shape, deviating slightly only in the ranges about 40° and 120°. Agreement for the v = 0 → 1 transition is good as well, with both theory and experiment being essentially flat for all except very small angles. The experimental data, which extend only to θ = 30°, never display the characteristic dipole-induced rise near θ= 0, while the theoretical points seem to start increasing in value at θ ∿ 40°, where the experimental data remain constant. We are pursuing the source of this discrepancy; however, the basic good agreement indicates that our hybrid method, with the incorporation of adiabatic vibrational excitation, can provide a realistic model of the dipole vibrational excitation process.

References

1. K. Rohr and F. Linder, J. Phys. B 8, L200 (1975);. K. Rohr and F. Linder, ibid., 2521 (1976); K. Rohr, Proc. Symp. on Electron-Molecule Collisions, Invited Papers, I. Shimamura and M. Matsuzawa, Eds., University of Tokyo, p. 67 (1979).

2. A. Herzenberg, Proc. Symp. on Electron-Molecule Collision, Invited Papers, I. Shimamura and M. Matsuzawa, Eds., University of Tokyo, p. 77 (1979) and references therein.
3. F. A. Gianturco and D. G. Thompson, J. Phys. B 10, L21 (1977).
4. C. W. Clark and J. Siegel, J. Phys. B 13, L31 (1980).
5. J. Siegel, J. L. Dehmer, and D. Dill, this report; Closure formula for vibrational excitation in electron-polar molecule scattering, J. L. Dehmer J. Siegel, J. Welch, and D. Dill, Phys. Rev. A 21, 101 (1980).
6. D. M. Chase, Phys. Rev. 104, 838 (1956).
7. G. Herzberg, Spectra of Diatomic Molecules, Van Nostrand, New York (1950).

HYBRID CALCULATION OF ELECTRON-POLAR MOLECULE SCATTERING: INTEGRATED AND MOMENTUM-TRANSFER CROSS SECTIONS FOR LiF *

Jon Siegel, J. L. Dehmer, and Dan Dill†

We describe in detail a hybrid method for calculation of electron-polar molecule scattering in which (1) low-ℓ S-matrix elements are calculated in the body frame using a potential which incorporates a realistic representation of the molecular core; (2) intermediate-ℓ elements are calculated in the body frame using an exact method with a point dipole potential; and (3) high-ℓ elements are calculated in the laboratory frame using the first Born approximation with a point dipole potential. By taking into account the dominant interactions of each ℓ-range when choosing the coordinate frame, potential, and calculational method, this hybrid framework achieves an exceptionally high level of efficiency and economy of calculation without sacrifice of accuracy. Using this method, we have calculated integrated and momentum-transfer cross sections for e-LiF scattering from 1 to 20 eV (differential cross sections have been reported

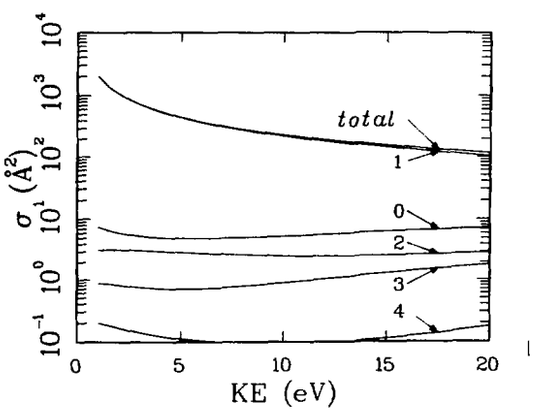

FIG. 1.--Electron-LiF scattering integrated cross sections for rotational transition from initial j =0 to indicated final j', plus total.

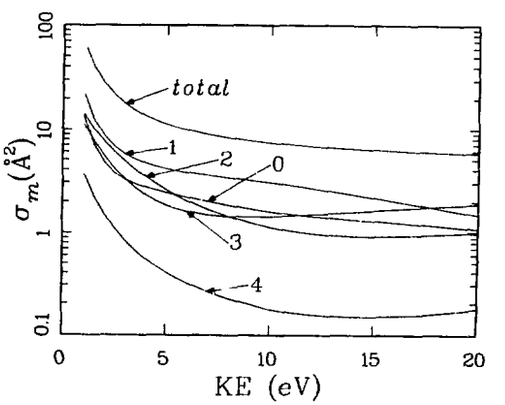

FIG. 2.--Electron-LiF scattering momentum-transfer cross sections. Notation and conditions as in Figure 1.

*Abstract of a paper to be submitted for publication.

†Consultant, RER Division. Permanent address: Department of Chemistry, Boston University, Boston, Mass. 02215.

elsewhere). The integrated cross section (Figure 1) is dominated (> 99%) by the $j = 0 \rightarrow 1$ rotational transition, whereas the momentum transfer cross section (Figure 2) is composed of comparable contributions from transitions to final $j' = 0$ through 3, owing to its de-emphasis of small-angle scattering. Eigenphase sums show no sign of resonant activity in this energy range.

ELECTRON SCATTERING FROM CsCl

Jon Siegel, J. L. Dehmer, and Dan Dill*

Cesium chloride (CsCl) is a highly polar (D = 4.09 a.u.),[1,2] 72-electron molecule whose electron scattering spectrum has been of great theoretical and experimental interest, in part because its large dipole moment exceeds the so-called "critical value" for binding of an electron.[3,4] However, no calculation[6,7] of e-CsCl scattering to date has incorporated the core potential in a realistic manner. This potential, which must reflect the strongly attractive singularities due to nuclear charges of 55 (Cs) and 17 (Cl), as well as the repulsion and exchange contributions of 72 electrons, will strongly influence the scattering at close range. In our hybrid method,[8,9] it is easily included by performing multiple-scattering calculations[10-12] for the low-ℓ partial waves. In contrast, the other hybrid method in current use[5] relies on a single-center expansion of the core potential, which might experience convergence difficulties with singularities such as occur at the Cs nucleus.

We have commenced a spectral study of e-CsCl scattering, starting with the energies 5 and 20 eV where comparison with experimental differential cross sections[13] is possible. We used the hybrid method given in Refs. 8 and 9, under calculational conditions to be presented in our full report.[14] Differential cross sections are presented in Figures 1 and 2.

At both energies, agreement is good over the entire angular range. At 5 eV (Figure 1), the calculated dip at $\sim 120°$ is more pronounced than the observed dip. This slight discrepancy persists, although to a much reduced extent, at 20 eV (Figure 2). Note that, at the higher energy, both theory and experiment display a shoulder near 30°. This is unusual behavior for dipolar scattering, which is typically extremely smooth in this angular range.

The only significant disagreement with the experimental data concerns the overall magnitude. The original data furnished to us by Vuskovic[13] were

*Consultant, RER Division. Permanent address: Department of Chemistry, Boston University, Boston, Mass. 02215.

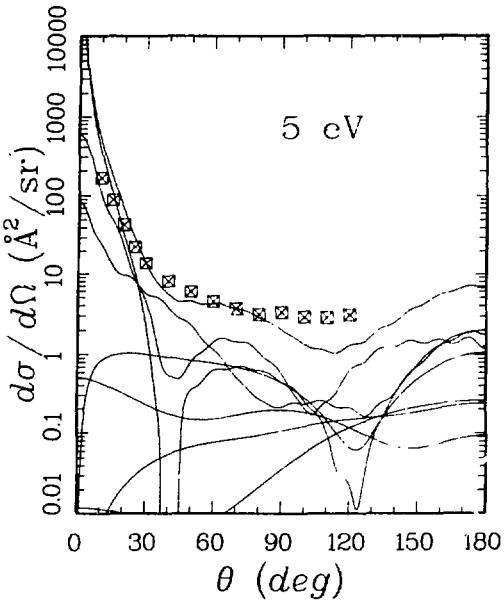

FIG. 1.--Electron-CsCl scattering differential cross section at 5 eV. Rotational partial cross sections from initial j = 0 to final j' = 0-6 are shown, but not identified owing to their complex shapes. Lower final j' dominates at small θ, and higher j' at large θ. The uppermost solid line is the total summed over j'. ⊠ , experimental results of Vuskovic, normalized at 30°.

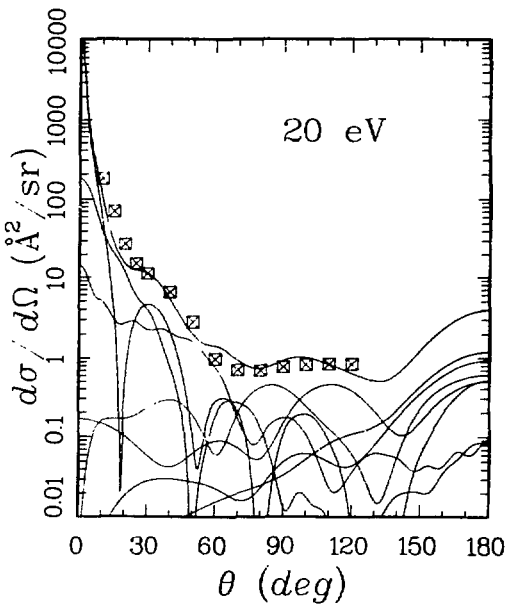

FIG. 2.--Electron-CsCl scattering differential cross section at 20 eV. Lines and symbols as in Figure 1.

in absolute units, having been normalized to the e-He cross section obtained under similar conditions in the same apparatus. However, in order to achieve the agreement shown in our figures, the absolute data had to be rescaled at both energies. In general, the dipole (small θ) component of the differential cross section should behave as E^{-1}, as do our results. The absolute results of Vuskovic, however, do not, leading us to believe that the difficulty lies with the experimental normalization.

References

1. A. J. Hebert, F. J. Lovas, C. A. Melendres, C. D. Hollowell, T. L. Story, and K. Street, J. Chem. Phys. 48, 2824 (1968).
2. R. L. Matcha and S. C. King, J.A.C.S. 98, 3420 (1976).
3. W. R. Garrett, Mol. Phys. 24, 465 (1972).
4. W. G. Becker, M. G. Fickes, R. C. Slater, and R. C. Stern, J. Chem. Phys. 61, 2283 (1974), but see Ref. 5 for a critical evaluation of Becker et al.'s data analysis.
5. L. Collins and D. W. Norcross, Phys. Rev. A 18, 467 (1978).
6. K. Onda, J. Phys. Soc. Japan 40, 1437 (1976).
7. M.R.H. Rudge, J. Phys. B 7, 1323 (1974).
8. C. Clark and J. Siegel, J. Phys. B 13, L31 (1980).
9. J. Siegel, J. L. Dehmer, and D. Dill, to be published.
10. D. Dill and J. L. Dehmer, J. Chem. Phys. 51, 692 (1974).
11. J. Siegel, D. Dill, and J. L. Dehmer, J. Chem. Phys. 64, 3204 (1976).
12. J. L. Dehmer and D. Dill, Electron-Molecule and Photon-Molecule Collisions, T. Rescigno, V. McKoy, and B. Schneider, Eds., Plenum Publ. Corp., New York (1979).
13. M. Vuskovic, to be published.
14. J. Siegel, J. L. Dehmer, and Dan Dill, to be published.

ELECTRON SCATTERING FROM HCN

Jon Siegel, J. L. Dehmer, and D. Dill*

Using our recently-developed hybrid model[1,2] of electron-polar molecule scattering, we have calculated scattering of electrons from first-row diatomics (LiF);[2,3] large, strongly polar systems (CsCl);[4] and systems showing pronounced vibrational effects (HCl, DCl).[5] The extension to HCN, for which initial results are reported here, marks both (1) the first such calculation on a polyatomic molecule, and (2) the first such calculation on a strongly polar system expected to display a characteristic shape resonance within a few eV of threshold. This resonance is related to the 2.4 eV π_g resonance[6] in N_2, with which HCN is isoelectronic. (Note that Gianturco and Thompson[7] calculated shape resonance in e-HCl scattering, but this molecule's dipole moment is so weak that no special techniques had to be used to accommodate it.)

A detailed account of the hybrid calculational method[1,2] has already been published; parametric details of the calculation will be given in our full report. Figures 1 to 3 compare our differential cross section (DCS) results with the experimental data of Srivastava et al.[8] at 3, 5, and 11.6 eV. At all three energies the agreement in shape is generally good, demonstrating that the core as well as the longer-ranged dipole interactions are modeled well by our hybrid treatment. The experimental data had to be renormalized to obtain such good agreement, as did the CsCl data[4] provided by the same group. At this early stage of our investigation, we are not able to say where the source of this discrepancy in magnitude lies.

The most significant part of this investigation concerns the expected π-channel shape resonance, whose study will require calculation on a much finer energy mesh than is presented here. Such resonances are accompanied by a sharp rise of $\sim \pi$ radians in the eigenphase sum associated with their particular channel; trial calculations by us,[9] for which the dipole potential was omitted

*Consultant, RER Division. Permanent address: Department of Chemistry, Boston University, Boston, Mass. 02215.

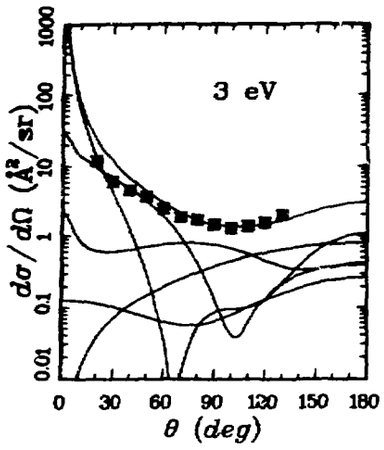

FIG. 1.--Differential cross section for e-HCN scattering at 3 eV. Solid lines, rotational partial DCS's from initial j = 0 to final j' = 0-6 (unlabeled), and their sum (uppermost line). Symbols ■, experimental data of Srvistava et al.,[8] normalized at 90°.

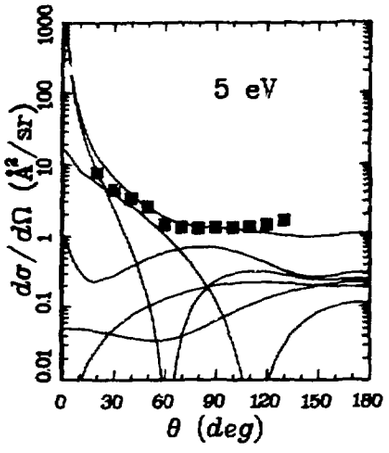

FIG. 2.--As for Figure 1, but at 5 eV.

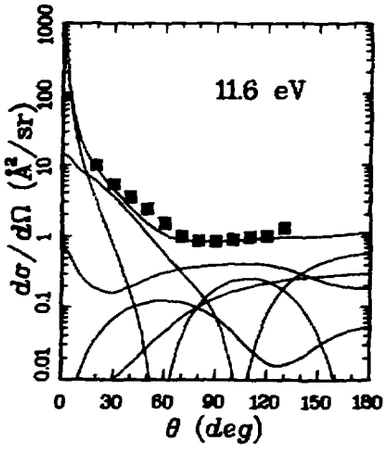

FIG. 3.--As for Figure 1, but at 11.6 eV.

for economy, clearly showed such a rise in the π channel in the expected energy range. The enhancement of the integrated cross section associated with this resonance is expected to be $\sim$ 10 to 25 $\mathring{A}^2$, far smaller than the "background" cross sections due to the HCN dipole moment. However, the dipole cross section is restricted to small θ, while resonant scattering is not. Therefore, we expect to see marked resonance effects in both the DCS and momentum-transfer cross section spectra.

References

1. C. Clark and J. Siegel, J. Phys. B 13, L31 (1980).
2. J. Siegel, J. L. Dehmer, and D. Dill, to be published.
3. J. Siegel, J. L. Dehmer, and D. Dill, J. Phys. B, in press.
4. J. Siegel, J. L. Dehmer, and D. Dill, "Electron Scattering from CsCl," this report.
5. J. Siegel, J. L. Dehmer, and D. Dill, "Vibrational Excitation in Electron-DCl Scattering," this report.
6. See, e.g., J. Siegel, J. L. Dehmer, and D. Dill, Phys. Rev. A 21, 85 (1980).
7. F. A. Gianturco and D. G. Thompson, J. Phys. B 10, L21 (1977).
8. S. K. Srivastava, H. Tanaka, and A. Chutjian, J. Chem. Phys. 69, 1493 (1978).
9. W. Kosman, J. Siegel, J. L. Dehmer, and D. Dill, to be published.

A PROPOSED TECHNIQUE FOR THE ABSOLUTE MEASUREMENT OF THRESHOLD STRUCTURES IN THE TOTAL VIBRATIONAL EXCITATION CROSS SECTIONS OF MOLECULES BY ELECTRON IMPACT

P. D. Burrow and D. Spence

Many recent electron-impact excitation experiments have revealed the existence of sharp structures tens of meV wide or less, at the threshold for excitation of vibrational levels of diatomic and polyatomic molecules,[1] and at the threshold for electron-impact excitation of electronic states of atoms and molecules.[2] Measurements indicate that in the case of vibrational excitation, these threshold structures cannot be explained solely on the basis of the molecular permanent dipole moment. Attempts have been made by Taylor et al.[3] to interpret HCl vibrational threshold structures on the basis of a resonance model, and by Dube and Herzenberg[4] from a consideration of virtual states. However, the real physical mechanisms responsible for the observed threshold structures remain unclear,[5] and any additional inforration concerning such structures is clearly of value.

In the case of most molecules studied to date, the physical reality of these structures is in no doubt. However, in other molecules such as CO_2, the widths of the observed structures are very narrow and there is some question as to whether the observed structures may be of an instrumental nature. This question arises because most observations of threshold structures have been made by electrostatic analyzers, where instrumental transmission properties for almost zero energy scattered electrons are notoriously difficult to characterize. One technique in which the "transmission" function remains constant down to essentially zero energy (within the instrumental resolution) is the trapped electron technique.[6] Unfortunately the resolution of the trapped electron technique is, in general, too poor ($\geq$ 80 meV, typically) to observe very narrow threshold structures.

However, it has recently been pointed out, and demonstrated,[7] that the measured ratio of two (or more) inelastic cross sections is totally independent of instrumental resolution. Consequently, a measurement of the ratio of a

cross section which peaks at threshold to one which decreases monotonically towards threshold will show a rapid increase as the scattered electron energy approaches zero from above. Spence[7] has recently demonstrated the existence of a sharp structure of width < 1 meV in He 2^1S cross section by a measurement of the $^1S/^3S$ ratio, even though the instrumental resolution was more than 100 times larger than the width of the structure. We propose that sharp structures in vibrational excitation cross sections be measured by this technique by making such measurements in a mixture of the gas in question and molecular hydrogen. The v = 1 level of H_2, at $\sim$ 0.52 eV is sufficiently far removed from vibrational levels of most other molecules for this measurement to be feasible. Moreover, the cross section for electron-impact excitation of the v = 1 level of H_2 is known to decrease monotonically towards threshold from above, and the slope of the cross section is known absolutely.[8] Consequently, it should be a relatively straightforward procedure to determine the magnitude of threshold structures in other gases on an absolute basis. The best resolution available to the trapped electron technique ($\sim$ 80 meV)[9] is sufficient to fully resolve the H_2 v = 1 level from at least the first vibrational level of all other gases.

References

1. K. Rohr, Proc. Symp. on Electron Molecule Collisions, Invited Papers, I. Shimamura and M. Matsuzawa, Eds., University of Tokyo, pp. 67-76 (1979).
2. N. Bose and F. Linder, Proc. Symp. on Electron Molecule Collisions, Invited Papers, I. Shimamura and M. Matsuzawa, Eds., University of Tokyo, pp. 179-186 (1979).
3. H. S. Taylor, E. Goldstein, and G. A. Segal, J. Phys. B 10, 2253 (1977).
4. L. Dube and A. Herzenberg, Phys. Rev. Letters 38, 820 (1977).
5. A. Herzenberg, Proc. Symp. on Electron Molecule Collisions, Invited Papers, I. Shimamura and M. Matsuzawa, Eds., University of Tokyo, pp. 77-94 (1979).
6. G. J. Schulz, Phys. Rev. 112, 150 (1958).
7. D. Spence, J. Phys. B: Atom. Molec. Phys. 13, L73 (1980).
8. P. D. Burrow and G. J. Schulz, Phys. Rev. 187, 97 (1969).
9. M. Michejda, Electron Scattering from Vibrationally Excited Nitrogen, Thesis, Yale University (1977).

TECHNIQUE TO ENHANCE AND SEPARATE NEGATIVE IONS FROM NEUTRAL AUTOIONIZING FEATURES IN SCATTERED ELECTRON SPECTRA IN THE IONIZATION CONTINUUM: APPLICATION TO NEGATIVE IONS IN NEON *

David Spence

Identification of autoionizing states in scattered electron, positive ion, and unresolved photoemission spectra following electron-impact excitation is often hindered by additional structures caused by the decay of Feshbach resonances (negative ions) associated with those autoionizing states. We describe a technique whereby negative ion structures in scattered electron spectra may be enhanced and energetically separated from structures caused by neutral autoionizing states, providing for an unambiguous identification. We apply this technique to negative ion states in Ne in the energy region 40 to 50 eV, where we locate 11 negative ion resonances. From a systematic study of possible neutral parent states, electron configurations are assigned to the 12 known resonances in this energy region. Our assignments are in good agreement with previous identifications, where comparisons can be made with other techniques.

Table 1. Comparison of N_e^- energies in eV, obtained in present experiments, with previous data

Present experiment	Sanche and Schulz[1]	Wilden et al.[2]	Roy et al.,[3]	Bolduc et al.[4]	Veillette and Marchand [5]	Mean value
42.13	41.98	42.10	42.11			42.08
43.09	43.05		43.07	43.12	43.0	43.06
43.71	43.67	43.68	43.67	43.72		43.69
44.00		44.04	44.06		44.10	44.05
44.37	44.35	44.40	44.36			44.37
45.15	45.18	45.18	45.18			45.17
45.42	45.43	45.47	45.39	45.41		45.42
46.59	45.58	46.50	46.39			46.52
46.89	46.86				46.90	46.88
47.61	47.58	47.60				47.60
		48.00				48.00
49.06	49.03		49.05	49.02		49.04

*Summary of a paper to appear in J. Phys. B: Atom. Molec. Phys.

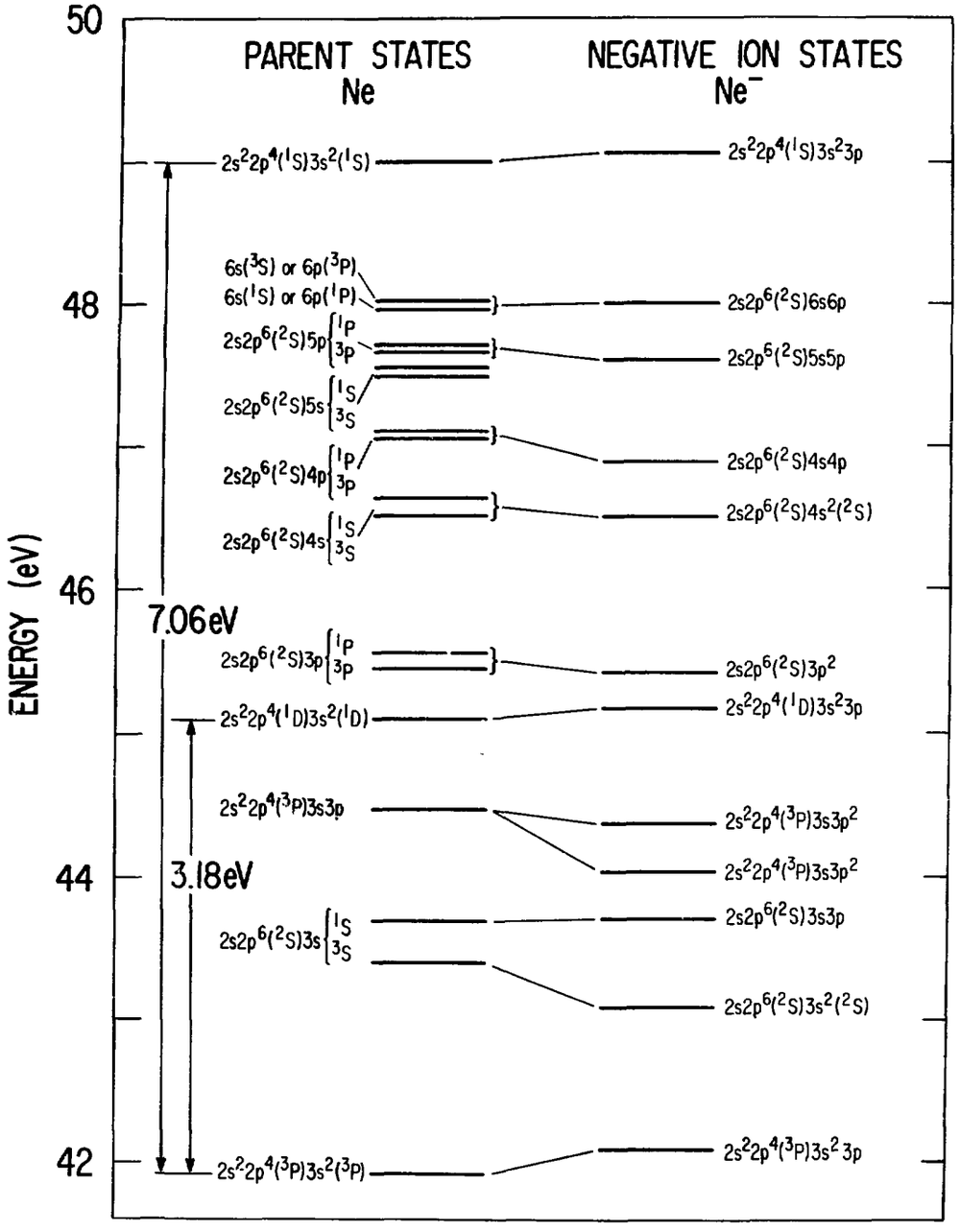

FIG. 1.--Energy level diagram and electron configurations of negative ion states observed in the 40 to 50 eV region of Ne, together with those of their probable parent states. (ANL neg. 149-79-142 R1)

Table 2. Comparison of electron configurations of Ne^- resonances from present and previous experiments. Where there is agreement between different experiments, the configurations are underlined. The resonance energies listed are the mean values from Table I.

Resonance energy, eV	Resonance Configurations			
	Present	Wilden et al. [2]	Roy et al. [3]	Sanche and Schulz 1†
42.08	$\underline{2s^2 2p^4(^3P)3s^2 3p}$	$\underline{2s^2 2p^4(^3P)3s^2 3p}$	$\underline{2s^2 2p^4(^3P)3s^2 3p(^2P)}$	$2s^2 2p^4(^3P)3s^2$
43.06	$\underline{2s2p^6(^2S)3s^2(^2S)}$	$\underline{2s2p^6(^2S)3s^2(^2S)}$	$\underline{2s2p^6(^2S)3s^2(^2S)}$	$2s2p^6(^2S)3s$
43.69	$\underline{2s2p^6(^2S)3s3p}$	$\underline{2s2p^6(^2S)3s3p}$	$\underline{2s2p^6(^2S)3s3p(^2P)}$	$2s2p^6(^2S)3s$
44.05	$\underline{2s^2 2p^4(^3P)3s3p^2}$	$2s2p^6\ 3s3p$	$\underline{2s^2 2p^4(^3P)3s3p^2(^2S)}$	
44.37	$\underline{2s^2 2p^4(^3P)3s3p^2}$		$\underline{2s^2 2p^4(^3P)3s3p^2(^2D)}$	$2s^2 2p^4\ 3s3p$
45.17	$\underline{2s^2 2p^4(^1D)3s^2 3p}$	$\underline{2s^2 2p^4(^1D)3s^2 3p}$	$2s2p^6 3p^2(^2S)$	
45.42	$\underline{2s2p^6(^2S)3p^2}$	$\underline{2s2p^6(^2S)3p^2}$	$2s^2 2p^4(^1D)3s^2 3p(^2P)$	
46.52	$\underline{2s2p^6(^2S)4s^2(^2S)}$	$\underline{2s2p^6(^2S)4s^2(^2S)}$	$\underline{2s2p^6(^2S)4s^2(^2S)}$	
46.88	$2s2p^6(^2S)4s4p$			
47.60	$2s2p^6(^2S)5s5p$			
48.00	$2s2p^6(^2S)6s6p$			
49.04	$\underline{2s^2 2p^4(^1S)3s^2 3p}$		$\underline{2s^2 2p^4(^1S)3s^2 3p(^2P)}$	

†Probable parent state configuration only.

The results of our measurements are tabulated in Tables 1 and 2, together with comparisons with energies and electron configurations of various Ne^- states obtained by previous workers. Figure 1 is an energy level diagram showing Ne^- states obtained in the present experiments, together with the energy levels of their probable parent autoionizing state.

Reference

1. L. Sanche and G. J. Schulz, Phys. Rev. A 5, 1672 (1972).

COMPARISON OF ENERGY LEVELS OF AUTOIONIZING STATES OF Ne OBTAINED BY NEAR-THRESHOLD ELECTRON-IMPACT TECHNIQUES*

D. Spence

Studies of autoionizing states of Ne by near-threshold electron impact have included the scattered electron measurements of Grissom et al.[1] and Spence,[2,3] electroionization measurements of Bolduc et al.,[4,5] broadband photon measurements of Veillette and Marchand,[6] and ejected electron spectra of Sharp et al.[7] and Wilden et al.[8] However, when a comparison of the energy location of autoionizing states is made, as shown in Figure 1, it is clear that the discrepancies among the various experiments is often well outside the quoted experimental error of 0.05 eV. Some of these near-threshold electron-impact measurements have given autoionizing state energies and identifications which may be in doubt for the following reasons.

Sharp et al.[7] suggested that electroionization measurements and broadband photon measurements may be subject to postcollision interaction (PCI) effects (Read,[9,10] and references therein), yielding incorrect energies in some cases. Additionally, Wilden et al.[8] suggested that these same spectra may also be contaminated by unidentified Feshbach (negative ion) resonances. Spence[3] has recently confirmed that the former suggestion is indeed correct for electroionization measurements. In the present report, we demonstrate that the latter suggestion of Wilden et al.[8] is true for broadband photon measurements, but not for electroionization measurements. Furthermore, we demonstrate that

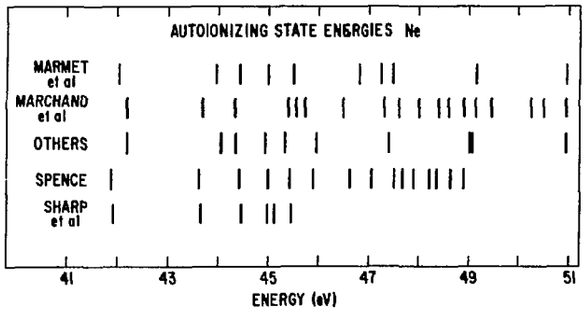

FIG. 1.--Comparison of energy levels of autoionizing states in Ne obtained by different threshold and near-threshold electron-impact techniques, showing large discrepancies among the various techniques. (ANL neg. 149-80-24)

*Synopsis of part of a paper submitted for publication.

broadband photon measurements are unaffected by PCI. The threshold scattered electron measurements of Grissom et al.[1] are, of course, also subject to PCI effects, and we show that their spectra exhibit only neutral autoionizing states and not a superposition of neutral- and negative-ion states as the authors believed.

1. Broadband Photon Spectra

Comparison of Energy Levels

The suggestion by Wilden et al.[8] that broadband photon spectra may contain negative-ion structures arose from their observation that some structures in the data of Veillette and Marchand[6] occurred near energies of know Feshbach resonances. A detailed comparison of such energy levels is now possible following several recent experiments which have accurately located many Feshbach resonances in the autoionization region.[11] The results of this comparison are shown in Figure 2 where the center column lists the energies of structures observed by Veillette and Marchand[6] in broadband photon spectra. Where they had, in fact, identified Feshbach resonances as such, we have indicated these levels by the zero above the level. In the right-hand column we show the energy levels of Feshbach resonances known to exist in this energy region. We have used the mean values of several authors as tabulated by Spence.[11] One should note that the energy differences between the six different sets of data tabulated by Spence[11] rarely exceeded 0.025 eV. In the left-hand column of Figure 2, we have listed all the known reliable energy levels of autoionizing states compiled from the many different techniques listed in Section 3 of this paper. Excluding the 3 structures identified by Veillette and Marchand[6] as negative-ion states, we find 9 other resonances to be only an average of 0.039 eV displaced from broadband photon structures. This is within the error and energy resolution quoted by the authors. On the other hand, these same broadband photon structures are, on the average, 0.096 eV displaced from the listed neutral autoionizing states, which is outside the quoted experimental error and resolution of Veillette and Marchand.[6] There does occur some correspondence between broadband photon structures and known neutral states, as is indeed expected, but Figure 2 demonstrates that agreement with resonance spectra is much closer where resonances are known to exist.

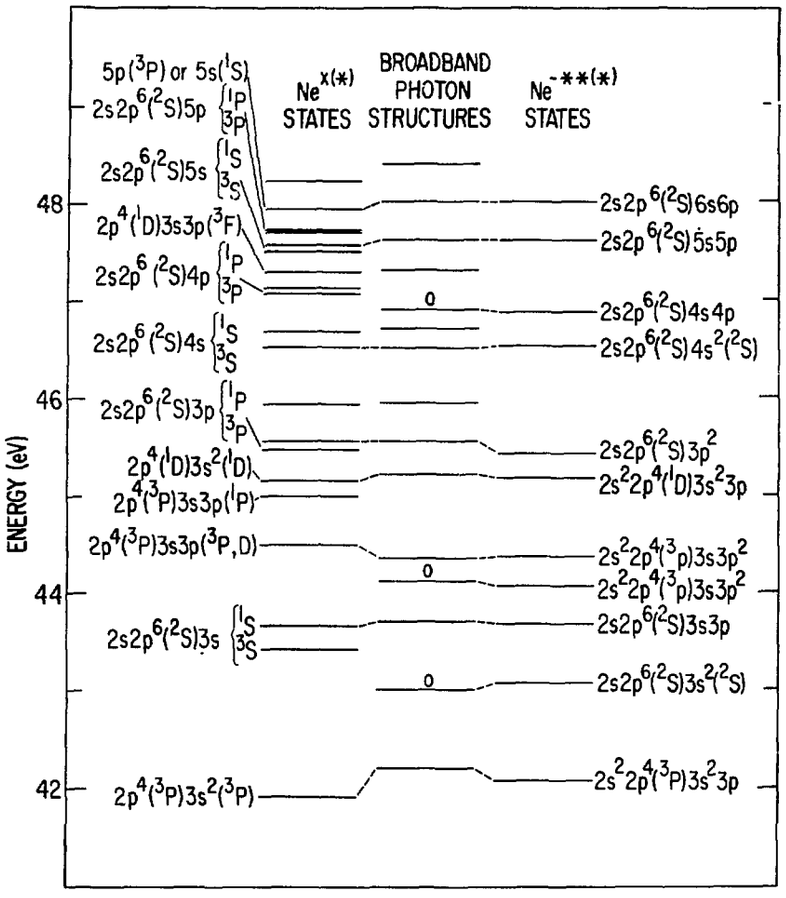

FIG. 2.--Energy level diagram showing a comparison between the energy locations of structures observed in the threshold electron-impact broadband photon detection spectrum of Veillette and Marchand[6] and those of known negative ion[11] and neutral autoionizing states.[12] The three states identified as negative ions by Veillette and Marchand are indicated by the zero above the energy level. Energy levels derived from broadband photon spectra are on the average only 39 meV from known negative ion resonances, within the error and resolution of the broadband photon experiments. These same structures are an average of 96 meV removed from known neutral autoionizing states, outside the error quoted in the broadband photon experiments. (ANL neg. 149-80-14)

Comparison of Threshold Scattered Electron and Broadband Photon Spectra

Before making a comparison between threshold scattered electron and broadband photon spectra, we must first ask, "Are Feshbach resonances expected to appear as strong features in broadband photon spectra in Ne?"

From a comparison of neutral- and negative-ion structures in resonance-enhanced threshold electron spectra, broadband photon spectra, and electroionization spectra in He, we have been able to show[12] that the ratio (negative ion/neutral) structure from the three types of experiment occurs in the ratio 2:1:1, respectively, i.e., resonance (negative ion) structures in broadband photon spectra will be about half as strong as in resonance-enhanced scattered electron spectra, when compared to neutral features. Furthermore, the above comparison in He suggests that whereas PCI energy shifts are observed in scattered electron and electroionization spectra, PCI is inoperative in this respect in broadband photon spectra.

With the knowledge that broadband photon data will contain resonance structures of about half the relative strength as in our resonance-enhanced spectra, and that broadband photon spectral features are almost certainly unaffected by PCI energy shifts, we show a comparison between our resonance-enhanced threshold scattered electron broadband photon spectra and the broadband photon spectrum of Marchand[6] in Figure 3.

Note that our "resonance-enhanced"[11,12] threshold spectra are very different in shape from the purely inelastic scattered electron spectrum, the latter containing only neutral autoionizing states. The locations of negative-ion resonances in the lower spectrum of Figure 3 are indicated by the straight vertical lines. Although the locations of several resonances in this spectrum are obvious, most of them can only be obtained unambiguously from a previous publication.[11] The whole of the lower spectrum of Figure 3 is, in fact, completely dominated by the often overlapping resonances, and it is not possible to extract any neutral state energies unambiguously from this spectrum. Although the indicated resonance structures are smaller than the underlying neutral structures in the broadband photon spectrum in the upper trace of Figure 3 (by about a factor of 2, as expected from the above argument), the

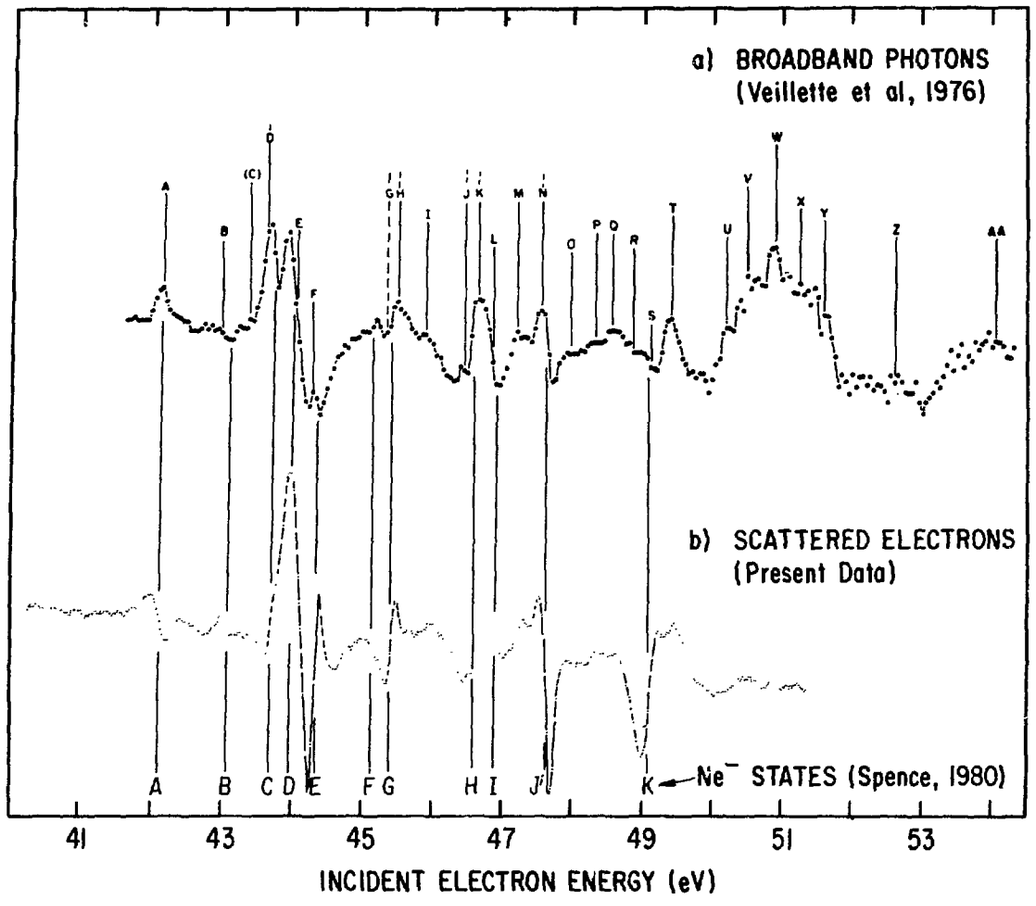

FIG. 3.--Comparison between broadband photon spectrum (upper curve), Veillette and Marchand[6] and the present threshold scattered electron spectrum with enhancement of negative-ion structures (lower curve). The resonance locations in the lower spectrum obtained by Spence[11] are shown by the vertical lines marked A to K. Structures identified as neutral autoionizing states by Veillette and Marchand[6] are labeled A to Z in the upper spectrum. The great similarity between the two spectra is discussed in the text. In addition to demonstrating that many strong features in the broadband photon spectrum are caused by previously unidentified negative ions, this figure provides evidence that the broadband photon spectrum is not subject to energy shifts caused by postcollision interactions. Note specifically the large peak due to the $(2s2p^6 3s)^1S$ in the lower spectrum which is shifted by PCI to 44.12 eV and split by resonance E, is unshifted from its true threshold of 43.66 eV in the broadband photon spectrum, and is split instead by resonance D.
(ANL neg. 149-80-23)

similarity between the two curves is striking. The similarity of the broadband photon curve to the present "resonance-enhanced" scattered electron spectrum suggests that it is also dominated by a convolution of resonance structures. At first glance, it would appear that a major difference in the two spectra of Figure 3 occurs in the energy location of the large double feature centered on 43.66 eV in the upper spectrum, and at slightly higher energy, 44.12 eV, in the lower spectrum. The reason for this is the PCI shift of neutral states in the threshold scattered electron spectrum, but not, as argued above, in the broadband photon spectrum. This shift causes the large neutral $2s2p^6\ ^1S$ state feature to be shifted upwards by about 0.4 eV from its true threshold in the scattered electron spectrum, the $3s\ ^1S$ structure being split by the overlapping resonance labeled E. This state is not shifted in the broadband photon spectrum and occurs at its true threshold of 43.66 eV, overlapping and being split by resonance D. This is the only notable difference in the two spectra, and is, in fact, additional support for our suggestion that broadband photon spectra in Ne, at least, are not subject to PCI threshold shifts, but are completely dominated by resonance structures.

2. Comparison with Electroionization Measurements

In the electroionization technique, structures are observed in the total ionization cross section as the incident electron energy is swept through the autoionization region. These structures arise from decay of both negative-ion states, $e + X \rightarrow (X^{**-}) \rightarrow X^+ + 2e$, and the neutral autoionizing states, $e + X \rightarrow X^{**} + e$, followed by $X^{**} \rightarrow X^+ + e_{ejected}$. However, for reasons similar to those given above for broadband photon spectra, electroionization measurements have been criticized as being subject to misidentification of negative-ion and neutral-autoionizing states, and also to PCI energy shifts. From a series of curve-fitting procedures, Bolduc et al.[4,5] were able to identify several of the most prominent features in their Ne electroionization spectrum as arising from decay of negative-ion resonances. There is little correlation in energy of the 10 features in the electroionization spectrum of Bolduc et al.,[4,5] not identified as negative-ion states by them, with other known negative-ion states (in

contrast with the broadband photon spectrum). It appears, therefore, that, in general, electroionization spectral analyses have not confused negative-ion states and neutral-autoionizing states.

However, there is considerable evidence that electroionization spectral features are subject to large energy shifts because of PCI. This effect is graphically illustrated in Figure 4, which is an energy level diagram showing a comparison between the energy locations of neutral autoionizing states obtained from electroionization spectra (set a) and from the present threshold scattered electron spectra[12] (set b). The excellent agreement in energy between these two sets of data is obvious, and is as expected from the above discussion. However, our threshold electron spectra are known to give incorrect energies because of PCI. The corrected energy locations of this set of states, obtained by using higher analysis energies[11] and thus eliminating PCI effects, are shown in Figure 4 as set c, the shift in energies being indicated by the sloping dashed lines. For the sake of completeness, we have included in Figure 4 a set of energy levels shown by lighter lines, obtained from techniques where PCI is not a complicating issue.[11,12] Note that there is no disagreement between set a and set b, although many disagreements between set a and the energetically correct set c are obvious.

3. Comparison with Previous Threshold Scattered Electron Spectra

Previous studies of near-threshold scattered-electron spectra in neon in the energy range 40 to 50 eV have been made by Grissom et al.[1] A comparison between the spectrum of Grissom et al.[1] and the present near-threshold spectrum[12] shows them to be essentially identical, although more fine structure is apparent in the present experiments because of the slightly better resolution. From the excellent energy calibration in their spectrum, Grissom et al.,[1] recognized that none of the features in their spectrum, except that located at 45.53 eV, coincided with any then known neutral-autoionizing state of Ne. The reason for this lack of agreement is, of course, now known to be due to PCI energy shifts, although this mechanism was unknown to the authors at the time of publication. Figure 4 shows the PCI threshold shift of the 45.53 eV peak to

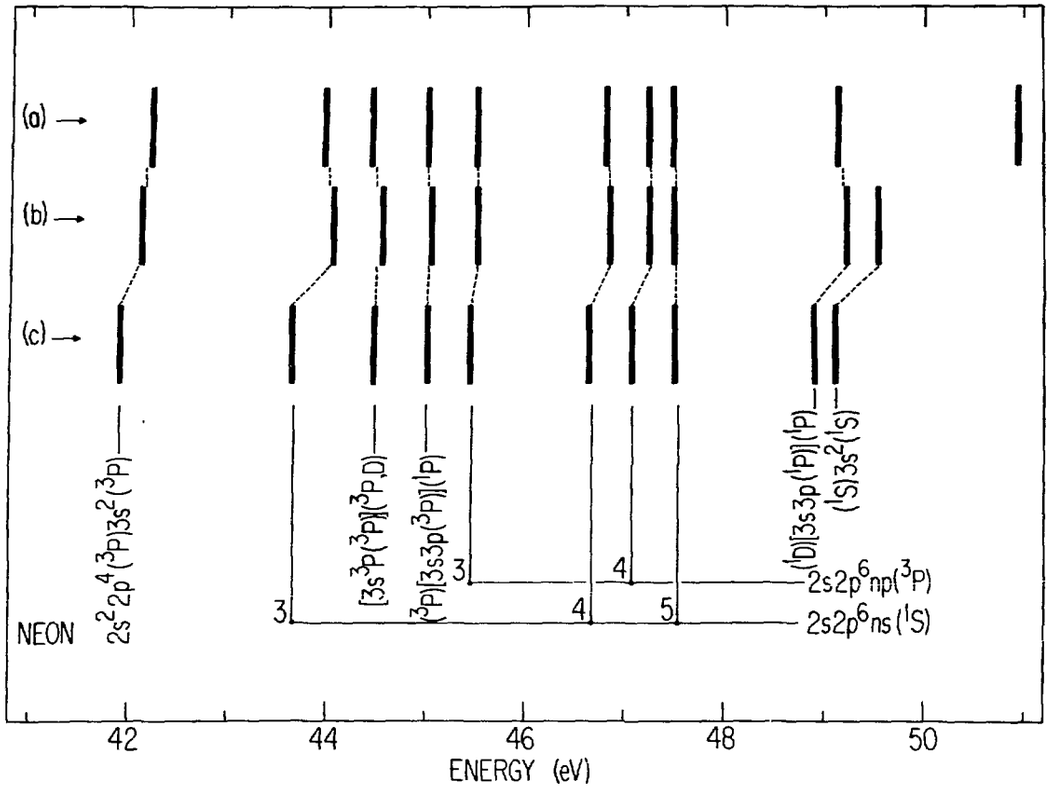

FIG. 4.--Comparison of energy levels of autoionizing states in Ne obtained by Bolduc et al.[4,5] from electroionization spectra (set a), present threshold scattered electron spectrum (set b), and the 1.9 eV residual scattered electron energy spectrum of Figure 2 (set c), in which the postcollision interaction energy level shifts have been eliminated. Known locations of autoionizing states[12] are listed at the bottom. This figure vividly demonstrates that the threshold electron-ionization spectrum of Bolduc et al.[4,5] is serously affected by PCI and cannot, in general, provide correct threshold energies of short-lived autoionizing states. (ANL neg. 149-80-17 Rev. 1)

be very small, of the order of 0.05 eV, explaining the agreement of Grissom et al.[1] with previous data. Because of lack of agreement between the rest of the structures in their spectrum with known neutral energy levels, Grissom et al.[1] suggested they may all be caused by decay of negative-ion resonances, especially the peak at 44.00 and dips at 44.51 and 49.86 eV. All of these features are reproduced in the present threshold spectra[12] which have been shown here and in a previous publication,[11] to be free of any negative-ion

resonance structures. In particular, it was shown unambiguously[11,12] that none of the features in the threshold scattered electron spectra are negative-ion resonances. One must conclude that none of the structures in the threshold trapped electron spectra of Grissom et al.[1] were negative-ion resonances either.

Conclusions

The most important conclusions of the present report can be summarized as follows:

1. From a detailed comparison between the present near-threshold scattered electron spectra and broadband photon spectra, we conclude that the broadband photon technique of Marchand and co-workers[6,13-15] appear not to be subject to near-threshold PCI energy shifts.

2. We have demonstrated that broadband photon spectra are, however, in the case of Ne and He at least, completely dominated by negative-ion resonance structures. This has resulted in the misidentification of resonances as neutral autoionizing states in broadband photon spectra. It is not possible, using the broadband photon technique alone, to separate negative-ion and neutral features, and this technique thus appears unsuited to the spectroscopy of autoionizing states.

3. In spectra obtained by the electroionization technique of Marmet and co-workers[4,5,16] it is possible by curve fitting to separate negative-ion and neutral features, and criticism of misidentification of structures, for these reasons, appear to be unfounded.

4. We have conclusively demonstrated that electroionization do suffer exactly the same PCI-induced energy shifts as do threshold scattered electron spectra. Unlike threshold scattered electron techniques, the electroionization technique has no adjustable experimental parameter by which the PCI-induced energy shift can be determined. It appears, therefore, that the electroionization technique is also unsuited to the location of neutral autoionizing states.

5. Through lack of knowledge of the PCI mechanism, structures observed in previous near-threshold trapped-electron spectra in Ne in the energy range 41 to 52 eV had been misinterpreted by Grissom et al.[1] as Feshbach

resonances when, in fact, none were present.

6. Though we have made no detailed comparison here, it is likely by extension of arguments given above that electron scavenger-type threshold techniques will also be unsuitable for location of autoionization states, as this technique also is unable to account for PCI shifts.

References

1. J. J. Grissom, W. R. Garrett, and R. N. Compton, Phys. Rev. Lett. 23, 1011-1014 (1969).
2. D. Spence, J. Phys. B: Atom. Molec. Phys. 11, L243-L247 (1978).
3. D. Spence, J. Chem. Phys. 68, 2980-2981 (1978).
4. E. Bolduc, J. J. Quenmener, and P. Marmet, J. Chem. Phys. 57, 1957-1966 (1972).
5. E. Bolduc and P. Marmet, Can. J. Phys. 51, 2108-2113 (1973).
6. P. Veillette and P. Marchand, Can. J. Phys. 54, 1208-1215 (1976).
7. J. M. Sharp, J. Comer, and P. J. Hicks, J. Phys. B: Atom. Molec. Phys. 8, 2512-2519 (1975).
8. D. G. Wilden, P. J. Hicks, and J. Comer, J. Phys. B: Atom. Molec. Phys. 10, 1477-1486 (1977).
9. F. H. Read, J. Phys. B: Atom. Molec. Phys. 10, L207-L212 (1977).
10. F. H. Read, J. Phys. B: Atom. Molec. Phys. 10, 449-458 (1977).
11. D. Spence, J. Phys. B: Atom. Molec. Phys., in press.
12. D. Spence, submitted for publication.
13. P. Marchand, Can. J. Phys. 51, 814-819 (1973).
14. P. Marchand, P. Veillette, and P. Marmet, J. Chem. Phys. 67, 2908-2910 (1977).
15. P. Marchand and J. Cardinal, Can. J. Phys. 57, 1624-1633 (1979).
16. J. J. Quenemer, C. Paquet, and P. Marmet, Phys. Rev. A 4, 494-498 (1971).

MEASUREMENT OF THE RATIO OF THE He $2^1S/2^3S$ ENERGY INTEGRATED TOTAL CROSS SECTIONS FROM THRESHOLD TO 0.10 eV: COMPARISON WITH THEORY*

David Spence

We point out that the measurement of energy-integrated total cross section ratios near their thresholds is independent of instrumental resolution when a trapped-electron technique is used. Relying on this fact, we have measured the He $2^1S/2^3S$ cross section ratio, which we find to decrease monotonically from ≈ 8 at 3 meV to ≈ 1.0 at 100 meV above threshold, in excellent agreement with theory.[1] Our measurements clearly indicate a sharp structure of width of a few meV near the 2^1S threshold, which has been predicted to arise from a ^2S virtual state.[2,3]

References

1. R. K. Nesbet, Phys. Rev. A 12, 444 (1975).
2. P. G. Burke, J. W. Cooper, and S. Ormonde, Phys. Rev. 183, 245 (1969).
3. K. A. Berrington, P. G. Burke, and A. L. Sinfailam, J. Phys. B: Atom. Molec. Phys. 8, 1459 (1975).

---

*Abstract of a paper appearing in J. Phys. B: Atom. Molec. Phys. 13, L73 (1980).

AUTOIONIZING STATES OF Ne IN THE ENERGY RANGE 41 TO 52 eV DERIVED FROM NEAR-THRESHOLD SCATTERED ELECTRON SPECTRA*

David Spence

Near-threshold electron-impact spectra in neon, demonstrably free of post-collision-interaction (PCI) effects and negative-ion resonance structures, have been obtained as a function of scattered energy over the incident energy range from 41 to 52 eV. Detailed comparisons with previous experimental data obtained by techniques were PCI and resonance structures are not a complicating issue are made in order to identify the autoionizing states in our scattered electron spectra, which have been published ina previous report.[1] We find that single-electron transitions $2s^2 2p^6 \rightarrow 2s2p^6\ n\ell$ dominate over two electron transitions $2s^2 2p^6 \rightarrow 2s^2 2p^4\ n\ell n'\ell'$, and that states of symmetry ^1S and ^3P are preferentially excited.

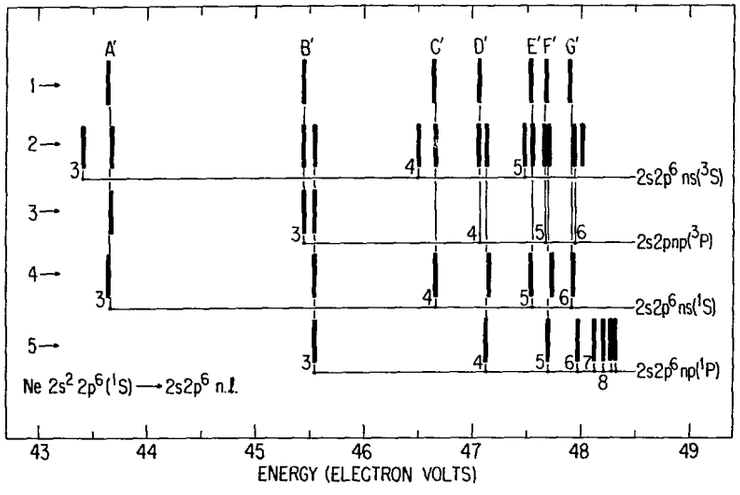

FIG. 1.--Energy level diagram showing a comparison of singly-excited ($2s2p^6 n\ell$) autoionizing state energies in Ne obtained from 5 different techniques. The technique used, source, and preferential symmetries excited in each of the data sets are: (1) low-energy scattered electron, present data, ^1S and ^3P; (2) 150 to 250 keV ion impact, Edwards and Rudd,[2] $^{1,3}S$ and $^{1,3}P$; (3) low-energy impact-ejected electron detection, Sharp et al.,[3] ^1S and ^3P (^1P weak); (4) 10 keV electron impact, Seigbahn et al.,[4] ^1S and ^1P; (5) photoabsorption, Codling et al.,[5] ^1P. (ANL neg. 149-80-18)

---

*Expanded abstract of a paper submitted for publication.

Table 1. Comparison of the values obtained by different authors for singly-excited autoionizing states, $(2s2p^6,n\ell)$, in neon. All energies are in eV.

Autoionizing state	Present data	Edwards and Rudd [2]	Sharp et al.[3]	Siegbahn et al.[4]	Codling et al.[5]	Mean
$3s^3S$		43.41				43.41
$4s^3S$		46.50				46.50
$5s^3S$		47.48				47.48
$3s^1S$	43.64	43.68	43.67	43.645		43.66
$4s^1S$	46.65	46.66		46.66		46.66
$5s^1S$	47.50	47.56		47.54		47.53
$6s^1S$	47.90			47.92		47.91
$3p^3P$	45.45	43.44	45.45			45.45
$4p^3P$	47.07	47.06				47.065
$5p^3P$	47.68	47.66				47.67
$6p^3P$		47.94				47.94
$3p^1P$		45.54	45.54	45.545	45.547	
$4p^1P$		47.14		47.16	47.123	
$5p^1P$		47.71		47.745	47.694	
$6p^1P$		48.01			47.967	
7p					48.116	
8p					48.207	
9p					48.271	
10p					48.313	

Table 2. Comparison of the values obtained by different authors for doubly-excited autoionizing states ($2s^2 2p^4, n\ell, n'\ell'$) in neon. All energies are in eV.

Present data Peak label	Energy	Veillette and Marchand [6]	Andersen and Olsen [7]	Edwards and Rudd [2]	Wilden et al. [8]	Codling et al. [5]	Mean	Configuration $2p^4$(core)[$n\ell, n'\ell'$]
a	41.90		41.95		41.87		41.91	$(^3P)3s^2(^3P)$
b	44.45		44.50		44.48		44.48	$(^3P)[3s3p(^3P)](^3P)$ or (^3D)
c	45.00			45.02	44.97	44.98	44.98 (opt)	$(^3P)[3s3p(^3P)](^1P)$
			45.15		45.12		45.14	$(^1D)3s^2(^1D)$
			45.65				45.65	$(^3P)[3s3p(^1P)](^3P)$ or (^3D)
d	45.90	45.95					45.93	
			47.10				47.10	$(^3P)\{3s4s(^3S)\}(^1P)$
		47.30	47.25				47.28	$(^1D)[3s3p(^3P)](^3F)$
			47.55				47.55	$(^1D)[3s3p(^3P)](^3P)$ or (^3D)
			47.70				47.70	$(^3P)[3s3d(^3D)](^1D,F,P)$
e	48.22						48.22	
f	48.35	48.40 (±0.1)	48.30				48.35	$(^3P)[3p^2(^3P)](^1D)$
g	48.65	48.60 (±0.1)					48.63	$(^3P)[3p^2(^3P)](^1S)$
h	48.90	48.90	48.90			48.907	48.91 (opt)	$(^1D)[3s3p(^1P)](^1P)$
i	49.11	49.15					49.13	$(^1S)[3s^2](^1S)$
j	49.35	49.45					49.40	$(^3P)[3p^2(^1D)]$
				49.88			49.88	
k	50.00		50.00				50.00	$(^1D)[3s3d(^1D)]$
		50.25		50.21			50.23	$(^3P)[3p^2(^1S)]$
l	50.50(±0.1)	50.50 (±0.1)	50.45				50.48	$(^1D)[3s3d(^3D)]$
		50.95	51.05			51.00	51.00 (opt)	$(^3P)3d3p(^1P)$
m	51.30 (±0.1)	51.30 (±0.1)	51.25	51.24		51.309	51.31 (opt)	$(^3P)3d3p(^1P)$
		51.60 (±0.1)	51.70	51.61			51.64	$(^1D)[3p^2(^3P)]$
				51.81			51.81	
				52.04			52.04	
n	52.60 (±0.1)	52.60 (±0.1)		52.63		52.62	52.62 (opt)	$(^1S)[3s3p(^1P)](^1P)$

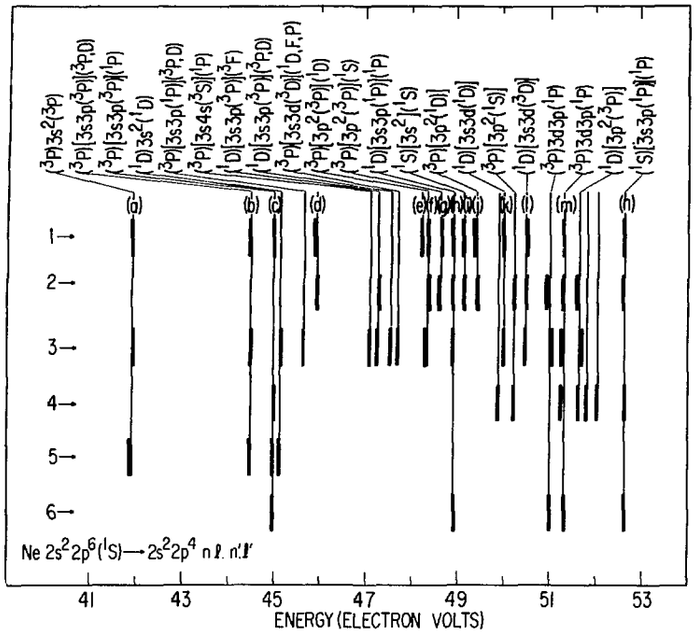

FIG. 2.--Energy level diagram showing a comparison of doubly-excited ($2s^2 2p^4$ $n\ell n'\ell'$) autoionizing state energies in Ne obtained from six techniques. The techniques used and source of these six sets are: (1) low-energy scattered electron, present data; (2) threshold electron-broadband photon detection, Veilette and Marchand[6] (mainly levels above 48 eV); (3) low-energy (0.5-15 keV) ion/neutral impact, Andersen and Olsen;[7] (4) 150 to 250 keV ion impact, Edwards and Rudd;[2] (5) near-threshold electron impact, ejected electron detection, sharp et al.,[3] Wilden et al.;[8] (6) photoabsorption, Codling et al.[5] (ANL neg. 149-80-19)

The energies and energy level diagram of singly-excited autoionizing states are shown in Table 1 and Figure 1, and those of the doubly-excited states in Table 2 and Figure 2.

References

1. D. Spence, Argonne National Laboratory Radiological and Environmental Research Division Annual Report, October 1976-September 1977, ANL-77-65, Part I, p. 92.
2. A. K. Edwards and M. E. Rudd, Phys. Rev. 170A, 140 (1968).
3. J. M. Sharp, J. Comer, and P. J. Hicks, J. Phys. B: Atom. Molec. Phys. 8, 2512 (1975).

4. K. Seigbahn, C. Nordling, G. Johansson, J. Headman, P. F. Heder, K. Hamrin, V. Gelius, T. Bergmark, L. O. Werme, R. Manne, and Y. Baer, ESCA Applied to Free Molecules, North Holland Publishing Co., Amsterdam, pp. 149-153 (1971).
5. K. Codling, R. P. Madden, and D. L. Ederer, Phys. Rev. 115A, 26 (1967).
6. P. Vewillette and P. Marchand, Can. J. Phys. 54, 1208 (1976).
7. N. Andersen and J. Osfgaard Olsen, J. Phys. B: Atom. Molec. Phys. 10, L719 (1977).
8. D. G. Wilden, P. J. Hicks, and J. Comer, J. Phys. B: Atom. Molec. Phys. 10, 1477 (1977).

CROSS SECTIONS FOR NEAR-THRESHOLD ELECTRON-IMPACT EXCITATION OF THE $(2s^2 2p^2 3s)\ ^4P$ and $(2s2p^4)\ ^4P$ STATES OF ATOMIC NITROGEN WITH IMPLICATIONS FOR [N] MEASUREMENTS IN THE AIRGLOW*

David Spence and P. D. Burrow†

Because of the difficulty in producing beams of atomic nitrogen of sufficient density in the laboratory, previous measurements of electron-impact excitation cross sections have been restricted to observations of the optical emission from dipole-allowed transitions.[1] Of necessity, these experiments were performed with rather poor electron beam energy resolution, and the measurements included contributions from cascading.

Although atomic nitrogen is a minor constituent (about 3 or 4% of the total species) above 100 km altitude,[2] it plays an important role in thermospheric chemistry.[3,4] Recent rocket measurements in the thermosphere[5] indicate that the density of N inferred from 1200 Å emission, $(2s^2 2p^2 3s)\ ^4P \rightarrow (2s^2 2p^3)\ ^4S$, differs by approximately 40% from that inferred from 1134 Å emission, $(2s2p^4)\ ^4P \rightarrow (2s^2 2p^3)\ ^4S$, using currently available cross section data,[1] and from the measured electron energy distribution in the upper atmosphere,[6] which is known to peak sharply at an energy of about 10.0 eV.

For these reasons, we have re-examined the cross sections for electron-impact excitation of these states of atomic N in the region near their thresholds using improved electron energy resolution ($\sim$ 0.10 eV). The experimental technique we used for these experiments has been described in a separate publication and will not be discussed here.

Results

The results of our measurements are shown in Figure 1. We find that the $(3s)\ ^4P$ cross section rises very rapidly at threshold, within our experiment resolution of about 0.10 eV, then falls off monotonically to half maximum about

*Summary of a paper to appear in J. Phys. B: Atom. Molec. Phys.

†Consultant, RER Division.

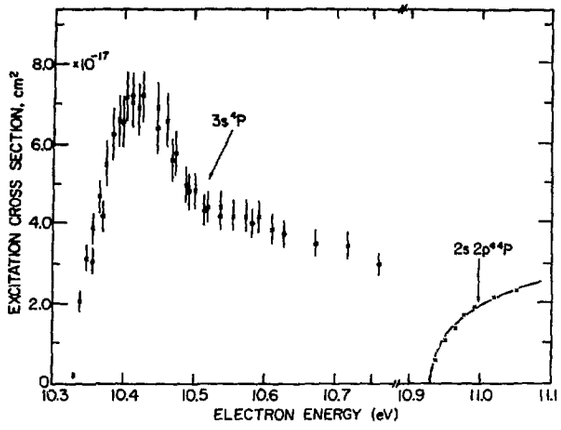

FIG. 1.--Cross sections for electron-impact excitation of the $(2s^2 2p^2(^3P)3s)\ ^4P$ and $(2s2p^4)\ ^4P$ states of atomic nitrogen as a function of incident electron energy. (ANL neg. 149-79-216 Rev. 1A)

0.45 eV above threshold. This threshold behavior is a fairly common feature in electron-impact excitation of states which have a temporary negative ion state (Feshbach resonance) close to the threshold energy.[7] In this particular case, the $(3s)\ ^4P$ threshold structure could be caused by a resonance of configuration $2s^2 2p^2(^3P)3s^2$ just below threshold or, more likely, a core-excited shape resonance such as $2s^2 2p^2 3s3p$ just above threshold.

The near-threshold cross section behavior of the $(3s)\ ^4P$ state obtained in the present experiments is at first sight in apparent conflict with the threshold behavior obtained by Stone and Zipf[1] from observation of 1200 Å emission from the $(3s)\ ^4P$ state following electron-impact excitation. Stone and Zipf[1] obtained a cross section which rose monotonically from threshold, reached a broad peak at about 30 to 40 eV incident energy, and then decreased slowly to a value about half the peak cross section at 400 eV. However, their measurements were made only at energy intervals of about 1.3 eV between threshold and 20 eV, which, combined with the use of unmonochromated electron beams, would preclude observations of the threshold structure.

The cross section for electron-impact excitation of the $(2p^4)\ ^4P$ state increases monotonically above threshold, as shown in Figure 1.

Several recent theoretical studies of electron scattering from atomic nitrogen have been carried out.[8] Using the R-matrix method, Berrington et al.[8] have calculated the total cross section for excitation of the $(2p^4)\ ^4P$

state in addition to that of several higher-lying states. Unfortunately, for computational reasons excited state configurations containing electrons in the $n \geq 3$ were not included, even though the $(3s)\ ^4P$ state is energetically the lowest-lying excited configuration of atomic nitrogen. Omission of this target state will certainly affect the accuracy with which cross sections for excitation to the higher states can be calculated. Because the $(2p^4)\ ^4P$ cross section of Stone and Zipf[1] contains contributions from cascading, a definitive comparison with the calculated cross section is not possible. Nonetheless, the shapes of the two cross sections are in good agreement. The experimental cross section of Stone and Zipf at maximum is 2.0×10^{-16} cm^2 ± 40%, about 2.7 times larger than that calculated by Berrington et al.[8] The threshold dependence of the theoretical cross section is entirely consistent with the present experimental measurements over the limited range of our data.

To determine whether the additional structure we have observed in the $(3s)\ ^4P$ cross section near threshold is of importance in aeronomy, our relative value must be put on an absolute scale. We have done this by renormalizing the theoretical peak cross section of the $(2p^4)\ ^4P$ state at 25 eV (7.3×10^{-17} cm^2) to the experimental value[1] (2.0×10^{-16} cm^2 ± 40%) at this energy. We then used the renormalized $(2p^4)\ ^4P$ theoretical cross section at 0.15 eV above its threshold to determine the cross section scale used in Figure 1. To the extent that cascading processes enter into the cross section of Stone and Zipf at its maximum, this procedure yields an upper bound to our measurement at threshold. However, an extrapolation of our $(3s)\ ^4P$ cross section to 11.0 eV yields a cross section value for the state in good agreement with the 11.0 eV value of Stone and Zipf,[1] which is their lowest energy data point for this cross section.

Discussion

The recent in situ rocket measurements by Meier et al.[2] show that the atomic nitrogen concentration in the thermosphere, as determined from 1200 Å emission ($(3s)\ ^4P$ to $(2s^2 2p^3)\ ^4S$ transitions), is 40% greater than that determined from 1134 Å emission ($(2p^4)\ ^4P$ to $(2s^2 2p^3)\ ^4S$ transitions) when the concentrations are derived from the atomic nitrogen excitation cross sections of Stone and

Zipf[1] in combination with thermospheric photoelectron flux measured by Doering et al.[6]

It is unlikely that the apparent discrepancy between the 1200 Å and 1134 Å rocket measurements can be explained by the large probable errors (±40%) in the cross section measurements of Stone and Zipf as this error is likely to be of the same sign for both the (3s) ^3P and ($2p^4$) ^4P states. At altitudes above 100 km the photoelectron flux has a maximum at about 10.0 eV, close to the (3s) ^4P threshold, and decreases by an order of magnitude between 10 eV and 20 eV. To examine the increased yield of 1200 Å photons one would expect from the (3s) ^4P state because of the threshold peak, we have convoluted measured photoelectron fluxes in the thermosphere[6] with a combination of the present and previous (3s) ^4P cross sections, and find that the threshold peak we observe accounts for only an additional 4 to 5% increase in photon yield. This is an order of magnitude too small to explain the observations of Maier et al.,[5] and an alternative explanation must be sought.

References

1. E. J. Stone and E. C. Zipf, J. Chem. Phys. 56, 4278 (1973).
2. P. Z. Takacs and P. D. Feldman, J. Geophys. Rev. 82, 5011 (1977).
3. E. S. Oran, P. S. Julienne, and D. F. Strobel, J. Geophys. Rev. 80, 3068 (1975).
4. D. F. Strobel, E. S. Oran, and P. D. Feldman, J. Geophys. Res. 81, 3745 (1976).
5. R. R. Meier, D. J. Strickland, P. D. Feldman, and E. P. Gentieu, submitted to J. Geophys. Res.
6. J. P. Doering, W. K. Peterson, C. O. Bostrom, and T. A. Poterma, Geophys. Res. Lett. 3, 129 (1976).
7. G. J. Schulz, Rev. Mod. Phys. 45, 378 (1973).
8. K. A. Berrington, P. G. Burke, and W. D. Robb, J. Phys. B: Atom. Molec. Phys. 8, 2600 (1975).

ANGULAR DEPENDENCE OF THE SCATTERED ELECTRON SPECTRUM OF Ne IN THE 43 eV TO 51 eV ENERGY LOSS RANGE

M. A. Dillon and David Spence

In the Born approximation the differential cross section, σ, for electron impact excitation to bound states is given qualitatively by the hydrogenic form,[1]

$$\sigma \sim \frac{C\,K^{2(m-1)}}{(\alpha^2 + K^2)^{L+m+5}} \quad . \tag{1}$$

Here C is a constant,

$$K = (k_o^{\,2} + k_n^{\,2} - 2k_o k_n \cos\theta)^{\frac{1}{2}} \tag{2}$$

is the momentum transferred by the projectile electron, and

$$\alpha = \sqrt{2I} + \sqrt{2(I-W)} \quad . \tag{3}$$

The quantities k_o and k_n are the magnitudes of the incident and scattered wave vectors, and θ is the scattering angle; I and W are, respectively, the ionization potential and excitation level of the target atom or molecule. The integer $m + 1$ is the index of the first non-zero transition moment according to electron impact selection rules and $L = \ell' + \ell$ where ℓ' and ℓ are the angular momentum numbers of the initial and final target states. Equation 1 shows that the angular distributions of inelastically scattered electrons corresponding to various excitation levels of an atom can provide a means of identifying the term symbol of the excited state. As an example the differential cross section for the $1^1S \rightarrow 2^1P$ transition in He, where $m = 0$ and $L = 1$, falls off much more rapidly with angle than the cross section curve for the $1^1S \rightarrow 2^1S$ transition ($m = 1$, $L = 0$). It is natural to inquire whether similar propensities in the angular distribution of inelastically scattered electrons can be used to delineate the nature of quasi-discrete autoionizing states.

Electron impact spectra of Ne in the 43 eV to 51 eV energy loss range are displayed in Figure 1. The spectra were determined with 200 eV incident electrons and an instrument resolution of 70 meV. The general description of the scattering apparatus used in this work is given elsewhere.[2] The scattered electron

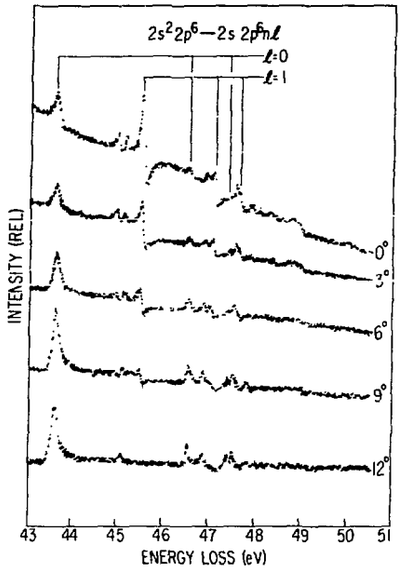

FIG. 1.--Electron energy-loss spectra of Ne as a function of scattering angle θ.

intensity varies by a factor of 15 over the 12° angular interval presented in the figure, and the spectra show marked changes. Under the operating conditions described above the structures in the 43 eV to 51 eV energy loss range arise entirely[3] from singlet excitations. We will concern ourselves with only the single-electron transitions of the type $2s^2 2p^4 \rightarrow 2s2p^6\, n\ell$. The locations of the leading two prominent series with term symbols ^1S and ^1P are included in the figure. Peaks corresponding to the allowed P series decrease much more rapidly with scattering angle than the optically forbidden S series. For example, the intensity of the first member of each series appears as if it could be represented qualitatively by Eq. 1. If such behavior proves characteristic of single electron transitions, then the angular dependence of electron-impact spectra in an autoionization region should provide an additional tool for spectral classification

References

1. K. N. Klump and E. N. Lassettre, J. Chem. Phys. 68, 886 (1977).
2. H. Tanaka, R. H. Huebner, O. J. Steingraber, and D. Spence, Argonne National Laboratory Radiological and Environmental Research Division Annual Report, July 1975-June 1976, ANL-76-88, Part I, p. 10.
3. S. Tahira, F. Nishimura, and N. Oda, J. Phys. B 6, 2306 (1975).

ATOMIC PROCESSES PERTINENT TO RADIATION PHYSICS*

Mitio Inokuti

The physics of electronic and atomic collisions is a key element in the understanding of action of ionizing radiation on matter. Studies on radiation action in turn are fundamental to various aspects of the nuclear fission and fusion energy technology, most notably its health aspect. The present lecture illustrates through selected examples the use of electron-collision cross-section data in radiation physics. The cross-section data for this use must be absolute and comprehensive (i.e., referring to all major final states of a target atom or molecule and covering a wide range of independent variables such as incident energy). For the determination of a comprehensive and trustworthy set of electron-collision cross-section data for a given atom or molecule, various theoretical constraints prove to be useful. Various outstanding problems, both experimental and theoretical, are suggested for work in the future.

* Abstract of an invited lecture presented at XIth International Conference on the Physics of Electronic and Atomic Collisions, Kyoti, 1979. Proceedings, edited by N. Oda and K. Takayanagi, North-Holland Publ. Co., Amsterdam, p. 31 (1980).

STATISTICAL FLUCTUATIONS IN THE IONIZATION YIELD AND THEIR RELATION TO THE ELECTRON DEGRADATION SPECTRUM*

Mitio Inokuti, D. A. Douthat,† and A.R.P. Rau‡

We discuss various indices that characterize the statistical fluctuations in the ionization yield for electron incidence. The indices include the variance, the moments, the central moments, and the cumulants, all defined in terms of the probability $P(T_0,j)$ that an electron of kinetic energy T_0 causes, upon complete slowing-down, exactly j ion pairs. Like the mean ionization yield, each of the indices is expressible as an integral over the current energy T of electrons. The integrand is a product of the Spencer-Fano degradation spectrum $y(T_0,T)$ for source energy T_0 with another factor, and displays contributions from different values of T to the quantity of interest. It has been shown for the first time that the cumulant of any order (including the variance as a special case) receives contributions from different T in nearly the same way as the mean ionization yield. Therefore, for T_0 greatly exceeding the first ionization threshold, every cumulant is roughly proportional to T_0, just as the mean yield is. This leads to a generalization of the Fano factor. Thus, our findings reinforce the importance of the cumulant notion in statistical physics in general.

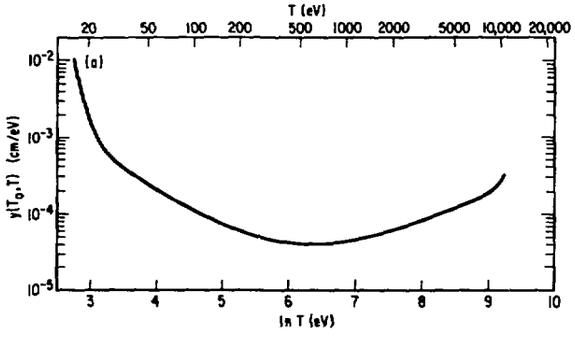

FIG. 1.--The electron degradation spectrum $y(T_0,T)$ in H_2 for the source-electron energy T_0 =10 keV. Data are taken from Ref. 1.

*Summary of a paper to appear in Phys. Rev. A.

†Consultant, Radiological and Environmental Research Division. Permanent address: Kennedy-King College, Chicago, Illinois 60621.

‡Department of Physics and Astronomy, Louisiana State University, Baton Rouge, LA 70803.

Numerical work on molecular hydrogen as an example substantiates the general conclusion and predicts the value 0.30 for the Fano factor for an electron of initial energy 10 keV. The four figures illustrate some of our results.

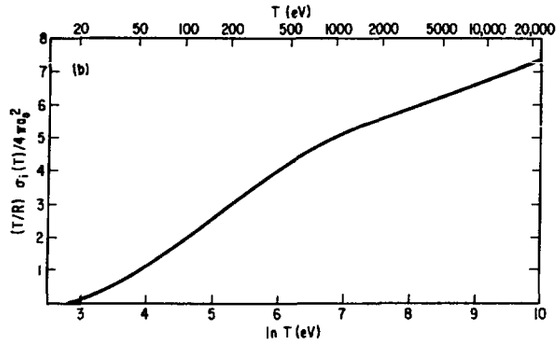

FIG. 2.--The Fano plot, i.e., the product $T\sigma_i(T)$ plotted against ln T for H_2. More precisely, the vertical scale is dimensionless since R is the Rydberg energy (13.6 eV) and a_0 is the Bohr radius (0.529×10^{-8} cm). The slope of the asymptotic straight-line behavior is 0.721, and represents the total dipole matrix element squared measured in a_0^2.

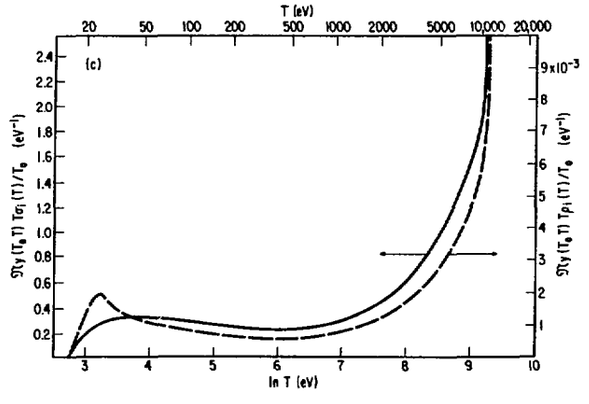

FIG. 3.--The mean number $N_i(T_0)$ and the variance $D(T_0)$ of ion pairs in H_2 for the source electron energy T_0 = 10 keV. These quantities are expressed[2] as

$$N_i(T_0) = \mathcal{N} \int_I^{T_0} d(\ln T)\, y(T_0,T)\, T\sigma_i(T),$$

and

$$D(T_0) = \mathcal{N} \int_I^{T_0} d(\ln T)\, y(T_0,T)\, T\rho(T),$$

where $\mathcal{N}$ is the number density of molecules and I is the ionization threshold energy. The symbol $\sigma_i(T)$ represents the ionization cross sections for electron of energy T, and $\rho(T)$ a quantity of the cross-section dimension. The area under the solid curve represents $N_i(T_0)/T_0$. The data were obtained by multiplying the values in Figure 1 and the values in Figure 2. The area under the broken curve represents $D(T_0)/T_0$.

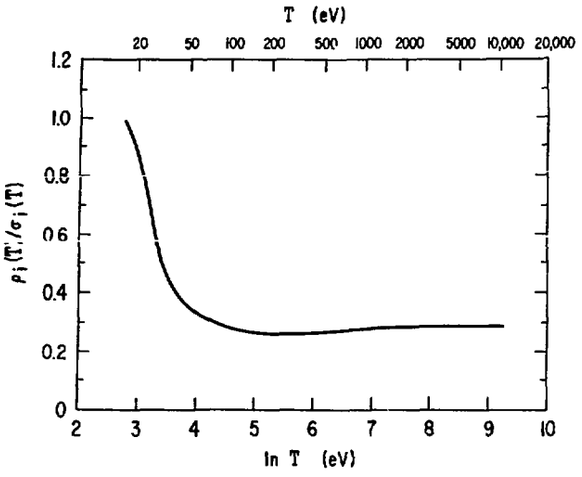

FIG. 4.--Plot of the ratio $\rho(T)/\sigma_i(T)$ evaluated numerically from the data of Ref. 1 for H_2 as a function of T. The ratio is nearly constant for T >500eV, except for noticeable departures at lower $\bar{I}$.

References

1. D. A. Douthat, J. Phys. B 12, 663 (1979).
2. A.R.P. Rau, M. Inokuti, and D. A. Douthat, Phys. Rev. A 18, 971 (1978).

ELASTIC AND INELASTIC ATOM-ATOM CROSS SECTIONS AT HIGH VELOCITIES FOR $Z \leq 18$*

George H. Gillespie† and Mitio Inokuti

When two complex atomic particles collide at high relative speeds, a variety of phenomena can occur. Bates and Griffing[1] initiated a study within the Born approximation of the various possible processes for collisions between two hydrogen atoms. Subsequent work[2] has provided calculations for many different processes, although only the simpler atomic systems have been studied in detail. More recently some work has been devoted to the establishment of certain general systematics of the relative importance of various phenomena relevant to fast collisions between complex atomic particles.[3,4] In extension of that work, we have undertaken a systematic study of the asymptotic (high-velocity) Born cross sections for atom-atom collisions.[5]

Because of the great number of possible final states of such collisions, it is useful to simplify the problem by grouping the processes into a few broad classifications. In particular, we consider four types of collision which can be categorized according to whether each of the collision partners is scattered elastically or inelastically. For atoms A and B initially in their ground state (g), these processes and their respective cross sections are the following:

$$A(g) + B(g) \rightarrow A(g) + B(g): \quad \sigma_{el,el} = 8\pi a_0^2 \left(\frac{\nu_0}{\nu}\right)^2 I_{el,el} \,, \tag{1}$$

$$A(g) + B(g) \rightarrow A(g) + B(\Sigma): \quad \sigma_{el,in} = 8\pi a_0^2 \left(\frac{\nu_0}{\nu}\right)^2 I_{el,in} \tag{2}$$

$$A(g) + B(g) \rightarrow A(\Sigma) + B(g): \quad \sigma_{in,el} = 8\pi a_0^2 \left(\frac{\nu_0}{\nu}\right) I_{in,el} \,, \tag{3}$$

$$A(g) + B(g) \rightarrow A(\Sigma) + B(\Sigma): \quad \sigma_{in,in} = 8\pi a_0^2 \left(\frac{\nu_0}{\nu}\right) I_{in,in} \,, \tag{4}$$

---

*Abstract of a paper presented at the XIth International Conference on the Physics of Electronic and Atomic Collisions, Kyoto, Japan, 29 August-4 September 1980. A full paper will appear in Phys. Rev. A.

†Physical Dynamics, Inc., P.O. Box 556, La Jolla, California 92038.

where in processes 1 to 4 we indicate by Σ that all possible inelastic processes, either excitation or ionization, have been included.

At high velocities the collision strengths ($I_{el,el}$, etc.) are independent of v and may be expressed in terms of compact momentum transfer integrals over products of atomic form factors or incoherent scattering functions for the atoms involved.[3-5] We have numerically calculated the collision strengths appearing in processes 1 to 4 for all possible combinations of atoms with $Z \leq 18$, using the tabulations of these functions given by Hubbell et al.[6]

As a result, we now answer questions such as, "What is the dominant collision process at high velocities?" In Figure 1 we display the answer as a function of $Z^{(A)}$ and $Z^{(B)}$. For atomic numbers of 3 or less, the doubly inelastic collision process is dominant, as noted by Bates and Griffing for H-H collisions.[1] At higher atomic numbers, purely elastic collisions are dominant.[3] When one of the collision partners is H (and in select cases He) then singly inelastic collisions are dominant if the other collision partner has an atomic number greater than 3.

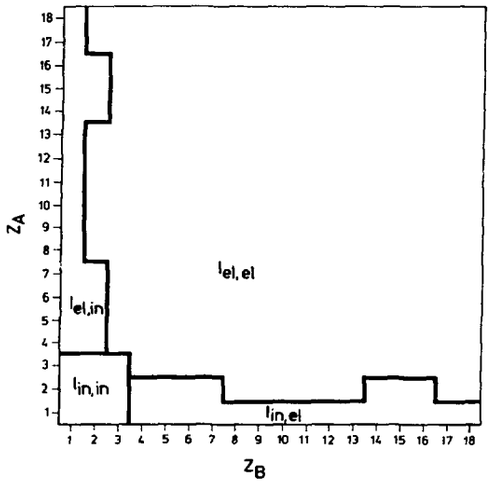

FIG. 1.--Domains indicating the largest collision strength for the processes 1 to 4 as a function of the atomic numbers of the collision partners.

References

1. D. R. Bates and G. W. Griffing, Proc. Phys. Soc. A 66, 961 (1953); 67, 663 (1954); 68, 90 (1955).

2. K. L. Bell and A. E. Kingston, Adv. Atom. Molec. Phys. 10, 53 (1974); Atomic Processes and Applications, P. G. Burke and B. L. Moiseiwitsch, Eds., North Holland Publ. Co., Amsterdam, p. 493 (1976).
3. M. Inokuti, Proc. Xth International Conference on the Physics of Electronic and Atomic Collisions, Paris, p. 280 (1977).
4. G. H. Gillespie, Phys. Rev. A 18, 1967 (1978).
5. G. H. Gillespie and M. Inokuti, in preparation.
6. J. H. Hubbell, Wm. J. Veigele, E. A. Briggs, R. T. Brown, D. T. Cromer, and R. J. Howerton, J. Phys. Chem. Ref. Data 4, 471 (1975); 6, 615 (1977).

STOPPING POWER FOR PARTIALLY STRIPPED IONS*

Yong-Ki Kim and Kwok-tsang Cheng

The Bethe formula for the stopping power for bare ions[1] is extended to the collisions between partially stripped ions and neutral atoms. The resulting formulas can be presented in the same form as the original Bethe formula by replacing the nucleqr charge of the projectile Z and the mean excitation energy I by Z_{eff_2} and I_{eff}, respectively: $-dE/dx = \text{const.} \times Z_{eff}^2 \ln(4T/I_{eff})$, where $T = \frac{1}{2} m v_{ion}$, with the electron mass m and ion velocity v_{ion}. Both Z_{eff} and I_{eff} contain contributions from excitations (including ionizations) of the target by the projectile, excitations of the projectile by the target, and mutual excitations. They are defined in terms of projectile and target properties that can be calculated from first principles. Expressions for Z_{eff} and I_{eff} reduce to those in the Bethe formula for bare incident ions. Details of the formulas for

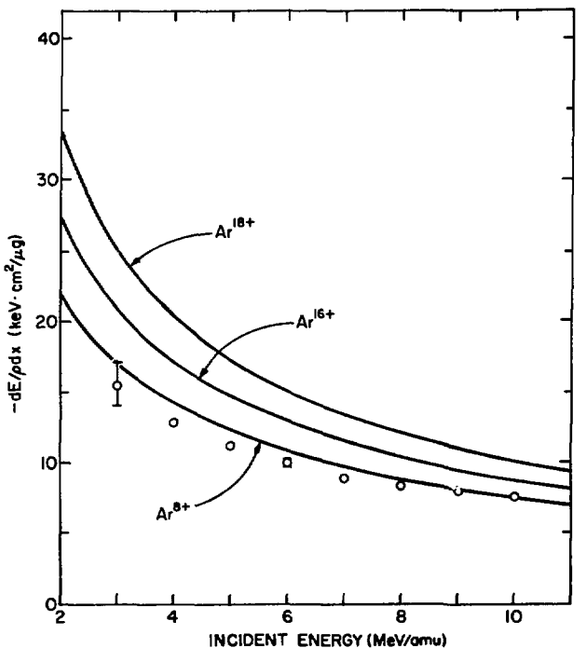

FIG. 1.--Stopping powers for $Ar^{\zeta+}$ in Ar gas at different ζ as functions of incident energy. Solid curves are based on the present theory, and the circles represent the experimental data by Martin and Northcliffe.[2]

*Summary of a paper in Phys. Rev. A 22, 61-67 (1980).

atom-atom and ion-ion collisions are presented in the paper to appear in the Physical Review A. Comparison with experimental data on Ar ions in Ar gas[2] indicates that the new formula is reliable for projectile energies greater than a few MeV/amu (Figure 1).

References

1. H. A. Bethe, Ann. Physik 5, 325 (1930).
2. F. W. Martin and L. C. Northcliffe, Phys. Rev. 128, 1166 (1962).

BETHE CROSS SECTIONS FOR THE IONIZATION OF C^{3+}, N^{4+}, AND O^{5+} *

Y.-K. Kim and K. T. Cheng

Introduction

A sum rule for the Born cross sections[1] gives the total cross section for inelastic scattering of fast electrons in the form:

$$\sigma_t = (A_t \ln T + B_t + C_t/T)/T \quad , \tag{1}$$

where the Bethe parameters A_t, B_t, and C_t are derived from the properties of the target ion, and T is the incident electron energy.

Since Eq. 1 includes all discrete, ionizing, and inner-shell excitations, we get the ionization cross section (including autoionization of inner-shell excited states) by subtracting the sum of all discrete excitation cross sections, σ_d.

Theory

Cross sections for discrete excitations also have the same form as Eq. 1 for fast incident electrons:

$$\sigma_d = (A_d \ln T + B_d + C_d/T)/T \quad . \tag{2}$$

Thus, the ionization cross section based on the sum rule is given by:

$$\sigma_i = (A_i \ln T + B_i + C_i/T)/T \quad . \tag{3}$$

The ionization cross section σ_i can be improved further by intorducing an exchange correction based on the Mott formula[1]

$$\sigma_x = (\text{const}/T^2)\sum_j [\ln (I_j/T) + 1] N_j \quad , \tag{4}$$

where I_j and N_j are the ionization potential and the occupation number of the jth orbital. Equation 4 reduces to the Ochkur approximation at high T, and it is valid when $1/T \ll 1$. The ionization cross section with exchange, σ_{ix}, is hence given by

---

*Presented at the XIth International Conference on the Physics of Electronic and Atomic Collisions, Aug. 29-Sept. 4, 1979, Kyoto, Japan.

$$\sigma_{ix} = (A_i \ln T + B_i + C_i/T + D_i \ln T/T)/T \quad . \tag{5}$$

Details

We calculated the Bethe parameters of σ_d directly from the Dirac-Fock (DF) wave functions for the Li-like ions ($2s - n\ell$: $n = 2 - 7$, $\ell = 0 - 4$), and extrapolated them to higher $n\ell$, using the quantum defect method.[1]

To calculate the Bethe parameters for σ_t, one needs the ground state wave function and the f values for all allowed transitions from the ground state. Again, we used the DF wave functions for $n < 8$, and extrapolated to higher n by the quantum defect method. Reliable continuum f values, however, are difficult to calculate, and we used the Dirac-Slater (DS) approximation for the continuum wave functions.

The DS approximation gives too low an ionization potential for the 1s electron, and it is likely to underestimate (by < 10%) the 1s contribution to B_t in Eq. 1. We included an estimated correction for the low ionization potential of 1s.

Results

The Bethe parameters for σ_{ix} are listed in Table 1. In Figures 1 to 3, our σ_{ix} are compared with the electron-impact databy Crandall et al.[2] and also with Coulomb-Born calculations by Moores[4] and by Golden and Sampson.[5]

The Fano plots presented in Figures 1 to 3 are powerful in checking consistency of asymptotic behavior of the experimental data. The slopes of the Bethe cross sections in the figures are reliable to a few per cent. Heights of the Bethe cross sections, however, are uncertain by $\sim$ 10% because of the inaccuracies in the continuum f values. Near the kinks in the experimental data (e.g., at T = 250 eV for C^{3+}), some autoionization peaks ($1s - n\ell$) are expected. The Bethe theory accounts only for dipole-allowed transitions among the K-shell excited states, whereas in reality, some forbidden transitions may be prominent near the threshold.

Table 1. Bethe parameters for ionization as defined in Eq. 5 (σ_{ix} in 10^{-16} cm^2 and T in eV).

	C^{3+}	N^{4+}	O^{5+}
A_i	5.12	3.59	2.65
B_i	-11.0	- 9.57	- 8.38
C_i	7196	7910	8513
D_i	-1954	-1954	- 1954

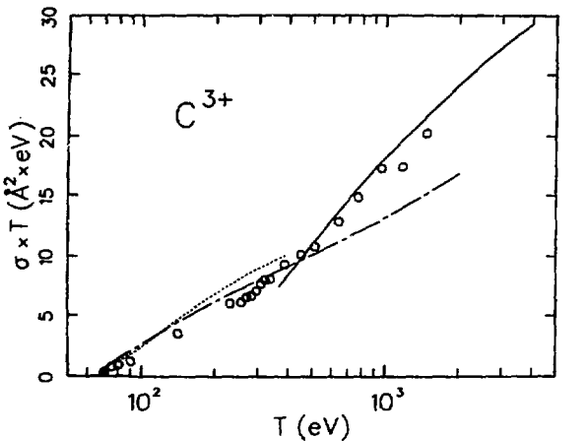

Fig. 1

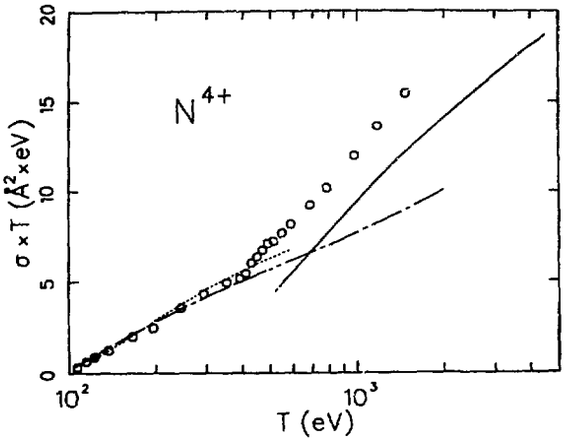

Fig. 2

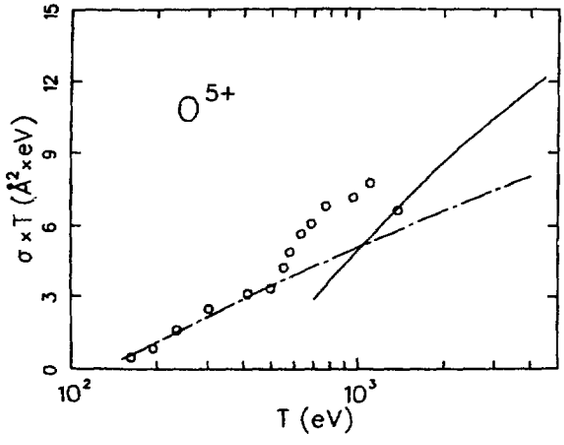

Fig. 3

FIGs. 1-3.--Fano plots for the ionization of C^{3+}, N^{4+}, and O^{5+} by electron impact. In these figures, O, Crandall et al., experiment, Refs. 2,3; —, Kim and Cheng, Bethe, present work; ----, Moores, Coulomb-Born, Ref. 4; -----, Golden and Sampson, hydrogenic Coulomb-Born, Ref. 5.

References

1. Y.-K. Kim and M. Inokuti, Phys. Rev. A 3, 665 (1971).
2. D. H. Crandall, R. A. Phaneuf, and P. O. Taylor, Phys. Rev. A 18, 1911 (1978).
3. D. H. Crandall, R. A. Phaneuf, B. E. Hasselquist, and D. C. Gregory, J. Phys. B 12, L249 (1979).
4. D. L. Moores, J. Phys. B 11, L1 (1978).
5. L. B. Golden and D. H. Sampson, J. Phys. B 10, 2229 (1977).

THE BETHE TOTAL CROSS SECTION FOR INELASTIC COLLISIONS OF FAST CHARGED PARTICLES WITH C^-, O^-, AND F^- IONS*

Mitio Inokuti, Kwok-tsang Cheng, and J. L. Dehmer

Recent experiments by Peart, Forrest, and Dolder[1,2] on electron detachment from C^-, O^-, and F^- by electrons of kinetic energies up to 990 eV have prompted us to study the topic in the title. The general framework of our study has been fully described earlier (see in particular Sec. 4.3, Ref. 3; Ref. 4) and it merits have been illustrated for the H^- ion;[4] indeed, the present work is an extension of that work in many respects.

The total cross section σ_{tot} for inelastic collisions of any structureless particle of charge ze and speed v (assumed nonrelativistic for brevity) with any atomic or molecular target is given[3] by

$$\sigma_{tot} = 4\pi a_0^2 z^2 (R/T)\, M_{tot}^2 \ln (4c_{tot}T/R) \quad , \tag{1}$$

where $T = \frac{1}{2}mv^2$, $R = 13.6$ eV, and $a_0 = 0.529 \times 10^{-8}$ cm. The two quantities M_{tot}^2 and c_{tot} depend on the target electronic structure only, and their dependable evaluation is the main object of our study.

Of the two quantities, M_{tot}^2 is both conceptually simpler and easier to evaluate; it is the sum of the squared dipole matrix elements (measured in a_0^2) over the entire spectrum that includes all continua as well as discrete spectra. The quantity M_{tot}^2 can be evaluated by virtue of a sum rule from the ground-state wave function of the target. We have thus obtained $M_{tot}^2 = 7.76$ for C^-, 4.55 for O^-, and 3.78 for F^- by calculations within the Hartree-Fock (HF) approximations. For F^-, we have deduced a better value, $M_{tot}^2 = 3.6$ from the configuration-interaction calculations of Tanaka and Sasaki.[5]

For comparison with the experiment,[1,2] we should first note that σ_{tot} should be a close upper bound to the electron-detachment cross section σ_{det} for all three negative ions because there appear to be no discrete bound states

---

*Abstract of a paper presented at the XIth International Conference on the Physics of Electronic and Atomic Collisions, Kyotok Japan, 28 August-4 September, 1979.

accessible by a dipole-allowed transition to the best of our knowledge.[6] Next, recall that a good way of analysis of any cross-section data for high incident speed is by the use of the Fano plot,[3,7] (as exemplified by Figure 2 of Ref. 1 and by Figure 3 of Ref. 2), in which one plots $T\sigma_{det}$ or $T\sigma_{tot}$ against ln T. The slope of the linear asymptote, as suggested by Eq. 1, should be comparable to our theoretical values for M_{tot}^2.

With these ideas in mind, we have examined the experimental data,[1,2] and have come to a tentative conclusion that for F^- and O^- the slopes of the Fano plots of these data at highest energies are probably compatible with our theoretical results, within uncertainties of 10%. For C^-, the theoretical slope is much larger than the experimental.

A more detailed result is forthcoming. By several means we are evaluating σ_{tot} (i.e., the second quantity in Eq. 1, which determines the intercept in the Fano plot).

We thank Professor Dolder for communicating the experimental results far in advance of publication.

References

1. B. Peart, R. Forrest, and K. T. Dolder, J. Phys. B 12, L115 (1979).
2. B. Peart, R. Forrest, and K. T. Dolder, J. Phys. B 12, 847 (1979).
3. M. Inokuti, Rev. Mod. Phys. 43, 297 (1971).
4. M. Inokuti and Y.-K. Kim, Phys. Rev. 173, 154 (1968).
5. K. Tanaka and F. Sasaki, Int. J. Quantum Chem. 5, 157 (1971).
6. H. Hotop and W. C. Lineberger, J. Phys. Chem. Ref. Data 4, 539 (1975).
7. U. Fano, Phys. Rev. 95, 1198 (1954).

NEAR-THRESHOLD STRUCTURE IN THE ATOMIC K-SHELL SPECTRA FOR IONIZATION BY PHOTONS OR FAST CHARGED PARTICLES*

Steven T. Manson† and Mitio Inokuti

Spectra of the optical and generalized oscillator strength for the K-shell ionization of all free atoms with $Z \leq 30$ have been calculated within the framework of a Hartree-Slater central potential.[1] A major result of this study is our finding that the spectra (at fixed small values of momentum transfer including the optical limit) are rich in structure. In other words, the spectral strength is non-monotonic in the kinetic energy of an ejected electron near the K-shell threshold, for all atoms with $Z \geq 8$. This is in sharp contrast to the hydrogenic result, according to which the spectral strength for every shell monotonically decreases with kinetic energy.[2,3] The magnitude of the near-threshold structure sometimes amounts to as much as 30%, but this varies, as does the spectral shape, along the periodic table.

The structure arises from the energy dependence of the normalization of the continuum wave function which, in turn, is determined by the potential over its entire range.[4] Thus it is seen that the spectral shape of an inner subshell can be strongly affected by the behavior of the potential outside the subshell. Among the important implications of these results is that great care must be taken in the interpretation of any structure in molecular and solid-state photoabsorption and photoemission data near threshold.

References

1. F. Herman and S. Skillman, Atomic Structure Calculations, Prentice-Hall, Englewood Cliffs, N.J. (1963).
2. H. Hall, Rev. Mod. Phys. 8, 358-397 (1936).
3. H. Bethe, Handbuch der Physik, H. Geiger and K. Scheel, Eds., Springer-Verlag, Berlin, Vol. 24/1, pp. 273-560 (1933).
4. J. Dehmer and U. Fano, Phys. Rev. A 2, 304-309 (1970).

*Summary of a paper published in J. Phys. B 13, L323 (1980).

†Department of Physics and Astronomy, Georgie State University, Atlanta, Georgia 30303.

A GENERALIZED POWER SERIES REPRESENTATION OF PHOTOIONIZATION OSCILLATOR-STRENGTH DISTRIBUTIONS

M. A. Dillon

A polynomial representation of continuum differential oscillator-strength distributions as a function of ejected electron energy is proposed. The representation is obtained from a simple analysis of the independent electron dipole matrix element. As examples, oscillator-strength curves of He, Li, Na, and K are reproduced by the least-square fitting technique.

In the course of analyzing and collating photoionization cross sections it is convenient to have a means of representing data points by a semi-empirical formula. A similar consideration led to the development[1] of a generalized power series representation for electron collision measurements. The method employed in that study can be readily adapted to the case of photoabsorption.

The differential oscillator strength, f, for photoionization is given by

$$f = A^2(k)\bar{f} \quad , \tag{1a}$$

where

$$\bar{f} = 2WC^2(k)\,|M|^2 \quad . \tag{1b}$$

All quantities are in atomic units; $W = I + \varepsilon$ is the excitation energy, I the ionization potential, and $\varepsilon = \frac{1}{2}k^2$ is the ejected electron energy. The product AC is a coefficient that normalizes the continuum final states on the energy scale with the hydrogenic contribution C given by

$$C = (1 + k^2)^{\frac{1}{2}}/(1 - e^{-2\pi/k})^{\frac{1}{2}} \tag{2}$$

for the $\ell = 1$ Coulomb wave. In Eqs. 1a and 1b the quantity ACM is the electric dipole matrix element where for $s \rightarrow p$ transitions,[2]

$$M = \frac{4\pi}{3}\int \psi_0(r)\, r\, \psi_k(r)\, r^2\, dr \tag{3}$$

in the independent particle approximation. Here $\psi_0 \xrightarrow{r\to\infty} (r^{1/\lambda-1})e^{-\lambda r}$ with $\lambda = (2I)^{\frac{1}{2}}$; ψ_k is a complete analytical function of k^2 and $\psi_k \sim r$ in the neighborhood of $r = 0$.

We would like to express M as a power series expansion in the variable

$g = g(\varepsilon)$ which converges for all positive ε. In order to find a plausible form for g, it is first necessary to locate the singularities of M in the complex k plane. An application of the technique employed by Lassettre[1] shows that only two singularities exist in the finite k plane of M located at

$$k = \pm i\lambda \quad . \tag{4}$$

The function

$$g = \frac{k^2}{k^2 + \lambda^2} = \frac{\varepsilon}{\varepsilon + I} \tag{5}$$

is the natural expansion variable[3] for $\bar{f}$ in the photoionization of atomic hydrogen. This is also true in the present more general case, for when M is considered a function of g, the singularities at $\pm i\lambda$ are mapped to ∞ in the g plane, and a singularity at $k = \infty$ is transformed to the circle of radius $|g| = 1$. Hence, we can write

$$|M|^2 = \sum_{n=0}^{n=\infty} a_n g^n \quad , \tag{6}$$

where Eq. 6 converges for all positive ε. The excitation energy W and the factor $(1 + k^2)$ in Eq. 2 can be absorbed in the power series Eq. 6. The exponential factor in Eq. 2 becomes important only for ejected electron energies larger than the 0 to 200 eV range considered here. Hence, we can put

$$\bar{f} \approx \sum_{n=0}^{n=\infty} b_n g^n \quad . \tag{7}$$

The normalization factor A in Eq. 1 makes a significant contribution to the variation of f with ε in the case of inner-shell ionization.[4] When needed, A can be constructed from eigenvalue data.[5] In the simple cases treated here, it is assumed that f and $\bar{f}$ differ at most by a constant which is independent of ε.

In order to test the fitting properties of Eq. 7, simulated photoionization data were generated for four diverse but simple $s \rightarrow p$ continuum transitions. Optical oscillator strengths for $He(1s \rightarrow p)$, $Li(2s \rightarrow p)$, $Na(3s \rightarrow p)$, and $K(4s \rightarrow p)$ transitions were obtained from calculations by Dehmer et al.[6] using the

independent electron model employing a Hartree-Slater potential from a tabulation of Herman and Skillman.

Data points normalized to unity at $\varepsilon = g = 0$ are presented in Figures 1 to 3. For He, Li, Na, and K, respectively, the upper limit $g \sim 0.9$ corresponds to 235 eV, 55 eV, 51 eV, and 45 eV ejected electron energies. The solid curves of Figure 1 represent least-square fits of Eq. 7 to the He and Li continuum oscillator-strength distributions. The choice of a third degree polynomial is used only for the purpose of illustration. For example, the complete range of He is well represented by a polynomial of second degree. The sodium and potassium oscillator-strength distributions displayed in Figures 2 and 3 exhibit a Cooper zero near $\varepsilon = 1$ eV and 0.5 eV, respectively. The curves show how rapidly the polynomial fit converges, even when the distributions contain complicated structure.

As long as the energy range is not too great, Eq. 7 can be used to fit the continuum oscillator strengths for outer-shell ionization of most simple atoms. When the ejected electron energy is so large that $g > 0.9$, then the polynomial in Eq. 7 must be furnished with an appropriate convergence factor. For example, in the case of an $s \rightarrow p$ continuum transition, f must tend asymptotically to $\varepsilon^{-3.5}$[2].

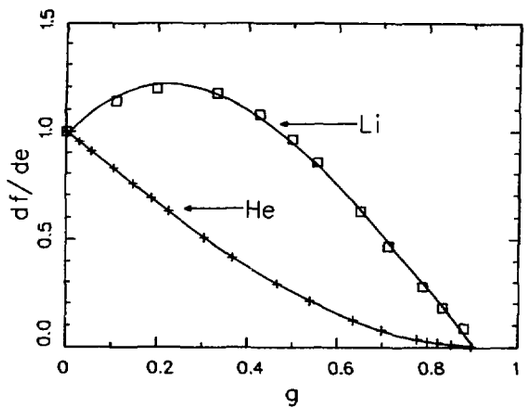

FIG. 1.--Differential oscillator strengths for the photoionization of He and Li. The curves are least-square fits of a third-degree polynomial to the simulated data points.

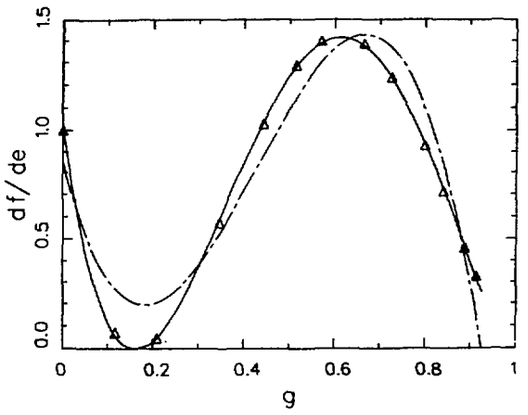

FIG. 2.--Differential oscillator strengths for the photoionization of Na. Broken and full curves compare, respectively, least-square fits with third- and fourth-degree polynomials.

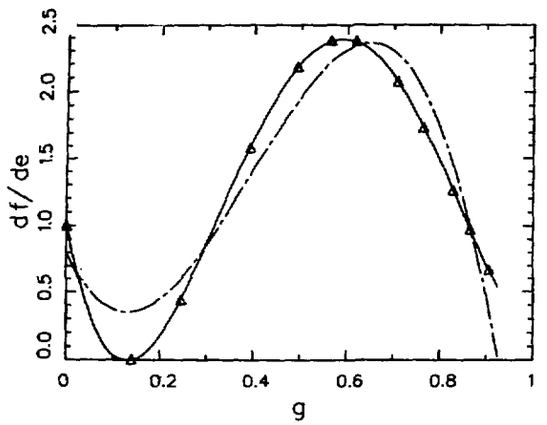

FIG. 3.--Differential oscillator strengths for the photoionization of K. Broken and full curves compare, respectively, least-square fits with third- and fourth-degree polynomials.

References

1. E. N. Lassettre, J. Chem. Phys. 40, 4479 (1965).
2. U. Fano and J. W. Cooper, Rev. Mod. Phys. 40, 441 (1968).
3. N. F. Mott and H.S.W. Massey, The Theory of Atomic Collisions, Oxford, Clarendon, p. 490 (1965).
4. S. Manson and M. Inokuti, to be published.
5. M. J. Seaton, Proc. Phys. Soc. 88, 815 (1966).
6. J. L. Dehmer, M. Inokuti, and R. P. Saxon, Phys. Rev. A 12, 102 (1975).

A METHOD FOR IMPLEMENTING ELECTRON COLLISION CROSS SECTION CALCULATIONS BY USE OF EXPERIMENTAL DATA

M. A. Dillon

A method is proposed in which data collected in the Born region can be used to implement the application of formulations more complicated than the Born approximation. The technique is applied to the electron-impact excitation of the 2^1S and 3^1S levels of helium in the Coulomb projected Born approximation.

In order to ascertain the merit of a particular theory it is necessary to compare a careful calculation with experiment. A satisfactory comparison is quite difficult in the field of electron atom inelastic collisions because of the requirement that such calculations incorporate accurate target wave functions. However, it is sometimes possible to use either experimental data or the results of simple theoretical calculations to facilitate the application of a more complicated approximation.

Formulation

An electron molecule scattering event may be characterized by a differential cross section, σ_{0f}, averaged over target orientations;

$$\sigma_{0f} = \frac{k_f}{k_0} \langle |A_{0f}|^2 \rangle. \tag{1}$$

All quantities are in atomic units; k_0 and k_f are the initial and final wave vectors of the projectile electron and the scattering amplitude, A_{0f}, is given by

$$A_{0f} = (2\pi)^{-1} T_{0f}$$

$$T_{0f} = \langle \bar{\Psi}^- |V| \Psi_0^+ \rangle \tag{2a}$$

$$= \langle \Psi_f^- |V| \bar{\Psi}^+ \rangle \quad . \tag{2b}$$

Here $\bar{\Psi}^-$ and $\bar{\Psi}^+$ are the exact solutions of the Schrödinger equation for the scattering problem and in the plane wave representation;

$$\Psi_0^+ = e^{i \underset{\sim}{k}_0 \cdot \underset{\sim}{r}} \Phi_0(\underset{\sim}{r}_i) \quad , \tag{3a}$$

$$\Psi^{*-} = e^{-i \underset{\sim}{k}_f \cdot \underset{\sim}{r}} \Phi_f(\underset{\sim}{r}_i) \quad . \tag{3b}$$

In this prescription Φ_0 and Φ_f are the initial and final state wave functions of the bound electron coordinates symbolized collectively by r_i and r is the positional coordinate of the projectile electron. For collisions involving target atoms

$$V = \sum_i \frac{1}{|r - r_i|} - \frac{z}{r} \delta_{0f} \quad . \tag{4}$$

We are interested in a class of approximations where

$$\bar{\Psi}^{*-} \cong \chi_f^{*-}(r) \, \Phi_f(r_i)$$

in Eq. 2b or

$$\bar{\Psi}^{+} \cong \chi_0^{+}(r) \, \Phi_f(r) \tag{5}$$

in Eq. 2a. For example, with Eq. 5, Eq. 2b becomes

$$T_{0f} = \int \chi_f^{*-} \, \chi_0^{+} \, e^{ik_0 r} \, V_{0f} \, d\underset{\sim}{r} \tag{6}$$

where

$$V_{0f} = \langle \Phi_0 | V | \Phi_f \rangle \quad . \tag{7}$$

It is convenient to write V_{0f} as the inverse of its Fourier transform V_{of};[1]

$$V_{0f} = (2\pi)^{-3} \int e^{-i \, q \cdot r} \tilde{V}_{0f} \, d\underset{\sim}{q} \quad , \tag{8}$$

where

$$\tilde{V}_{0f} = \frac{4\pi}{q^2} \left\langle \Phi \left| \sum_i e^{-i \, q \cdot r_i} \right| \Phi_n \right\rangle = \frac{4\pi}{q^2} F(q) \quad . \tag{9}$$

The generalized oscillator strength defined by

$$f = \frac{W}{2} K^2 \left\langle \left| 2K^{-2} F(K) \right|^2 \right\rangle \tag{10}$$

is a quantity that can be measured at high incident electron energies. Here W is the excitation level of the atom and $\underset{\sim}{K} = \underset{\sim}{k}_0 - \underset{\sim}{k}_f$ is the momentum transferred by the colliding electron. The function, $-((2/K^2)F(K))$ is the collision amplitude in the Born approximation. When the quantity, $\Phi_0\Phi_f$, is independent of angle,

$$\langle |F(K)|^2 \rangle = [F(K)]^2$$

so that

$$F = K\left(\frac{f}{2W}\right)^{\frac{1}{2}} . \tag{11}$$

Hence, in the case of angular independent transition densities, F can be measured in principle and inverted by Eq. 8. This suggestion immediately applies to inelastic electron collisions involving transitions between the s states of an atom.

Application

In the case of $1^1S \rightarrow n^1S$ electron impact excitation, a minor variation of the procedure used by Lassettre[2] and Vriens[3] shows that F may be represented by a rapidly convergent power series;

$$F = \frac{K^2}{(K^2+\alpha^2)^3} \sum A_n \left[\frac{K^2}{K^2+\alpha^2}\right]^n , \tag{12}$$

where

$$\alpha = \sqrt{2I} + \sqrt{2(I-W)}$$

and I is the ionization potential of the atom. Then Eq. 8, together with Eqs. 11 and 12, gives

$$V_{0f} = r^{-1} \sum_{n=0}^{n=\infty} \frac{a_n}{(n+2)!} \left(\frac{d}{dx^2}\right)^{n+2} x^{2n} e^{-xr}\Big|_{x=\alpha} . \tag{13}$$

Thus we obtain the a_n by fitting series (12) via Eq. 11 to either experimental or calculated data, and then T_{0f} in Eq. 6 is reduced to a single three-dimensional integration.

As an example, we consider the Coulomb projected Born approximation introduced by Geltman[4,5] to take into account interaction of the projectile

electron with the atomic nucleus. His approach consists in letting

$$\chi^{-*} = e^{\frac{1}{2}\pi\sigma}\,\Gamma(1 - i\sigma)e^{-i\,k_n \cdot r}\,{}_1F_1(i\sigma, 1, ik_n r + k_n \cdot r) \quad , \tag{14}$$

where $\sigma = z/k_n$ and ${}_1F_1$ is the confluent hypergeometric function. The resulting integration can be performed analytically;

$$T_{0f} = 4\pi\left(\frac{2\pi\sigma}{1 - e^{-2\pi\sigma}}\right)^{\frac{1}{2}} \sum_{n=0}^{n=\infty} \frac{a_n}{(n+2)!}\left(\frac{d}{dx^2}\right)^{n+2} x^{2n} J\Big|_{x=\alpha} \quad , \tag{15}$$

where

$$J = (K^2 + x^2)^{-1 + i\sigma}\,(x^2 - 2ikx + 2W)^{-i\sigma} \quad . \tag{16}$$

In order to pursue this example further we consider the electron-impact excitation of the $1^1S \rightarrow 2^1S$ and $1^1S \rightarrow 3^1S$ transitions in helium for which accurate values of f have been calculated by Kim and Inokuti.[6] The polynomial coefficients a_n for both transitions were obtained by a least square fit of the tabulated values to Eq. 12.

It is convenient to define an apparent generalized oscillator strength by

$$f_a = \frac{W}{2}K^2\frac{k_0}{k_n}\,\sigma \quad . \tag{17}$$

When $k_0, k_n \rightarrow \infty$ ${}_1F_1 \rightarrow 1$ and Eq. 17 approaches the Born approximation of Eq. 10. The K^2 dependence of f_a for the two transitions is shown in Figures 1 and 2. The Born approximation limit labeled B in the figures were obtained by letting $k_n = 10^{10}$ in Eq. 15. The resulting f values differ from the original calculations[6] by less than 0.1%. In general, the f_a curves in Figure 1 exhibits a trend with $E = \frac{1}{2}k_0^2$ characteristic of what is observed experimentally.[7] The magnitude of f_a near $K^2 = 1$ decreases with decreasing E while the reverse occurs for $K^2 \geq 5$. This behavior tends to conserve the integral, $\int_0^\infty f_a\, d\ln K$ so that the total cross section Ω is given approximately by

$$\Omega = \frac{2\pi}{EW}\int_0^\infty f_a\, d\ln K$$

remains roughly the same regardless of whether f_a or the Born f is used in the

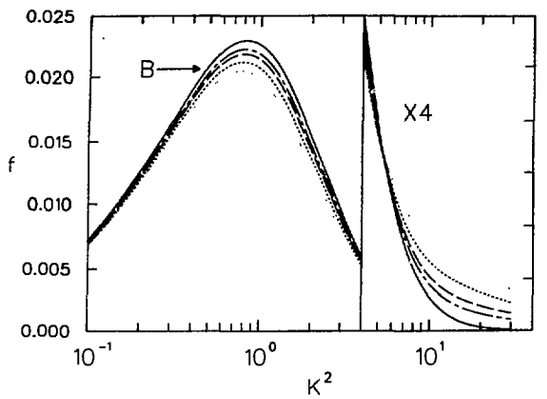

FIG. 1.--Apparent generalized oscillator-strength curves for the $1^1S \rightarrow 2^1S$ transition in helium as a function of incident electron energy. The Born approximation of Kim and Inokuti[6] is labeled B. 800 eV, ———; 500 eV, -.-.-.; 300 eV, ----; 200 eV, ····.

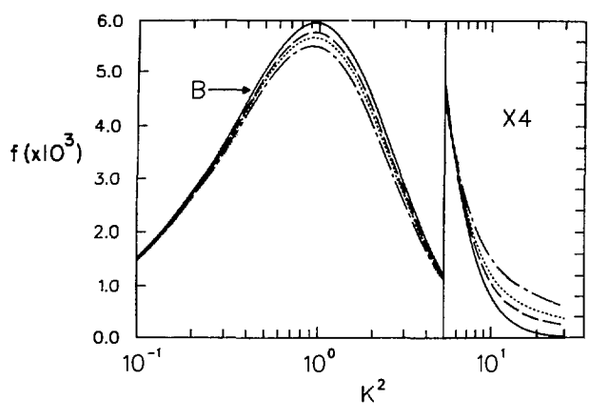

FIG. 2.--Apparent generalized oscillator-strength curves for the $1^1S \rightarrow 3^1S$ transition in helium as a function of incident electron energy. The Born approximation of Kim and Inokuti[6] is labeled B. 800 eV, ———; 500 eV, -.-.-; 300 eV, ----; 200 eV, ···· .

integration. This observation is in general accordance with both experiment[7] and the results of previous calculations.[5]

The calculated curves displayed in Figures 1 and 2 serve to illustrate the general utility of the procedure outlined above. The method can be applied to electron atom elastic scattering as well as to excitations where the transition density contains angular terms. In the latter case, it would be necessary to use calculated rather than experimentally derived Born amplitudes.

References

1. E. N. Lassettre, J. Chem. Phys. 57, 4357 (1972).
2. E. N. Lassettre, J. Chem. Phys. 43, 4479 (1965).
3. L. Vriens, Phys. Rev. 160, 100 (1967).
4. S. Geltman and M. Hidalgo, J. Phys. B 4, 1299 (1971).

5. M. Hidalgo and S. Geltman, J. Phys. B 5, 617 (1972).
6. Y.-K. Kim and M. Inokuti, Phys. Rev. 175, 176 (1968).
7. M. Dillon and E. N. Lassettre, J. Chem. Phys. 62, 2327 (1975).

RELATIVISTIC RANDOM-PHASE APPROXIMATION*

W. R. Johnson, † C. D. Lin, ‡ K. T. Cheng, ** and C. M. Lee ††

The relativistic random-phase approximation (RRPA) is developed from linearized time-dependent Hartree-Fock theory. Applications of the resulting relativistic many-body equations to determine excitation energies and oscillator strengths along the He, Be, Mg, Zn, and Ne isoelectronic sequences are discussed and compared with other recent experimental and theoretical work. The multichannel RRPA treatment of photoionization is described and applications are given to total cross sections, branching ratios, angular distributions and to autoionizing resonances.

* Abstract of a paper published in Phys. Scripta 21, 409 (1980).

† Physics Department, University of Notre Dame, Notre Dame, IND 46556.

‡ Physics Department, Kansas State University, Manhattan, Kansas 66506.

** Postdoctoral appointee from the University of Notre Dame, Notre Dame, IND.

†† Laboratory on Laser Energetics, University of Rochester, Rochester, N.Y. 14627; permanent address: Institute of Physics, Academy of Science, Peking, China.

SPIN POLARIZATION OF ns → εp PHOTOELECTRONS FROM XENON, KRYPTON, AND ARGON ATOMS*

K. T. Cheng,† K.-N. Huang,‡ and W. R. Johnson‡

Photoelectrons ejected from ns subshells of closed-shell atoms by unpolarized radiation are polarized as a result of the spin-orbit interaction. This usually small effect is dramatically enhanced near the "Cooper minimum" of the ns cross section. We present theoretical values of the spin polarization photoelectrons from outer ns subshells of the rare-gas atoms Xe, Kr, and Ar, obtained in the relativistic random-phase approximation. It is shown that a degree of polarization ranging up to 53% is possible for unpolarized radiation incident on Xe atom near the 5s cross section minimum. Furthermore, it is found that for linearly polarized radiation, up to 99% polarization can be achieved while for circularly polarized radiation, photoelectrons with up to 70% polarization can be produced.

---

*Abstract of a paper published in J. Phys. B. 13, L45 (1980).

†Postdoctoral appointee from the University of Notre Dame.

‡Physics Department, University of Notre Dame, Notre Dame, IND 46556.

THEORETICAL STUDY OF SPIN POLARIZATION OF PHOTOELECTRONS FROM NOBLE GASES*

K.-N. Huang,[†] W. R. Johnson,[†] and K. T. Cheng[‡]

Recent measurements by Heinzmann et al.[1] of the spin polarization of photoelectrons ejected from xenon by unpolarized light are in serious disagreement with various theoretical calculations. This letter reports an ab initio study of spin polarization with use of relativistic random-phase approximation. Excellent agreement is obtained between the present calculations and the experimental measurements by Heinzmann et al. for xenon, krypton, and argon.

Reference

1. U. Heinzmann, G. Schönhense, and J. Kessler, Phys. Rev. Lett. 42, 1603 (1979).

---

*Abstract of a paper published in Phys. Rev. Lett. 43, 1658 (1979).

†Physica Department, University of Notre Dame, Notre Dame, IND 46556.

‡Postdoctoral appointee from the University of Notre Dame.

RELATIVISTIC ENERGY LEVELS OF Fe XXI*

J. P. Desclaux,† K. T. Cheng,‡ and Y.-K. Kim

Energy levels of carbon-like iron, Fe XXI, with configurations $2s^2 2p^2$, $2s2p^3$, and $2p^4$ are calculated with the multiconfiguration Dirac-Fock method. The relativistic electron-electron interactions represented by the Breit operator are calculated with wave functions of definite angular symmetry instead of averaging over configurations. We find that the Breit interaction substantially improves the agreement between theory and experiment on the fine structures of the triplet states, while the Lamb shift corrections are very important in attaining accurate transition energies between configurations. Our results for energy levels agree with experiment to within 1% for all of the eighteeen levels compared, whereas corresponding non-relativistic results are off by 10 to 30%.

*Abstract of a paper published in J. Phys. B 12, 3819 (1979).

†Centre d'Etudes Nucléaires de Grenoble, 38041, Grenoble, France.

‡Postdoctoral appointee from the University of Notre Dame, Notre Dame, IND.

ELECTRIC DIPOLE AND ELECTRIC QUADRUPOLE TRANSITIONS BETWEEN LOW-LYING STATES OF Ni-LIKE IONS*

K. T. Cheng† and Y.-K. Kim

The low-lying spectra of Ni-like ions are studied using the relativistic multiconfigurational Hartree-Fock method. Electric dipole and electric quadrupole transitions from the ground state $3d^{10}\ {}^1S$ to the upper excited states $3d^9 4s\ {}^{1,3}D$ and $3d^9 4p\ {}^{1,3}P^o$ are calculated in both the length and velocity gauges. The theoretical wavelengths of the forbidden E2 transitions $3d^{10}$ $(J = 0)$ — $3d^9 4s$ $(J = 2)$ of Ni-like Mo are in good agreement with the observed lines in the soft x-ray spectrum of the TFR Tokamak.[1]

Reference

1. M. Klapisch, J. L. Schwob, M. Finkenthal, B. S. Fraenkel, S. Egert, A Bar-Shalom, C. Breton, C. DeMichelis, and M. Mattioli, Phys. Rev. Lett. 41, 403 (1978).

---

*Abstract of a paper presented at the DEAP meeting of the American Physcial Society at Houston, Texas, on 10-12 December 1979.

†Postdoctoral appointee from the University of Notre Dame, Notre Dame, IND 46556.

ENERGY LEVELS, WAVELENGTHS, AND TRANSITION PROBABILITIES OF Cu-LIKE IONS*

K. T. Cheng† and Y.-K. Kim

Wavelengths, oscillator strengths, and transition probabilities for the electric dipole transitions between low-lying states (n = 4, 5, 6) of Cu-like ions are presented. The data are calculated from relativistic Hartree-Fock wave functions.

*Abstract of a paper published in Atomic Data Nuclear Data Tables 22, 547 (1978).

†Postdoctoral appointee from the University of Notre Dame, Notre Dame, IND. 46556.

PUBLICATIONS BY THE STAFF OF THE FUNDAMENTAL MOLECULAR PHYSICS AND CHEMISTRY SECTION FOR THE PERIOD OCTOBER 1978-SEPTEMBER 1979.

MAJOR PAPERS

H. Bichsel, D. H. Peirson, J. W. Boring, A. Green, M. Inokuti, and G. Hurst. Average Energy Required to Produce an Ion Pair, ICRU Report 31, International Commission on Radiation Units and Measurements, Washington, D.C. (May 1979).

Kwok-tsang Cheng and Yong-Ki Kim, Energy levels, wavelengths, and transition probabilities of Cu-like ions, Atomic Data and Nuclear Data Tables 22, 547-563 (December 1978).

Kwok-tsang Cheng and Yong-Ki Kim, Excitation energies and oscillator strengths in silver isoelectronic sequence, J. Opt. Soc. Am. 69(1), 125-131 (January 1979).

J. L. Dehmer and Dan Dill, Connections between molecular photoionization and electron-molecule scattering with emphasis on shape resonances, Invited Paper, Symposium on Electron-Molecule Collisions, University of Tokyo, Japan, Sept. 6-7, 1979, I. Shimamura and M. Matsuzawa, Eds., University of Tokyo, pp. 95-104 (1979).

J. L. Dehmer, Jon Siegel, and Dan Dill, Shape resonances in e-SF_6 scattering, J. Chem. Phys. 69(1), 5205-06 (December 1978).

J. L. Dehmer and D. Dill, The continuum multiple-scattering approach to electron molecule scattering and molecular photoionization, Electron and Photon Molecule Collisions, V. McKoy, T. Rescigno, and B. Schneider, Eds., Plenum Publ. Corp., New York, pp. 225-265 (1979).

J. L. Dehmer, Dan Dill, and Scott Wallace, Shape-resonance-enhanced nuclear-motion effects in molecular photoionization, Phys. Rev. Lett. 43, 1005-1008 (October 1979).

J. L. Dehmer and Dan Dill, Shape resonance-enhanced nuclear motion effects in electron-molecule scattering and molecular photoionization, Electronic and Atomic Collisions, Invited papers and progress reports, Kyoto XIth ICPEAC Meeting, N. Oda and K. Takayanagi, Eds., Kyoto, 29 August-1 September 1979, pp. 195-208.

P. M. Dehmer and J. L. Dehmer, Photoelectron spectroscopy using a supersonic molecular beam source. The $^2B_{3u} + e^- \leftarrow {}^1A_g$ transition in ethylene, J. Chem. Phys. 70(10), 4574-4580 (May 1979).

Dan Dill, Scott Wallace, Jon Siegel, and J. L. Dehmer, Molecular-photoelectron angular distributions as a probe of dynamic symmetry breaking, Phys. Rev. Lett. 41(8), 1230-1233 (October 1978).

D. A. Douthat, Energy deposition and electron energy degradation in molecular hydrogen, J. Phys. B: Atom. Molec. Phys. 12(4), 663-678 (1979).

M. Inokuti (Book Review), Annual Review of Energy, Vol. 1, J. M. Hollander and M. K. Simmons, Eds.; Vol. 2, J. M. Hollander, M. K. Simmons, and D. O. Woods, Eds., Annual Reviews, Inc., Palo Alto, CA (1976-1977), Butsuri (Proc. Phys. Soc.) Japan 32, 1005-1006 (December 1978) (in Japanese).

M. Inokuti, Atomic processes pertinent to radiation physics, Electron and Atomic Collisions, Invited papers and progress reports, Kyoto XIth ICPEAC Meeting, N. Oda and K. Takayanagi, Eds., Kyoto, 29 August-4 September 1979, pp. 31-45.

Mitio Inokuti, Electron-scattering cross sections pertinent to electron microscopy, Ultramicroscopy 3, 423-427 (1979).

W. R. Johnson and K. T. Cheng, Quantum defects for highly stripped ions, J. Phys. B: Atom. Molec. Phys. 12(6), 863-879 (March 1979).

W. R. Johnson and K. T. Cheng, Photoionization of the outer shells of neon, argon, krypton, and xenon using the relativistic random-phase approximation, Phys. Rev. A 20(3), 978-988 (September 1979).

M. Matsuzawa, S. Mitsuoka, and M. Inokuti, Integrals of the squared form factor over the momentum transfer, J. Phys. B: Atom. Molec. Phys. 12(18), 3033-3046 (September 1979).

David Spence and P. D. Burrow, Resonant dissociation of N_2 by electron impact, J. Phys. B: Atom. Molec. Phys. 12(5), L179-L184 (March 1979).

David Spence and P. D. Burrow, Resonant dissociation in N_2 by electron impact: A source of heating in the thermosphere and auroras? Invited paper, Symposium on Electron-Molecule Collisions, University of Tokyo, Japan, Sept. 6-7, 1979, I. Shimamura and M. Matsuzawa, Eds., University of Tokyo, pp. 129-134 (1979).

Roger Stockbauer, B. E. Cole, D. L. Ederer, John B. West, Albert C. Parr, and J. L. Dehmer, Effects of shape resonances on vibrational intensity distributions in molecular photoionization, Phys. Rev. Lett. 43(1), 757-761 (September 1979).

S. Wallace, D. Dill, and J. L. Dehmer, Spectral variation of molecular photoelectron angular distributions: Valence shells of N_2 and CO, J. Phys. B: Atom. Molec. Phys. 12(4), L417-L420 (July 1979).

CONFERENCE PAPERS AND ABSTRACTS

Annual Meeting of the American Physical Society, Chicago, Ill., March 19-23, 1978. Abstracts published in Bull. Am. Phys. Soc. 24, 1979.

J. Siegel, J. L. Dehmer, and D. Dill, Energy-dependent continuum exchange in atomic photoionization, p. 511.

G. Das, R. C. Raffenetti, and Y.-K. Kim, Low-lying states of $(Cs_2)^{++}$, Proc. Heavy Ion Fusion Workshop, Argonne National Laboratory, September 19-26, 1978, p. 195.

10th Annual Meeting of the Division of Electron and Atomic Physics, Madison, Wisconsin, 29 November-1 December 1978. Abstracts published in Bull. Am. Phys. Soc. 23(9), November 1978).

J. Siegel, J. L. Dehmer, D. Dill, and J. Welch, Integrated and differential elastic and vibrationally inelastic cross sections for e-N_2 scattering, p. 1082.

M. G. Lynch, J. Welch, D. Dill, J. Siegel, and J. L. Dehmer, Elastic cross sections for e-CO_2, CS_2, COS scattering and vibrational excitation in e-CO_2 scattering, p. 1082.

Steven T. Manson and Mitio Inokuti, Generalized oscillator strength for ionization of the K and L inner shells of atoms, p. 1090.

K. T. Cheng and Y.-K. Kim, Oscillator strengths of the resonance transitions in the neon isoelectronic sequence, p. 1092.

J. L. Dehmer, J. Siegel, and D. Dill, Shape resonances in the e-SF_6 scattering, p. 1104.

P. M. Dehmer and J. L. Dehmer, Photoelectron spectra using a supersonic molecular beam source, p. 1106.

Abstracts of Papers, Joint American Chemical Society/Chemical Society of Japan Congress, April 1-6, 1979, Honolulu, Hawaii.

J. L. Dehmer and Dan Dill, Shape resonances in molecular photoionization, p. 108.

Spring Meeting of the American Physical Society, Washington, D.C., April 23-26, 1979. Abstract published in the Bull. Am. Phys. Soc. 24(4), April 1979.

K. T. Cheng, W. R. Johnson, and C. D. Lin, Photoionization of the outer shells of rare gases using the relativistic random-phase approximation, p. 561.

Abstracts of the 6th International Congress of Radiation Research, May 13-19, 1979, Kyoto, Japan

Yong-Ki Kim, Stopping power of partially stripped ions, p. 88.

Taizo Sasaki, Kazumi Fujima, Akira Mikuni, and Mitio Inokuti, Absorption cross sections of solids and polymers containing PO_4^{---} in the region of P $L_{2,3}$ excitation, p. 90.

Mitio Inokuti and D. A. Douthat, Statistical fluctuations in the yield of initial molecular species and their relation to the Spencer-Fano electron degradation spectrum, p. 199.

Daryl A. Douthat, Recent developments in electron degradation theory, p. 16.

XIth International Conference on the Physics of Electronic and Atomic Collisions, Kyoto, Japan, Aug. 29-Sept. 4, 1979, Abstracts of Contributed Papers.

P. M. Dehmer and J. L. Dehmer, Photoelectron spectroscopy using a supersonic molecular beam source Renner-Teller splitting in the bending vibration of $N_2O^+X^2\Pi$ at 584 Å, p. 44.

S. Wallace, J. R. Swanson, Dan Dill, and J. L. Dehmer, Molecular photoelectron branching ratios and angular distributions from 0 to 10 Ry. Effects of shape resonances and nuclear motion, p. 46.

M. Inokuti, K. T. Cheng, and J. L. Dehmer, The Bethe total cross sections for inelastic collisions of fast charged particles with C^-, O^-, and F^- ions, p. 220.

J. Siegel, J. L. Dehmer, and Dan Dill, Effects of shape resonances, nuclear motion, and dipole fields on electron-molecule scattering from 0-1000 eV, p. 300.

George H. Gillespie and Mitio Inokuti, Elastic and inelastic atom-atom cross section at high velocities for $Z \leq 18$, p. 442.

Hajime Ishimaru, K. Muto, Z. Igarashi, S. Hiramatsu, S. Shibata, J. E. Griffin, and M. Inokuti, Measurement of ionization cross section of gaseous molecules for 0.02-385 GeV protons, p. 640.

Isao Shimamura and Mitio Inokuti, Bounds on mean excitation energies in terms of oscillator-strength moments, p. 1014.

Yong-Ki Kim and Kwok-tsang Cheng, Bethe cross sections for ionization of C^{3+}, N^{4+}, and O^{5+}, p. 218.

David Spence and P. D. Burrow, Cross section for resonant dissociation of N_2 by electron impact, p. 372.